UNIVERSITY OF NAPLES FEDERICO II
DEPARTMENT OF PHARMACY

Ph.D. THESIS
IN
"PHARMACEUTICAL SCIENCE"

Extra-ribosomal functions of ribosomal protein uL3 in response to

drug-induced nucleolar stress in colon cancer cells lacking p53

SUPERVISOR: **COORDINATOR:**

Ch.ma Prof.ssa   Prof.ssa Maria Valeria D'Auria
Giulia Russo

CANDIDATE:
Annalisa Pecoraro

XXXIII cycle
2018/2021

INDEX

1. INTRODUCTION

1.1 Nucleolus: canonical and non-canonical functions

The nucleolus is a well-characterized sub-nuclear compartment without membrane, visible by microscopy inside the cellular nucleus. In humans, it originates around the nucleolar organizer region (NOR) of five chromosomes (13, 14, 15, 21 and 22) each containing tandem clusters of ribosomal genes (rDNA) (Pederson, 2011). The nucleolus is not visible during all phases of the cell cycle. It is present throughout interphase acquiring a dynamic structure to accommodate its canonical function: the biogenesis of ribosomes. Nucleolar disassembly occurs at the beginning of mitosis to ensure that the machineries necessary to assemble the nucleoli are inherited by the two daughter cells (Pederson, 2011).

The ribosome biogenesis is an energy-consuming and well-orchestrated process, functionally organized to take place in three sub-nucleolar compartments: the fibrillar compartment (FC), the dense-fibrillar compartment (DFC), and the granular compartment (GC) (Pederson, 2011). During ribosome biogenesis all the constituents of the ribosomes are synthetized, modified, assembled in the nucleolus, and finally carried into the cytoplasm to build up the mature ribosomal subunits, the small 40S subunit and the large 60S subunit. The 40S subunit, consisting of the 18S ribosomal RNA (rRNA) and 33 ribosomal proteins (RPs), decodes messenger RNAs by aminoacyl–transfer RNA (tRNA); whereas the 60S subunit, composing of 5S, 5.8S, 28S rRNAs and 47 RPs, catalyses peptide bond formation by the peptidyltransferase reaction (Thomson et al., 2013).

Besides the constituents of the ribosomes, a large number of molecular players are involved in ribosome biogenesis, such as RNA polymerases (RNA Pol), small nucleolar RNAs (snoRNAs), regulatory, processing, assembling, and maturation factors (Thomson et al., 2013).

Ribosome biogenesis starts in the FC, where the transcription of rDNA genes by the RNA Pol I leads to the synthesis of the 47S rRNA precursor (pre-rRNA), which is characterized by the presence of the 5′ and 3′ external transcribed spacers (ETS) and two internal transcribed spacers (ITS1 and ITS2). These transcribed spacers contain multiple cleavage sites targeted by endo- and exonucleases, leading to the generation of the mature 18S, 28S, and 5.8S rRNAs. In the nucleus, the RNA Pol III synthesizes 5S rRNA that will be subsequently accumulated in the nucleolus. RP genes transcription is driven by RNA Pol II and, after RPs

synthesis in the cytoplasm, they are imported into the nucleolus where they assemble with the nascent pre-rRNAs (Thomson et al., 2013). The processing of the 47S pre-rRNA occurs in the DFC, an area surrounding the FC, to be further completed in the GC, where the mature rRNAs and RPs are assembled to build up the pre-ribosomal subunits (40S and 60S), ready to be transferred to the cytoplasm to form the mature ribosomes (Thomson et al., 2013).

Taking into account that protein synthesis is strictly coordinated with cell growth and proliferation, and directly dependent on ribosome biogenesis, it is not surprising that ribosome biogenesis represents an essential cellular process highlighting the crucial role of nucleolus to maintain cellular homeostasis (Grummt, 2013). Based on this observation, in the last decades, a huge number of studies have deeply investigated the nucleolar functions that are independent from ribosome biogenesis, providing a new concept of "pluri-functional nucleolus". Specifically, the non-canonical functions of the nucleolus are strictly related to the regulation of a large number of cellular processes including the maintenance, repair and stability of the genome, the cell cycle progression, cellular senescence, response to stress, telomere maintenance, and the nuclear architecture (Pederson, 2011).

In the last decades, different studies have reported that nucleolar dysfunctions are implicated in several human disease. More specifically, mutations in genes encoding ribosome components or ribosome biogenesis factors are related to a class of human inherited disorders called "ribosomopathies" (Tsai et al., 2014). The nucleolus has also been linked with numerous viral infection and nucleolar activities showed to be essential for virus replication and/or pathogenesis (Tsai et al., 2014). In addition, several types of cancers are associated with alteration in both canonical and non-canonical nucleolar functions (Stępiński, 2018). The expression of several RPs has been found to be altered in human tumors such as colorectal cancer, esophagus cancer, and hepatocellular carcinoma suggesting a role for these RPs as oncogenes or tumor suppressors (Russo et al., 2017[a]). To date, mutations in uL5 (RPL11) are observed in melanoma and T-cell acute lymphoblastic leukemia, and deletions or inactivating mutations of uL18 (RPL5) occurs in T-cell acute lymphoblastic leukemia and in multiple myeloma, melanoma, glioblastoma and breast cancers (De Keersmaecker et al., 2013; Fancello et al., 2017).

Intriguingly, it has been reported that ribosomopathies are associated to an elevated cancer risk. Within the context of RP mutations in ribosomopathies and cancer, different evidences support the notion that ribosomes with different composition exhibit peculiar functions with preferential translation of particular mRNAs. These ribosomes are also known as "specialized ribosomes" or "onco-ribosomes" in order to underline their ability to translate preferentially

oncogenes supporting malignant transformation (Kampen et al., 2020). However, it remains to be elucidated how specialized ribosomes achieve the selectivity of specific mRNAs.

1.2 Nucleolar stress

The nucleolus is being considered as a central hub in sensing and reacting to various cellular stressors. In fact, it has been reported that various stress stimuli are able to impair ribosome biogenesis, i.e., exposure to UV and gamma radiation, de-regulation of oncogenes or tumor suppressor, nutrient and growth factor deprivation, rRNA or RPs unbalance, hypoxia, and chemotherapeutic agents causing the activation of the so-called nucleolar stress response, allowing the cells to adapt to the new environment (Russo et al., 2017[a]). The nucleolar stress pathways involves several molecular networks, some of which required p53 tumor suppressor activity while others are independent (Russo et al., 2017[a]). Nevertheless, a key step in the activation of nucleolar stress response is the accumulation of several RPs and nucleolar proteins into the nucleoplasm leading to cell cycle inhibition, induction of apoptosis, DNA damage response and senescence (Figure 1). In this context, a multitude of studies have indicated that several RPs possess extra-ribosomal functions, defining them as "moonlight ribosomal proteins" (Molavi et al., 2018). One of the most intriguing extra-ribosomal roles of RPs is their participation in mediating p53-dependent or -independent nucleolar stress signaling pathways.
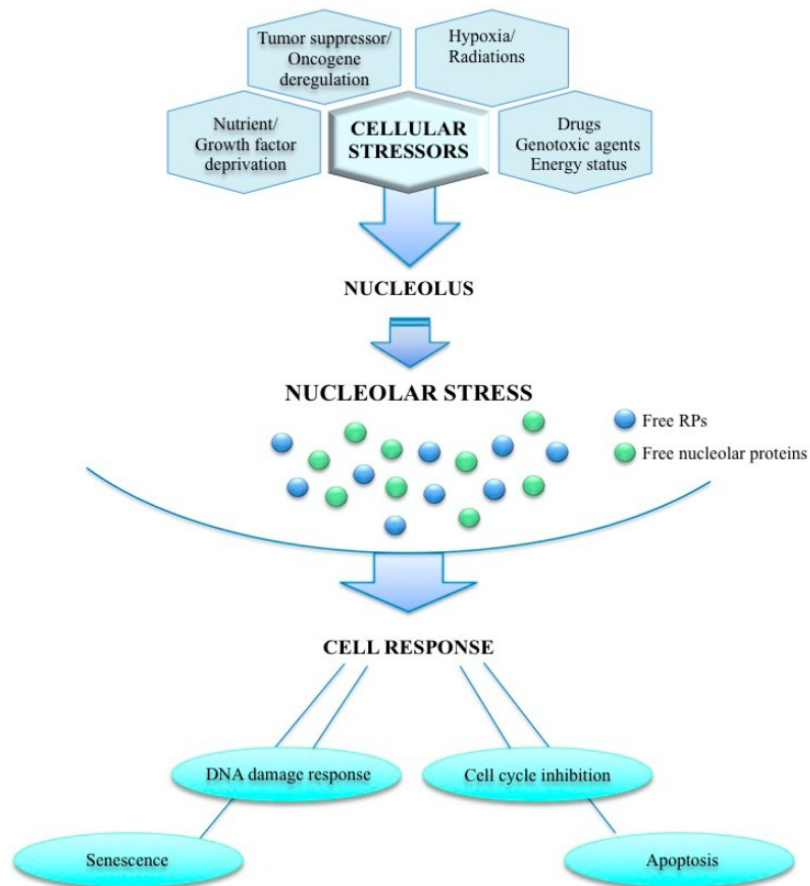
Figure 1. The nucleolar stress response pathway. Nucleolus can be exposed to a multitude of cellular stressors that impair ribosome biogenesis activating a complex cellular response namely "nucleolar stress". This stress pathway is mediated by several RPs and/or nucleolar proteins and its activation leads to cell cycle arrest, apoptosis, DNA damage and senescence. (Carotenuto et al., 2019)

1.2.1 Role of ribosomal proteins in p53-dependent response pathways to nucleolar stress

The tumor suppressor p53 protein is a transcription factor that regulates the expression of more than hundred target genes involved in essential cellular processes such as cell cycle progression, DNA repair, apoptosis, autophagy, senescence and differentiation (Sullivan et al., 2018). In physiological condition, p53 activity is finely controlled by MDM2 (murine double minute 2), the ubiquitin E3 ligase that negatively regulates p53 promoting its degradation via ubiquitination (Sullivan et al., 2018). Therefore, in the absence of stress signals MDM2 mainly acts to restrict the growth-suppressive function of p53 maintaining low cellular p53 levels (Figure 2A).

It has been reported that various cellular stressors can lead to the activation of p53 by interfering with its binding to MDM2 (Sullivan et al., 2018). Specifically, in condition of nucleolar stress several RPs from the large and small subunits translocate to the nucleoplasm

and bind to MDM2 resulting in p53 stabilization and consequent induction of p53-mediated cell cycle arrest or apoptosis (Figure 2B) (Russo et al., 2017[a]). To date, uL5 (RPL11) and uL18 (RPL5) are essential to mediate p53 stabilization in response to nucleolar stress (Fumagalli et al., 2012).

These two RPs in association with 5S rRNA form a ribosomal subcomplex, known as the 5S ribonucleoprotein particle (5S RNP). In unstressed cells, the 5S/uL18 (RPL5) complex is already present in the nucleoplasm whereas uL5 (RPL11) is present exclusively in the cytoplasm and nucleolus. In condition of nucleolar stress, uL5 (RPL11) translocates into the nucleoplasm and associates with pre-existing 5S/uL18 (RPL5) complex to form 5S RNP that binds to MDM2 with consequent upregulation of p53 levels (Onofrillo et al. 2017).

Other RPs exert their extra-ribosomal functions directly stimulating p53 mRNA translation independently from MDM2. For instance, in stressed cells uL24 (RPL26) binds to 5′-untranslated region (UTR) of p53 mRNA inducing p53 translation (Figure 2B). Intriguingly, the effect of uL24 (RPL26) on the p53 expression level is regulated in turn by MDM2. In fact, MDM2 could bind and ubiquinate uL24 (RPL26), which results in the attenuated promoting effect of this ribosomal protein on p53 translation in unstressed cells (Ofir-Rosenfeld et al., 2008).
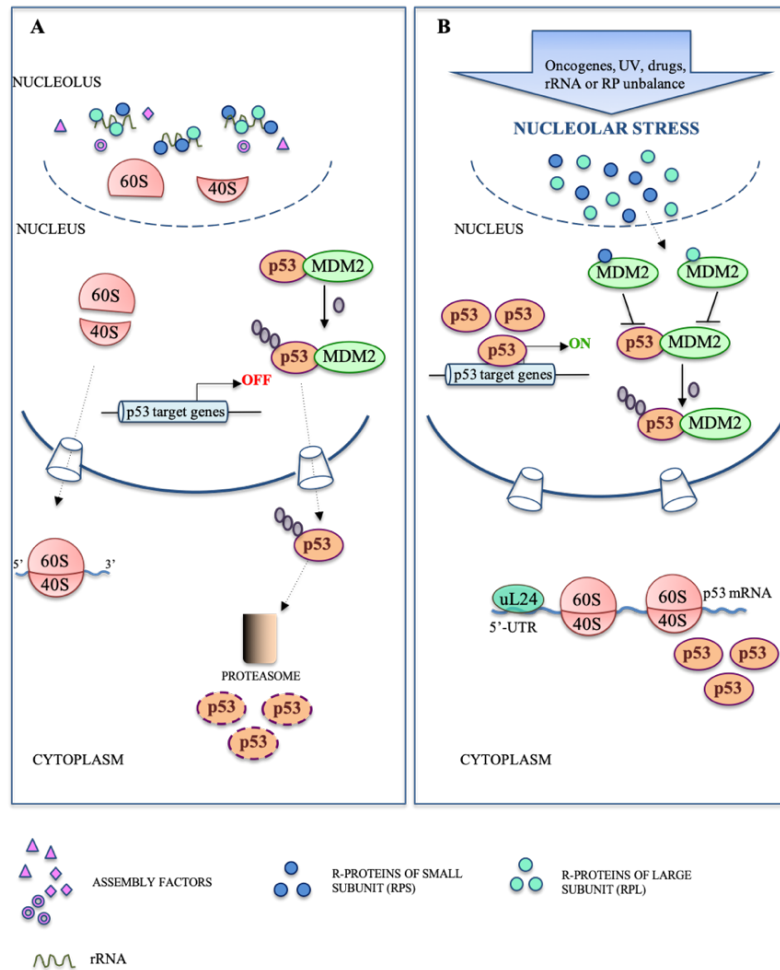
Figure 2. Role of RPs in p53 activation upon nucleolar stress. (A) Under physiological conditions, p53 activity is maintained at low levels through its degradation induced by ubiquitinylation mediated by MDM2 (mouse double minute). (B) Upon nucleolar stress, RPs are released as ribosome free form and accumulated into the nucleoplasm where they interact with MDM2, thus inhibiting its ubiquitin ligase activity with consequent p53 stabilization. In the cytoplasm, ribosome-free uL24 (RPL26) binds to 5′-UTR of p53 mRNA promoting p53 translation. Accumulated p53 induce the expression of its target genes involved in the activation of events that ultimately leads to cell cycle arrest and apoptosis. (Image adapted from Russo et al., 2017[a])

1.2.2 Role of ribosomal proteins in p53-independent response pathways to nucleolar stress

It is well established that over 50% of human cancers contain mutant p53 or no p53 at all (Mantovani et al., 2019). In recent years, some emerging evidence have revealed that nucleolar stress response is activated and leads to cell cycle arrest and/or apoptosis also in p53 deleted cells indicating the existence of additional stress response pathways that are p53-independent but still dependent on some RPs (Russo et al., 2017[a]).

It has been observed that the inhibition of RNA Pol I in p53-/- cells caused a reduction in the expression levels of E2F1, a transcription factor which regulates the expression of genes

whose products are necessary for the entry and passage through the S phase of cell cycle (Bertoli et al., 2013). In physiological conditions, E2F1 half-life is prolonged by the interaction with MDM2, which prevents its degradation via other E3 ligases responsible for E2F1 ubiquitination (Zhang et al., 2005).

In stressed cells, the selective inhibition of rRNA synthesis led to the release of uL5 (RPL11), which binds to MDM2, thus preventing its stabilizing function on the E2F1 (Figure 3). The consequent reduction of E2F1 caused the down-regulation of its target genes required for G1/S transition leading to the inhibition of cell proliferation (Donati et al., 2011).

The oncoprotein c-Myc is a key transcription factor which regulates the expression of many genes implicated in cell growth and proliferation (Dang, 1999). Moreover, it has been reported that c-Myc activity is also required for essential steps in ribosome biogenesis. Different studies demonstrate that some RPs negatively regulates c-Myc by directly suppressing its transcriptional activity and/or promoting its degradation through the miRNA-mediated mechanism (Russo et al., 2017[a]). In condition of nucleolar stress, ribosome-free uL18 (RPL5) and uL5 (RPL11) act in cooperative manner to suppress c-Myc expression. In particular, they form a complex that binds to c-Myc mRNA at its 3' untranslated region (3'-UTR) thus recruiting miRISC (micro-RNA-induced silencing complex) to c-Myc mRNA and leading to its degradation (Figure 3). Specifically, uL5 (RPL11) directly binds to c-Myc MBII (Myc homology box II) domain, thus preventing the recruitment of c-Myc and its cofactor TRRAP (transformation/transcription domain-associated protein) to the promoters of c-Myc target genes. Moreover, uL5 (RPL11) is able to recruit miR-24 to c-Myc mRNA (Dai et al., 2007; Challagundla et al., 2011). uL18 (RPL5) binds to 3'UTR of c-Myc mRNA and to two subunits of RISC, TRBP (HIV-1 TAR RNA-binding protein) and Ago2 (Argonaute 2), targeting c-Myc mRNA for miRNA-mediated degradation (Liao et al., 2014). Additionally, it has been reported that uS11 (RPS14) also acts as a negative regulator of c-Myc expression. Zhou et al. have demonstrated that uS11 (RPS14) binds to the MBII and bHLH-LZ (C-terminal basic helix-loop-helix leucine zipper) domains of c-Myc and interferes with its transcriptional activity by inhibiting the recruitment of c-Myc and its cofactor, TRRAP, to the promoter of its target gene, Nucleolin. Furthermore, uS11 (RPS14) is able to interact with Ago2 triggering Ago2/miR-145 mediated c-Myc mRNA degradation (Figure 3) (Zhou et al., 2013).
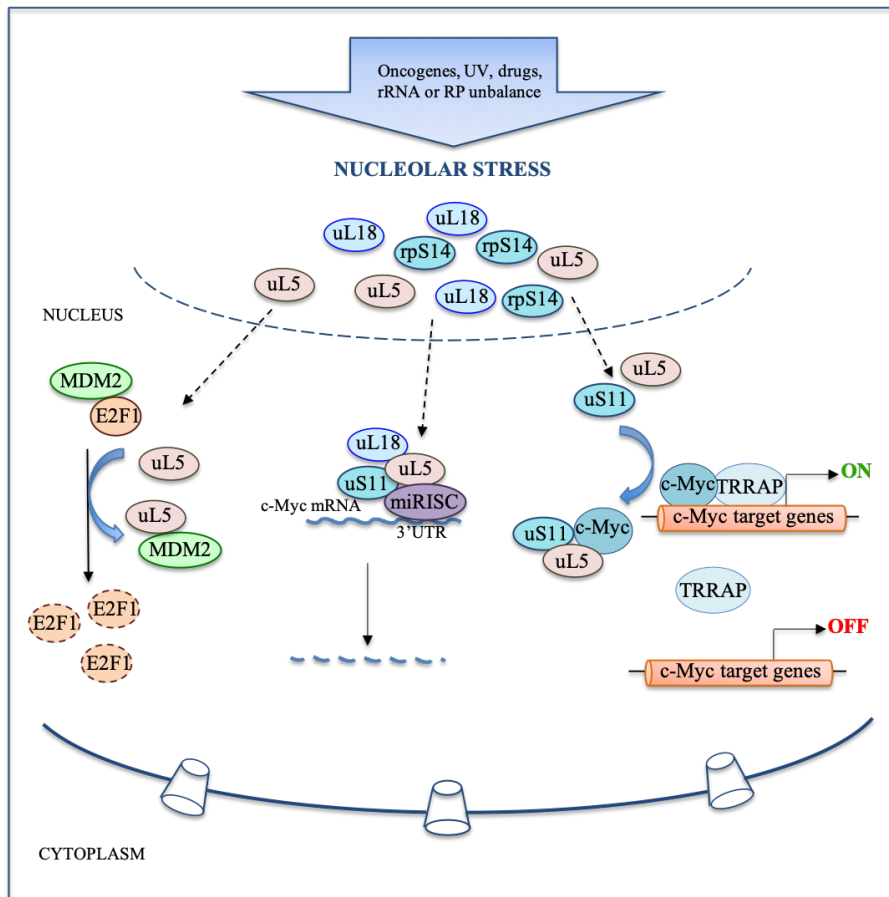
Figure 3. p53-independent and RPs-dependent nucleolar stress response pathways. Ribosome-free uL5 (RPL11) binds MDM2 causing the release of E2F1 and its subsequent degradation; ribosome-free uL18 (RPL5), uL5 (rpL11) and uS11(RPS14) bind to 3′-UTR of c-Myc mRNA inducing the recruitment of miRISC (miRNA-induced silencing complex) for c-Myc degradation; uL5 (rpL11) and uS11(RPS14) bind to c-Myc box II domain and inhibit the recruitment of c-Myc co-activator TRRAP to c-Myc target gene promoters. The activity of these RPs leads to c-Myc suppression causing the inhibition of cell proliferation. (Image adapted from Russo et al., 2017[a])

1.3 uL3 protein: ribosomal and extra-ribosomal functions

Ribosomal protein L3 (formerly RPL3 and reported in the text and in the figures as uL3, according to new nomenclature) is a universally conserved component of the large 60S subunit of cytoplasmic ribosomes. This protein plays a crucial role for both ribosome biogenesis and ribosome structure and function. Rosado et al. have reported that uL3 depletion impairs the nucleocytoplasmic export of pre-60S ribosomal particles indicating its essential role for the assembly of early pre-60S particles (Rosado et al., 2007). The tridimensional structure of uL3 is characterized by 3-fingered structure that consists of a globular domain and three extensions, the N-terminal extension, the "tryptophan" finger" (finger W) and the "base thumb", that reach up to the central core of the large 60S subunit nearly to the peptidyl transferase center (PTC). Different studies have revealed that mutations in these regions cause profound alterations in the ribosomes function (Mailliot et al., 2016). In addition, it has been reported that uL3 modulates translational elongation by coordinating both the accommodation of charged tRNAs and the binding of elongation factor 2 (eEF2); in this light, uL3 has been described as the "gatekeeper to the A-site" (Meskauskas et al., 2007). A recent study has demonstrated that uL3 promotes translational elongation fidelity; in particular, this function depends on methylation of uL3 at histidine 243 that lies close to the PTC in a functionally important region of uL3 known as the "basic thumb" (Al-Hadid et al., 2018).

Although uL3 has long been studied as fundamental ribosome component, a growing amount of data demonstrate that it exerts additional functions, independently from the ribosome biogenesis, well known as extra-ribosomal functions. In this scenario, it is not surprising that the expression levels of uL3 need to be finely regulated. We have previously demonstrated that uL3 protein autoregulates its own expression through the association of alternative splicing and nonsense-mediated mRNA decay (AS-NMD). Specifically, we have identified an alternative spliced nonsense codon-bearing transcript from the human *uL3* gene that is a natural target of NMD (Cuccurese et al., 2005).

Interestingly, the ribosome-free form uL3 protein acts as a sensor of its own expression. In physiological condition, the canonical transcript is the predominant isoform and encodes the uL3 protein; when uL3 is present in excess, the canonical splicing is suppressed and the alternative splicing is induced resulting in an increase of alternative uL3 mRNA, which is unproductive and is targeted by NMD. This event leads to a decrease in the intracellular levels of uL3 protein (Cuccurese et al., 2005). This post-transcriptional feedback loop regulates the

amount of ribosome-free uL3 avoiding wasteful production of the protein. The regulation of *uL3* gene expression via alternative splicing associated to NMD (AS-NMD) requires heterogeneous nuclear ribonucleoprotein H1 (hnRNP H1), K-homology splicing regulatory protein (KHSRP) and Nucleophosmin (NPM, also known as B23). Specifically, NPM interacts with hnRNP H1 and intron 3 pre-mRNA, thus preventing the binding of hnRNP H1 to the cis-acting regulatory elements "G runs" in uL3 intron 3. In this way, NPM suppress the alternative splicing of *uL3* gene. Upon uL3 accumulation, uL3 interacts with NPM causing its release from the ribonucleoprotein complex, and associated with KHSRP and other transacting proteins, thus favoring the interaction of hnRNP H1 with enhancer elements "G runs" in uL3 intron 3. These rearrangements within the ribonucleoprotein complex promote the selection of the 3′-splice site in intron 3 transcript leading to the production of the alternative splicing isoform (Russo et al., 2010; Russo et al., 2011).

The extra-ribosomal functions of uL3 have been deeply investigated by our group and the results pointed out its crucial role in the nucleolar stress response activated by different conventionally used chemotherapeutic drugs such as Actinomycin D (Act D), 5-Fluorouracil (5-FU), Oxaliplatin (OHP) and Niclosamide in lung and colon cancer cells lacking functional p53 (Russo et al., 2013; Esposito et al., 2014; Russo et al., 2016[a]; Russo et al., 2016[b]; Pagliara et al., 2016). Overall, these studies have strongly indicated the favourable anticancer potential of uL3 and revealed the existence of nucleolar stress response pathways that are p53-independent and uL3-dependent (Figure 4).

Upon drug-induced nucleolar stress, uL3 protein accumulates as ribosome-free form in the nucleoplasm where it acts as a transcription factor and affects *p21* (also known as p21[WAF1/Cip1]) and *CBS* (cystathionine-β-synthase) gene expression in opposite way. The cyclin-dependent kinase inhibitor p21 mediates its various biological activities primarily by binding to and inhibiting the kinase activity of the cyclin-dependent kinases (CDKs) causing growth arrest at specific stages in the cell cycle (Al Bitar et al., 2019), whereas CBS is one of three principal enzymes involved in the biosynthesis of H_2S in various mammalian cells and plays a crucial role in promoting cellular bioenergetics, proliferation and migration in tumors (Szabo, 2016). Specifically, in condition of nucleolar stress ribosome-free uL3 induces the phosphorylation of ERK (extracellular signal-regulated kinase), thus allowing the activation of ERK protein targets (Russo et al., 2016[b]). It has been hypothesized that activation of the MEKs/ERKs pathway triggered by uL3 could induce the consequent phosphorylation of the transcription factor Sp1 (specificity protein 1) and the binding of Sp1/uL3 complex to the *p21* promoter (Russo et al., 2016[b]). In addition, uL3 is able to bind to phosphorylated Sp1 and

this interaction could be essential to remove Sp1 from the *CBS* promoter resulting in the inhibition of *CBS* transcription. Concomitantly, free uL3 recruits phosphorylated Sp1 on the *p21* promoter with consequent induction of *p21* expression. In the cytoplasm, ribosome-free uL3 regulates the stability of p21, CBS and also of IκB-α (inhibitor alpha of nuclear factor kappa B) proteins. In particular, uL3 positively affects the half-life of p21 protein by modulating p21 interaction with its negative regulator MDM2 (Russo et al., 2016[b]). In contrast, uL3 binds to CBS protein and promotes its traslocation into the mitochondria for degradation causing a consequent decrease of CBS catalytic activity and a reduction of H_2S levels (Pagliara et al., 2016). These effects are correlated to the release of cytocrome c from mitochondria and the activation of caspases that ultimately lead to apoptosis (Pagliara et al., 2016). Moreover, ribosome-free uL3 also regulates NFκB (nuclear factor kappa-light-chain-enhancer of activated B cells), a key mediator of inflammatory responses that play a crucial role in tumorigenesis as survival factor (Zhang et al., 2006). It has been suggested that uL3 stabilizes IκB-α protein and prevents its degradation via proteasome thus inhibiting nuclear translocation of NFκB and its transcriptional activity (Russo et al., 2016[d]) (Figure 4).

Results from our group have also demonstrated a strong correlation between intracellular levels of uL3 and the regulation of DNA repair mechanisms such as homologous recombination (HR) and non-homologous end joining (NHEJ) (Esposito et al., 2014). In particular, in condition of drug-induced nucleolar stress ribosome-free uL3 could inhibit DNA repair in p21-dependent and p21-independent manner (Esposito et al., 2014).

These findings add more relevance to the multitude of mechanisms activated upon drug-induced nucleolar stress in which uL3 protein acts as a key mediator independently from p53.
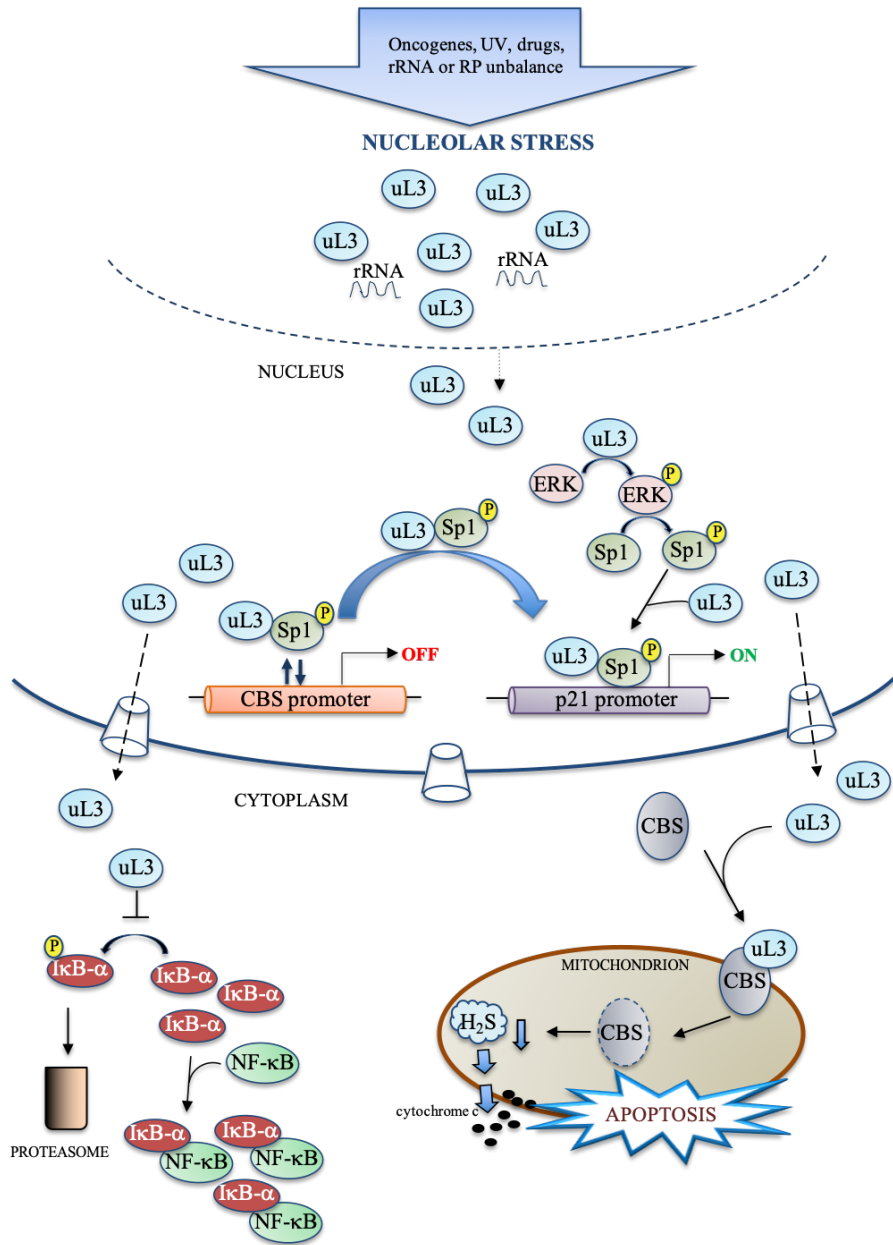
Figure 4. Schematic representation of proposed model for p53-independent and uL3-dependent nucleolar stress response pathways. (Image adapted from Russo et al., 2017[a])

1.4 Targeting nucleolus in cancer

Data from the literature largely demonstrated the existence of a close interconnection between nucleolus and cancer. Different cytological and histopathological studies have revealed that almost all tumor types are characterized by abnormalities in the morphology and numbers of nucleoli probably due to the hyperactivation of ribosome biogenesis required for sustaining the uncontrolled growth of cancer cells (Stępiński, 2018). Indeed, in some type of tumors nucleolar size has been used as predictive and prognostic biomarker in chemotherapeutic treatment and clinical outcomes (Stępiński, 2018). In light of these observations, many authors suggest that tumor cells are "addicted" to the hyperactivation of ribosome biogenesis and this concept is fundamental in cancer therapy. In addition, it has been reported that alteration in the nucleolar stress pathway are often associated to the development of cancer (Russo et al., 2017[a]). Therefore, in the last decades many efforts have been made to develop therapies that specifically target nucleolar components or nucleolar functions (Figure 5) (Carotenuto et al., 2019).
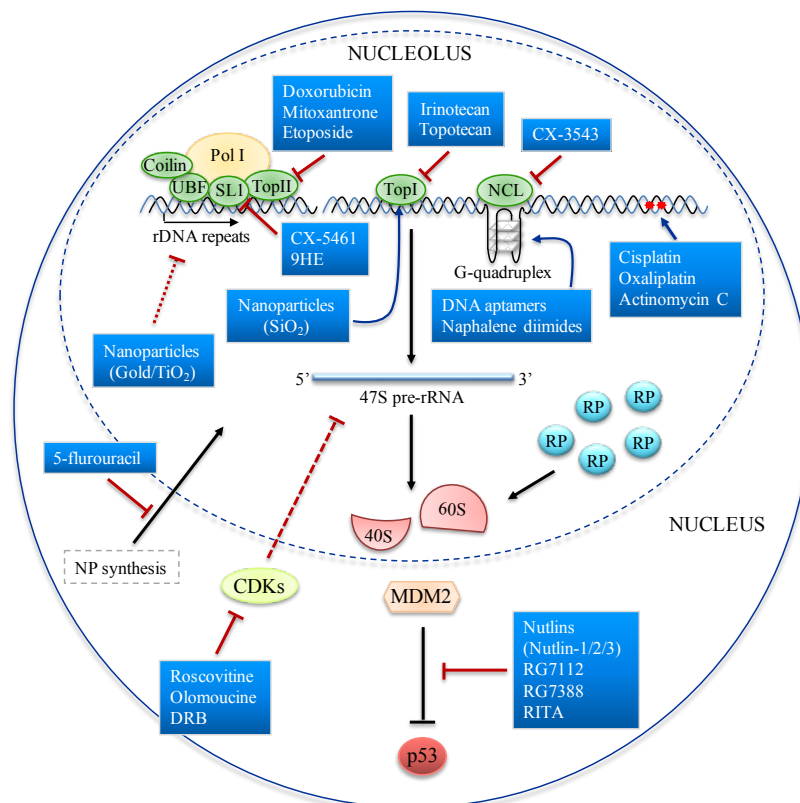
Figure 5. Targeting nucleolus in cancer treatment. Schematic representation of main anti-cancer molecules targeting nucleolar structures and/or functions. Pol I: RNA polymerase I; UBF: Upstream Binding Factor; SL1: Selective Factor 1; Top I/II: Topoisomerase I/II; NCL: Nucleolin. (Image adapted from Carotenuto et al., 2019)

1.4.1 Compounds targeting nucleolar components

It has been showed that during tumorigenesis, a series of oncogenic stimuli converge at the nucleolus causing the alteration of rRNA transcriptional machinery (Bywater et al., 2013). Particularly, the activity of RNA Pol I, the key enzyme in the synthesis of rRNA precursor, is often higher in tumor cells compared to normal cells. The overactivation of RNA Pol I activity is correlated with adverse prognosis in several tumor types (Bywater et al., 2012). In this light, the inhibition of RNA Pol I activity could be a useful strategy in targeted anti-cancer therapy. Interestingly, recent investigations have demonstrated that several of currently used antineoplastic drugs directly or indirectly interfere with RNA Pol I-driven transcription. These anticancer agents can be classified accordingly to their mechanism of action into the following groups: DNA-alkylating agents, nucleotide analogues, antibiotics that bind/intercalate with DNA preventing RNA synthesis; and plant alkaloids that prevent cell division (Burger et al., 2010).

Alkylating-like platinum drugs such as Cisplatin and Oxaliplatin are able to inhibit RNA Pol I through the formation of platinum adducts within rDNA that negatively interfere with RNA Pol I activity (Bywater et al., 2013). Furthermore, platinum adducts are also able to displace the transcription factor UBF from rRNA, thus inhibiting the formation of the pre-initiation complex at the rDNA promoter (Hamdane et al., 2015).

The uracil analogue 5-Fluorouracil, broadly used in many first-line clinical approved protocols, exerts its anticancer effect through the inhibition of thymidylate synthase (TS), an enzyme involved in nucleotide synthesis, thus impairing both rDNA and rRNA synthesis. In addition, it has been reported that metabolites derived from 5-FU are able to intercalate within rRNA leading to RNA damage and consequent nucleolar stress (Sun et al., 2007; Burger et al., 2010).

Many antibiotics belong to the anthracycline class, such as Doxorubicin and Mitoxantrone, act as DNA intercalators but also as inhibitors of Topoisomerase II (Top II), a group of enzymes that remove DNA supercoils. The formation of DNA adducts causes double strand breaks which prevent DNA replication and induce cell death. Since it has been reported that Top II promotes the formation of the pre-initiation complex at the rDNA promoter, it is not surprising that treatment of cells with these antibiotics could inhibit rDNA transcription and leading to nucleolar stress (Ferreira et al., 2020).

Actinomycin D (Act D), otherwise Dactinomycin, is a well-known antibiotic belong to the actinomycin group. This compound exhibits high anticancer activity and is used or the treatment of Wilm's tumor and several type of sarcoma. The main mechanism of action of

Act D is due to its ability to intercalate with both double and selective single stranded DNA, especially at the 3′ side of guanine residues, in the dinucleotide site GpC causing the consequent inhibition of transcription. Notably, Act D at low concentration (i.e. 5 nM) preferentially intercalates into GC-rich regions of rDNA leading to the inhibition of RNA Pol I driven transcription at the level of elongation. While, it has been reported that higher doses of Act D impairs the transcription driven by all three RNA polymerases (Burger et al., 2010).

Representative examples of plant alkaloids are Camptothecin and its analogues, Irinotecan and Topotecan, and Epipodophyllotoxins (Etoposide) that exert their potent anti-neoplastic action by poisoning Topoisomerase, enzymes that remove DNA supercoils and have long been known to associate with RNA Pol I interfering with rDNA transcription. Thus, it is not surprising that these compounds are potent disruptors of nucleolar structure with consequent induction of nucleolar stress (Ferreira et al., 2020).

Moreover, it has been reported that CDKs (Cyclin-dependent kinases) inhibitors are able to impair the nucleolar structure. In particular, Roscovitine, Olomoucine and DRB (5,6-dichlorobenzimidazone-1-β-d-ribofurano-side) specifically inhibits rRNA processing thus promoting nucleolar disintegration (Burger et al., 2010).

In the last decade, different studies have suggested nanoparticles (NPs), as drug carrier systems, could be employed to target specific cellular components in cancer cells (Russo et al., 2016[a]; Russo et al., 2016[c]; d'Angelo et al., 2018). Interestingly, SiO_2-, TiO_2- and Gold-NPs have been intensively studied for their ability to target the nucleolus in a variety of tumor cell lines. Chen et al. have indicated the uptake of SiO_2-NPs in the nucleus where they cause the formation of aberrant clusters of Topoisomerase I and other nuclear proteins leading to the inhibition of transcription and cancer cell proliferation (Chen et al., 2005). In addition, other studies have revealed that nanoconjugates composed of DNA oligonucleotides attached to TiO_2-NPs specifically localized at rDNA, thus indicating that nanocomposites specific for nucleolar target sequence could be a promising strategy for targeted anti-cancer therapy (Paunesku et al., 2007). In this scenario, more recently Kodiha et al. have been shown that the treatment with Gold-NPs induces changes to nucleolar organization and function in breast cancer cells. In particular, Gold-NPs affect rDNA transcription and alter the intracellular distribution of several nucleolar and nuclear proteins such as B23, RPA194 (RNA Polymerase I Subunit A), hsp70 (Heat shock protein 70) and O-GlcNAc-modified proteins (Kodiha et al., 2016).

Lastly, it has been reported that various small compounds exert their anticancer activity through the binding to G-quadruplex (G4) structures, which are four-stranded helical

structures that can form in DNA and RNA due to the presence of four Guanines in close proximity (Esposito et al., 2017; Esposito et al., 2018[(a)]; Virgilio et al., 2020). Typically, G4 structures are located in in functional regions of the genome including rDNA. In this context, the DNA aptamers and naphthalene diimides (NDIs) are representative examples of this new class of small compounds able to selectively bind and stabilize G4 structures leading to the inhibition of cancer cells proliferation (Pirota et al., 2019).

1.4.2 Compounds targeting nucleolar functions

A growing amount of evidence are accumulating about the multitude of cancer-related signal transduction pathways able to modulate nucleolar functions through the regulation of ribosome biogenesis. The alteration of key signaling pathways such as the oncogenic signaling mediated by c-Myc, Ras/ERK, mTOR, and Akt/PKB or tumor suppressor signaling mediated by p53, Rb, ARF, and PTEN ultimately lead to deregulation of RNA Pol I activity, which is strictly correlated to cancer initiation and progression (Ruggero, 2012). In particular, the oncogenic signalling RAS/RAF/ERK and PI3K/AKT/mTOR (mammalian target of rapamycin) control many essential components of the RNA Pol I complex as RRN3 (RNA polymerase I transcription factor), UBF (upstream binding factor), and SL1 (selective factor 1) leading to the upregulation of rRNA synthesis in cancer cells (Ruggero, 2012). In addition, it has been reported that the oncogene c-Myc is also a direct regulator of ribosome biogenesis; in fact, c-Myc positively controls the formation of the pre-initiation complex at rDNA promoter or the expression of the rDNA transcription factors UBF, SL1, TIF-1A (transcription initiation factor 1A), and POLR1B (polymerase I polypeptide B) , thus promoting the hyperactivation of rDNA transcription (Ruggero, 2012). Furthermore, it has been shown that the transcriptional activity of RNA Pol I is also induced by the cell cycle regulator pathway CDK-cyclinD/INK4/pRB/E2F through the phosphorylation of UBF. Notably, p53 signaling pathways negatively regulates RNA Pol I activity. In fact, p53 binds to SL1 and prevents the SL1/UBF association, thus interfering with the formation of the pre-initiation complex at rDNA promoter (Zhai et al., 2000). Another study have revealed that the tumor suppressor p14[ARF], a crucial regulator of p53, is also able to hinder RNA Pol I activity interfering with the formation of pre-initiation complex and inhibiting the nuclear traslocation of TTF-1 (transcription termination factor 1) (Ayrault et al., 2006). In the light of these findings, the specific inhibition of RNA Pol I activity mediated by small compounds represents a useful strategy in targeted anti-cancer therapy. The first compound described to

be able to specifically inhibit RNA Pol I activity is the small molecule fluoroquinolone derivative CX-3543. Drygin et al. have shed light on the mechanism of action of this compound demonstrating that CX-3543 disrupts nucleolin/rDNA G-quadruplex complexes in the nucleolus leading to the inhibition of RNA Pol I driven transcription and triggering apoptosis in tumor cells (Drygin et al., 2009). Subsequently, a second more selective and direct RNA Pol I transcription inhibitor (CX-5461) was developed by Cylene Pharmaceuticals that acts by preventing the binding of SL1 to the rDNA promoter (Drygin et al., 2011). Notably, it has been reported that anticancer effect of CX-5461 is specific for tumor cells and it is effective in a large panel of cancer cell lines (Drygin et al., 2011).

In addition, a recent study has demonstrated that CX-5461 binds and stabilize G-quadruplex structures inducing DNA damages (Xu et al., 2017). Since the repair of G-quadruplex associated DNA damage is directly dependent on the correct functionality of homologous recombination (HR) and non-homologous end joining (NHEJ) pathways, this compound could be a promising strategy for treatment of HR and NHEJ deficient cancers (Xu et al., 2017).

As outlined above, a large number of commonly used chemotherapeutic agents such as alkylating agents, platinum-based drugs, and anthracyclines are able to activate p53-mediated nucleolar stress pathway through the induction of DNA damages that ultimately lead to cell cycle arrest and apoptosis (Russo et al., 2017[a]). However, this therapeutic approach is not able to distinguish between tumorigenic and normal cells, thus causing adverse effects. In this light, different non-genotoxic therapeutic strategies have been developed to specifically target MDM2-p53 axis by restoring the tumor suppressor function of p53 or modulating the activity of MDM2 in cancer cells. The main therapeutic approaches can be classified accordingly to their mechanism of action into the following groups: MDM2 antagonists, inhibitors of the MDM2-p53 interaction, and MDM2 antisense targeting the MDM2 expression.

The most well studied small compounds able to inhibit MDM2-p53 interaction are Nutlins, a group of cis-imidazoline analogs, that binds to MDM2 with high affinity. In particular, Nutlins act by mimicking the alfa-helical conformation of the p53 peptide, thus disrupting the physical interaction between MDM2 and p53 (Cheok et al., 2011).

Among Nutlin derivatives, RG7112 is the first developed and optimized compound with enhanced cellular potency and pharmacokinetics. In fact, RG7112 exhibits increased MDM2-binding affinity and exerts its anti-tumor effects in a huge number of *in vitro* and *in vivo* pre-clinical cancer models and in patients with liposarcoma associated to MDM2 gene amplification (Andreeff et al., 2016).

The RG7388, also known as Idasanutlin, is the only MDM2 antagonist that has entered phase III clinical trials. This compound is able to significantly induce p53, as highlighted by the upregulation of p21 expression, thus triggering cell cycle arrest in several cancer cell lines (Skalniak et al., 2018).

Another promising therapeutic approach is the small molecule RITA (reactivation of p53 and induction of tumor cell apoptosis) identified by the National Cancer Institute in 2004 (Issaeva et al., 2004). RITA acts differently from the above described compounds by binding directly to p53 rather than MDM2, thus inhibiting p53-MDM2 interaction. In addition, it has been reported that RITA is also able to induce DNA damage signaling (Cheok et al., 2011). Interestingly, a recent study have established that the sensitivity of different colon cancer cell lines to RITA seems to be independent of p53 status and is associated to enhanced antiproliferative response to 5-FU and OHP (Wiegering et al., 2017). Moreover, Ristau et al. have indicated that RITA is able to trigger apoptosis and repress mRNA translation by promoting the phosphorylation of the alpha subunit of the eukaryotic translation initiation factor 2 (eIF2α) independently from p53; and, unexpectedly, they found that the reactivation of p53 caused by RITA treatment is strictly dependent on eIF2α phosphorylation (Ristau et al., 2019).

Overall, the reported studies suggest that understanding the molecular mechanisms by which these small molecules are able to exert their antitumor activity is essential for the development of new targeted therapeutic strategies in cancer treatment.

2. MATERIALS AND METHODS

2.1 Cell cultures, transfections and drug treatment

HCT 116$^{p53-/-}$ cells and uL3ΔHCT 116$^{p53-/-,}$ a cell line derived from HCT 116$^{p53-/-}$ cells and stably silenced for uL3 (Pagliara et al., 2016), were cultured in Dulbecco's Modified Eagle's Medium (DMEM) supplemented with 10% fetal bovine serum (FBS), 2 mM L-glutamine, penicillin-streptomycin 50 U/ml.

Drug treatments were performed by adding to cells Act D (Sigma), AdoMet (New England Biolabs) or ODNs (synthesized by research group of Prof. Aldo Galeone – Dept of Pharmacy, University of Naples Federico II). Transfection of pHA-uL3 plasmid, pGFP-uL3 plasmid, PARP-1 plasmid (Addgene, cod. 111575) and pGL2-AN containing the entire E2F-1 promoter (Addgene, cod. 20950) was performed in cells using Lipofectamin 2000 (Invitrogen) according to the manufacturer's instructions. siRNA transfections were performed using Oligofectamine Reagent (Invitrogen) according to the manufacturer's instructions.

2.2 RNA extraction and RT-qPCR

Total RNA was isolated from cells using EuroGold Trifast™ kit (Euroclone) according to the manufacturer's instructions. RNA was first retrotranscribed using SensiFAST™ cDNA Synthesis kit (Bioline) and then realtime PCR was carried out using SensiFAST SYBER® No-ROX kit. The primers are indicated in Table 1. The comparative Ct method was used to calculate the relative abundance of the mRNA and compared with that of β-actin expression (Schmittgen et al., 2008).

Table 1. Sequence of oligonucleotides used in RT-qPCR analysis.

Gene	Sequence
ATG13	Forward: 5' – GACCTTCTATCGGGAGTTTCAG – 3' Reverse: 5' – GGGTTTCCACAAAGGCATCAAAC – 3'
ATG101	Forward: 5' – CCCAGGATGTTGACTGTGAC – 3' Reverse: 5' – ACATCTGCCCCAGCCCATCG – 3'
CDK1	Forward: 5' – CATGGCTACCACTTGACCTGT – 3' Reverse: 5' – AAGCCGGGATCTACCATACC – 3'
CycA	Forward: 5' – TTCATTTAGCACTCTACACAGTCACGG – 3' Reverse: 5' – TTGAGGTAGGTCTGGTGAAGGTCC – 3'
CycB	Forward: 5' – CAGTCAGACCAAAATACCTACTGGGT – 3' Reverse: 5' – ACACCAACCAGCTGCAGCATCTTCTT – 3'
CycD1	Forward: 5' – ACGGCCGAGAAGCTGTGCATC – 3' Reverse: 5' – CCTCCGCCTCTGGCATTTTGGAG– 3'

CycE1	Forward: 5' – TGAGCCGAGCGGTAGCTGGT – 3'
	Reverse: 5' – GGGCTGGGGCTGCTGCTTAG – 3'
Bax	Forward: 5' – CCCGAGAGGTCTTTTCCGAG – 3'
	Reverse: 5' – CCAGCCCATGATGGTTCTGAT – 3'
B23	Forward: 5' – AGAAAAAGCGCCAGTGAAGA – 3'
	Reverse: 5' – TGGTGTT GATGATTGGTTTTGA – 3'
β-actin	Forward: 5' – CCAACCGCGAGAAGATGA – 3'
	Reverse: 5' – CCAGAGGCGTACAGGGATAG – 3'
Bcl-2	Forward: 5' – ATGTGTGTGGAGAGCGTCAACC – 3'
	Reverse: 5' – GCATCCCAGCCTCCGTTATC – 3'
E2F1	Forward: 5' – GTGTAGGACGGTGAGAGCAC – 3'
	Reverse: 5' – TCAAGGGTAGAGGGAGTTGG – 3'
MCM6	Forward: 5' – ATCCTCTTGCCAAGGATTT – 3'
	Reverse: 5' – GAAAAGTTCCGCTCACAAGC – 3'
MCM7	Forward: 5' – CACGGAGTCTCTCAGCACAG – 3'
	Reverse: 5' – AACATCTGTCTGATGGGGGA – 3'
Rb	Forward: 5' – ATTCTGCATTGGTGCTAAAAG – 3'
	Reverse: 5' – CTCCTGTTCTGACCTCGC – 3'
p21	Forward: 5' – CCTCAAATCGTCCAGCGACCTT – 3'
	Reverse: 5' – CATTGTGGGAGGAGCTGTGAAA – 3'
TFEB	Forward: 5' – CAAGGCCAATGACCTGGAC – 3'
	Reverse: 5' – AGCTCCCTGGACTTTTGCAG – 3'
ULK1	Forward: 5' – CTGGTCCTCTTGCTTCCGTC – 3'
	Reverse: 5' – ACACCAGCCCAACAATTC – 3'
uL3	Forward: 5' – CAAAGGCTACAAAGGGGT – 3'
	Reverse: 5' – CTCAGTGCGGTGATGGTAG – 3'
uL5	Forward: 5' – GGGATCCAGGAACACATCGA – 3'
	Reverse: 5' – AGAAGTCCAGGCCGTAGATACCA – 3'
uL11	Forward: 5' – AGTCGTATACCTGAGGTGCACCGGA – 3'
	Reverse: 5' – GCCATCAACATTACAGCCCACTGAC – 3'
uL18	Forward: 5' – TGGAACCGTCCCAAAATGTC – 3'
	Reverse: 5' – GAGGAAGCTTGCCTTCTTTTGAG – 3'
uS12	Forward: 5' – CGAGACCAGAAGTGGCATGA – 3'
	Reverse: 5' – GCATGAGAAGCACCTCCAAAAG – 3'
47S	Forward: 5' – GCTGACACGCTGTCCTCTG – 3'
	Reverse: 5' – ACGCGCGAGAGAACAGCAG – 3'
45S	Forward: 5' – GCCTTCTCTAGCGATCTGAGAG – 3'
	Reverse: 5' – CCATAACGGAGGCAGAGACA – 3'
36S	Forward: 5' – GCGGAGGTTTAAAGACCC – 3'
	Reverse: 5' – CCAGACGAGACAGCAAAC – 3'
32S	Forward: 5' – GTCAGCGGAGGAGAAGAA – 3'
	Reverse: 5' – CTCGATCAGAAGGACTTGG – 3'
30S	Forward: 5' – CCTCTGACGCGGCAGACAGC – 3'
	Reverse: 5' – CTCCAGGAGCACCGCAAGGG – 3'
18S precursors	Forward: 5' – GTTCAAAGCAGGCCCGAGCC – 3'
	Reverse: 5' – AGCGGCGCAATACGAATGCC – 3'
28S	Forward: 5' – CAGGGGAATCCGACTGTTTA – 3'
	Reverse: 5' – ATGACGAGGCATTTGGCTAC – 3'
18S	Forward: 5' – AAACGGCTACCACATCCAAG – 3'
	Reverse: 5' – CCTCCAATGGATCCTCGTTA – 3'
5.8S	Forward: 5' – CTCTTAGCGGTGGATCACTC – 3'
	Reverse: 5' – GACGCTCAGACAGGCGTAG – 3'

2.3 Nuclear Run-On

Nuclear run-on was performed following the protocol previously reported by Juli et al., 2016. Nuclei from approximately from 10^8 cells were incubated in a buffer containing 10 mM Tris, pH 7.5; 10 mM MgCl2; 300 mM KCl; 0.5 mM each of ATP, CTP, and GTP; 15 μL [α^{-32}P]UTP [3000 mCi/mL]), and incubated at 30 °C for 30 min. Labeled RNA was extracted by using Trizol reagent (Invitrogen, Life Technologies, Carlsbad, CA, USA) according to the manufacturer's specifications. Plasmid DNAs were immobilized on a GeneScreen Plus membrane using a dot-blot apparatus. pCDNA3 plasmid was used as control. pCDNA3 was spotted on membrane and incubated with ^{32}P-labeled RNA from untreated HCT 116$^{p53-/-}$, HCT 116$^{p53-/-}$ cells transfected with 1μg of pHA-uL3 and HCT 116$^{p53-/-}$ cells treated with Act D. Observed signals for pCDNA3 in all samples represent the background signal. Intensity of signals was normalized on pcDNA3 signal. Hybridization was carried out as indicated in GeneScreen Plus manual.

2.4 Fluorescence microscopy, image processing and fluorescence signal quantifications

HCT 116$^{p53-/-}$ cells were plated on coverslips at a density of 2×10^4 cells per well into 35 mm tissue culture plates and treated with 5 nM Act D. 18 h later, cells were fixed with 3,7% paraformaldehyde for 20 min. After washing, coverslips were mounted with PBS 1X-Glicerol (1:1) and stained with 4,6-diamidino-2-phenylindole (DAPI) (Vector Laboratories, CA, USA) to visualize the nuclei. Images have been acquired by using the Zeiss Cell Observer system composed by a motorized inverted microscope (Axiovert 200M) and a digital camera (Axiocam H/R). The fluorescence of was measured with Zeiss acquisition software (Axiovision 4.8.1). Fluorescence images obtained from immunofluorescence were processed in ImageJ software (version 1.49 v with 64 bit Java Platform; NIH) and exported as TIFF mode files in red/green/blue (RGB) channels. To normalize individual cell differences, in general 30 cells were examined for quantification of average fluorescent intensity. The absolute fluorescence intensity and line plots were obtained from bit channel files before the images were transferred to RGB channel files. The relative fluorescence intensity (RFI) was calculated as RFI = Ncl/Npl where Ncl was the absolute intensity in the nucleolus area, Npl was the average the average intensity in nucleoplasmatic region.

2.5 Immunofluorescence

HCT 116$^{p53-/-}$ and uL3ΔHCT 116$^{p53-/-}$ cells seeded on slides were fixed for 10 min with Methanol (Sigma-Aldrich, St. Louis, MO, USA), followed by incubation with blocking–

permeabilization solution: 0.5% BSA, 0.1% saponin, and NH$_4$Cl 50 mmol/L in phosphate buffered saline for 30 min. Primary antibodies anti-LC3B (Novus Biologicals, Centennial, CO, USA) and anti-LAMP1 (Developmental Studies Hybridoma Bank) were diluted in blocking–permeabilization solution and added to the cells for 1 h. Then, secondary antibodies were incubated for 45 min. Lastly, cells were counterstained with Hoechst (Thermo Fisher Scientific, Uppsala, Sweden). Samples were examined under a confocal microscope (Zeiss LSM 700; Carl Zeiss AG, Jena, Germany) equipped with 40x and 63× 1.4 NA oil objective. Colocalization between specific markers was quantified using Zeiss Zen 2012 software.

2.6 Nucleolar isolation

HCT 116$^{p53-/-}$ cells plated in 100 mm petri dishes were washed twice with 20 mL cold solution I (0,5 M sucrose, 3 mM MgCl$_2$, 1X EDTA-free Roche protease inhibitor cocktail). Collected cells were sonicated on ice at 50% power, 10 s on, 10 s off, for five cycles. The sonicated cell suspension was layered over 1,4 mL precooled solution II (1 M sucrose, 3 mM MgCl$_2$, 1X EDTA-free Roche protease inhibitor cocktail) and centrifuged at 1800 × g for 10 min at 4 °C. The resulting pellet contained the isolated nucleoli. The samples were resuspended in 200 μl of 8 M urea and incubated at 56 °C for 40 min. Then, each sample was analyzed by western blotting.

2.7 Western blotting

Total proteins were obtained using RIPA lysis buffer and the protein concentration was measured by the Bradford method (Bio-Rad, Milan, Italy). Equal amounts of protein (40 μg/sample) were mixed with gel loading buffer (50 mm Tris/10% SDS/10% glycerol 2-mercaptoethanol/2 mg bromophenol in a final volume of 1 mL) in a ratio of 1:1 and boiled for 3 min. Each sample were analysed by electrophoresis through a 12% discontinuous polyacrylamide minigel. Proteins were transferred onto PVDF membrane, according to the manufacturer's instructions (Bio-Rad, Segrate, Milano, Italy).

The membranes were challenged with anti-E2F1 (Elabscience®, Houston, TX, USA), anti-uL3 (Primm, Milan, Italy), anti-CycD1, anti-pRbSer612, anti-CycE1, anti-CycA2, anti-CycB1, anti-Atg7, anti-procaspase 3, anti-procaspase 9, anti-procaspase 8, anti-PARP-1, anti-uL5, anti-uL18, anti-LC3BI/II, anti-p62, anti-GAPDH (Cell Signaling Technology, Danvers, MA, USA), anti-B23, anti-p21, anti-Bax, anti-Bcl2, anti-Bad, anti-α-tubulin, anti-β-actin, anti-nucleolin, anti-vinculin, anti-HA (Santa Cruz, Dallas, TX, USA), anti-POLR1B (Abcam, Cambridge, UK). Proteins were visualized with enhanced chemiluminescence detection

reagent according to the manufacturer's instructions (Elabscience®, Houston, TX, USA) or exposed to X-ray film. All films were scanned by using Image J software (National Institutes of Health, Bethesda, MD, USA).

2.8 Immunoprecipitation

HCT 116$^{p53-/-}$ cells were solubilized in lysis buffer and 1mg of protein lysate was incubated with 30 µl of protein A/G agarose beads coated with 5 µg of anti-uL3 (Primm, Milan, Italy) at 4 °C for 12 h. The beads were washed and boiled in the SDS sample buffer. The eluted proteins were loaded on 12% SDS-PAGE and detected by western blotting.

2.9 Luciferase assays

Luciferase assays were performed with the Dual-Glo Luciferase assay system (Promega, Milan, Italy) following manufacturer's instructions. Samples were read with Turner Luminometer and expressed as relative luciferase, i.e., R_T/R_C, where R_T and R_C are (Firefly luciferase)/(Renilla luciferase).

2.10 Protein half-life analysis

HCT 116$^{p53-/-}$ cells and uL3ΔHCT 116$^{p53-/-}$ cells were treated with Cycloheximide (CHX, Sigma-Aldrich, St. Louis, MO, USA) 0,1 mg/ml for different times, and subsequently harvested and lysed using RIPA lysis buffer (50 mM Tris-HCl pH 7.4, 1% NP40, 0,5% Na-deoxycolate, 150 mM NaCl, 1 mM Na3VO4, 1 mM NaF, 1X EDTA-free Roche protease inhibitor cocktail). Protein extracts from samples were analyzed by western blotting.

2.11 Wound healing assay

Cell motility was assessed using a wound healing assay. HCT 116$^{p53-/-}$ cells and uL3ΔHCT 116$^{p53-/-}$ cells (1 × 10^6 per well) were seeded into 35 mm tissue culture plates and, after 24 h, the confluent monolayer cells were then carefully wounded using a sterilized pipette tip. Monolayer cells were photographed at 0, 6, 24 and 30 h with an objective 10X. Quantitative analysis of wound assay was performed by measuring the gap area. The gap area was defined by using ImageJ Software (National Institute of Health, USA). Data is expressed as the fold-decrease of area respect to controls set as 100%. Bars represent the mean of triplicate experiments; error bars represent the standard deviation.

2.12 Cell cycle analysis by flow cytometry

HCT 116$^{p53-/-}$ cells and uL3ΔHCT 116$^{p53-/-}$ cells were seeded into 35 mm tissue culture plates at a confluency about 50-60% (5×10^5 cells). Then, cells were starved overnight treated with CQ (25 μM) or transiently transfected with pHA-uL3 (1 μg) for 24 h. After treatment, the cells were harvested and centrifuged at 400 g for 5 min, washed once with cold PBS and resuspended and fixed by adding 0.5 mL ice-cold 70% ethanol dropwise. Then, the cells were incubated on ice overnight. The cells were spun down and washed twice with PBS (Dulbecco's Phosphate-Buffered Saline, Sigma-Aldrich, St. Louis, MO, USA). They were resuspended in a 500 μL of PBS and incubated with 50 μg/mL PI (Propidium Iodide, Sigma-Aldrich, St. Louis, MO, USA) for 30 min protected from light. Cell cycle distribution was analyzed using BD Accuri C6 Plus flow cytometer (BD Biosciences, San Jose, CA, USA).

2.13 Cell death assay

HCT 116$^{p53-/-}$ and uL3ΔHCT 116$^{p53-/-}$ cells (5×10^5) were seeded in 6-well plate per well, starved overnight and treated with CQ (25 μM) or transiently transfected with pHA-uL3 (1 μg) for 24 h. The cells were washed with PBS, harvested by trypsinization and washed twice with PBS. Then, they were stained with Propidium Iodide (PI) and Annexin V Alexa Fluor® 488 (or Annexin V-FITC). Specifically, cells were re-suspended with 1× Binding Buffer at a density of 1×10^6 cells/mL. Then, PI (10 μL) and Annexin V Alexa Fluor® 488/ Annexin V-FITC (5 μL) was added to cell suspension (100 μL) before further incubation for 20 min at RT in the dark. Stained cells were diluted with 1× binding buffer and the percentage of Annexin V+/PI− (early apoptosis), Annexin V$^+$/PI$^+$ (late apoptosis), and Annexin V$^-$/PI$^+$ (necrosis) cells was analyzed by BD AccuriTM C6 flow cytometer (BD Biosciences, San Jose, CA, USA). The data are represented as rate of total apoptotic cells with both early and late apoptotic rate indicated. Analysis was carried out by triplicate determination on at least three separate experiments.

2.14 Cell viability assay

HCT 116$^{p53-/-}$ cells and uL3ΔHCT 116$^{p53-/-}$cells were plated in serum-containing media in 96-well plates at the proper density. After 24 h incubation, the cells were treated with increasing concentrations of AdoMet (from 72 to 1000 μM) or with different ODNs at a final concentration of 10 and 50 μM from 24h to 72 h. Then, cell viability was assessed by adding MTT assay. The absorbance values of the solution in each well were detected at 570 nm using a Bio-Rad IMark microplate reader (Bio-Rad Laboratories, Milan, Italy). All MTT

experiments were performed in triplicate. Cell viability was expressed as the percentage of absorbance values in treated samples with respect to that of the control (100%). For the treatments, AdoMet plus 5-FU, uL3ΔHCT 116$^{p53-/-}$ cells were seeded at proper density in 96-multiwell plates. After 24 h incubation, the cells were treated with different concentrations of AdoMet (from 125 to 1000 µM) and 5-FU (12.5 to 100 µM), alone or in combination, for 72 h and cell viability was detected by the MTT assay.

2.15 Determination of ROS by DCFH-DA Assay

Colon cancer cells were seeded in 6-well plates at the proper density, and after 24 h of incubation, the cells were treated with AdoMet 500 µM for 72 h. The positive control was represented by the cells treated with menadione at the final concentration of 100 µM for 1 h at 37 °C. After treatment, cells were stained with 10 µM DCFH-DA (2′,7′-dichlorofluorescein Diacetate) for 30 min at 37 °C in the dark. DCFH-DA can freely pass the cell membrane where it is trapped after being hydrolyzed by intracellular esterases in a non-fluorescent compound (DCFH). Then, DCFH can be oxidized to the fluorescent DCF by reacting with intracellular ROS. Following incubation, cells were washed twice with PBS, trypsinized, resuspended in PBS, and immediately analyzed with a BD Accuri™ C6 flow cytometer (BD Biosciences). For each sample, 20,000 events were recorded. Analysis was carried out by triplicate determination on at least three separate experiments.

2.16 LysoTracker-Red staining

HCT 116$^{p53-/-}$ and uL3ΔHCT 116$^{p53-/-}$ cells were seeded in a 6-well plate and treated with 500 µM AdoMet for 48 h, using CQ as the positive control. LTR was added to each well for 20 min at 37 °C at a final concentration of 0.1 µM in medium. The cells were then washed with PBS and observed by fluorescence microscopy. The fluorescence intensity of the cells was then analyzed by flow cytometry. Briefly, the cells were detached by incubation with EDTA-trypsin, washed twice with PBS, and collected by centrifugation. For the quantitative evaluation of LTR, FlowJo software was used to calculate the median fluorescence intensities (MFI) by the formula (MFI-treated/MFI-control), where MFI-treated is the fluorescence intensity of cells treated with the various compounds and MFI-control is the fluorescence intensity of the untreated cells. For each sample, 20,000 events were acquired. Analysis was carried out by triplicate determination on at least three separate experiments.

2.17 Statistical analysis

Experiments were performed at least three times with replicate samples. Data are expressed as mean ± standard deviation (SD). p-values were determined using unpaired two-tailed Student's t-test. * $p < 0.05$ was considered significant, ** $p < 0.01$, *** $p < 0.001$ were considered highly significant.

For image quantification, GraphPad Prism software (version 8.0) was used to analyse and plot all data. Statistical analysis was performed with two-tailed unpaired t-test with 95% confidence interval. In box and whisker plots, the box showed the top and bottom quartiles (25–75%) with a line at the median and the whiskers showed the minimum to the maximum values of all data. p -values indicated the significances of differences.

3. RESULTS

SECTION I

Role of uL3 in regulating cell cycle progression in response to nucleolar stress

The cell cycle is a tightly regulated process controlled by a complex series of multiple and different pathways. In tumor cells, as a consequence of genetic mutations, this process fails properly function leading to uncontrolled cell proliferation (Evan et al., 2001).

Beyond its canonical role in ribosome biogenesis, the nucleolus is strictly interconnected to cell cycle regulation. In fact, the nucleolus operates as a first-responder to stress stimuli that impair cell growth. This condition, known as nucleolar stress, is able to activate p53-dependent or p53-independent stress response signaling pathways leading to cell cycle arrest and/or apoptosis (Russo et al., 2017[a]).

In condition of nucleolar stress, some RPs are release from the nucleolus and in the nucleus are able to modulate important cell cycle regulators as Cyclins, cyclin-dependent kinases (CDKs), cyclin-dependent kinase inhibitors (CKIs) and the E2 factor (E2F) family of transcription factor (Molavi et al., 2019). To cite, eL6 (RPL6) and uS15 (RPS13) could promote G1/S transition of gastric cancer cells increasing Cyclin E expression and inhibiting p27^{Kip1} mRNA expression, respectively (Gou et al., 2010; Guo et al., 2011); uS4 (RPS9) induces G2/M phase transition upregulating CDK1 expression (Iizumi et al., 2013). In contrast, reduced intracellular levels of uL10 (RPLP0) are associated to the decreased expression of Cyclin D, Cyclin E, CDK2, and CDK4 leading to the inhibition of G1/S transition (Wang et al., 2019). Results from our group have indicated that the enforced expression of uL3 protein is associated to the upregulation of p21, a main negative cell cycle regulator. In particular, uL3 in a complex with Sp1 and NPM is able to positively transactivate p21 promoter leading to a dual effect: cell cycle arrest in G1 phase or apoptosis (Russo et al., 2013).

Accordingly to this, the aim of this study is to better clarify the mechanism by which uL3 contributes to cell cycle progression upon drug induced nucleolar stress in colon cancer cells devoid of p53.

3.1 Alteration of uL3 intracellular levels impairs in rRNA processing

Starting from the notion that the deregulated expression of some RPs is able to activate nucleolar stress we wondered whether uL3 might *per se* elicit nucleolar stress pathway through impairing of ribosomal gene processing as already demonstrated for other RPs (Russo et al, 2017[a]). To this aim, we analyzed the production of rRNA precursors and rRNA mature transcripts (Figure 6A) upon alteration of uL3 expression levels in colon cancer cells (HCT 116[p53−/−]). Total RNA was extracted from HCT 116[p53−/−] cells transiently transfected with pHA-uL3 and uL3ΔHCT 116[p53−/−], a cell subline stably silenced of uL3 (Pagliara et al., 2016); then, the relative abundance of intermediates and mature rRNA transcripts was assessed by RT-qPCR with specific primers (Table 1). Overexpression of uL3 in HCT 116[p53−/−] cells was associated to a reduction of about 60% of the 47S rRNA precursor while in condition of uL3 silencing the production of this transcript was significantly induced (Figure 6B). To better understand the role of uL3 in pre-rRNA processing we analyzed the level of other rRNA intermediates. As shown in Figure 6A, the initial cleavage of the 47S rRNA precursor at sites A' in the 5′-ETS and 02 in the 3′-ETS led to the generation of 45S rRNA precursor (Aubert et al., 2018). Our results indicated that the enforced expression of uL3 in HCT 116[p53−/−] cells caused the accumulation of 45S rRNA precursor (Figure 6B). This transcript is further processed either by cleavage of the 5′ETS or by elimination of the ITS1 at site 2 to generate mature rRNAs (Figure 6A). Of note, the upregulation of uL3 strongly induce the accumulation of 30S rRNA precursor which was associated to increased production of its corresponding mature transcript, 18S rRNA. In this condition, the production of other two mature rRNAs were also affected; in particular, 28S rRNA was increased while 5,8S rRNA was reduced (Figure 6B).

In condition of uL3 silencing we also observed an alteration in rRNA processing. Of interest, we noticed a strong increase of 36S rRNA precursor. This transcript is typically expressed at low levels in normal cells; hence, the presence of 36S rRNA precursor is probably due to the inhibition of processing at site 2 within ITS1. The enrichment of 36S rRNA precursor may not influence the following maturation steps that lead to mature 5,8S and 28S rRNAs (O'Donohue et al., 2010). Indeed, in cells stably depleted for uL3 we observed only a slight increase of these transcripts compared with control, HCT 116[p53−/−] cells (Figure 6B).

These data clearly demonstrate that the alteration in uL3 expression levels plays a crucial role in rRNA processing.
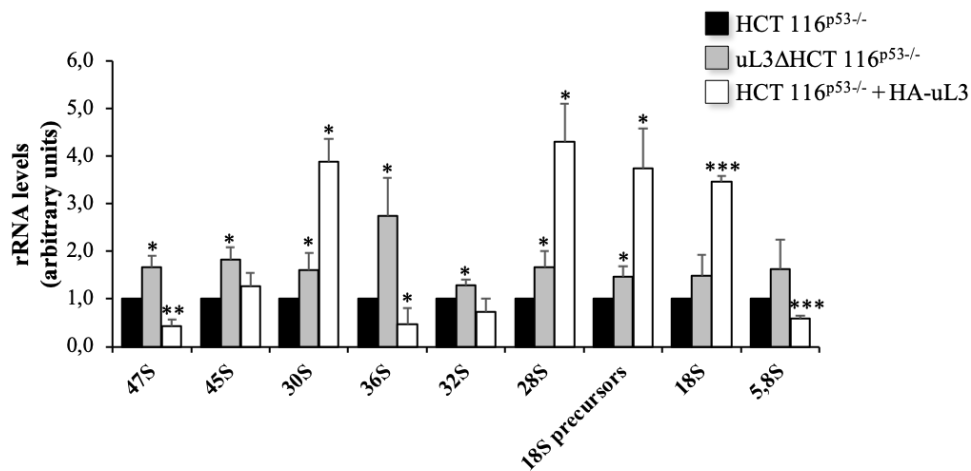
A
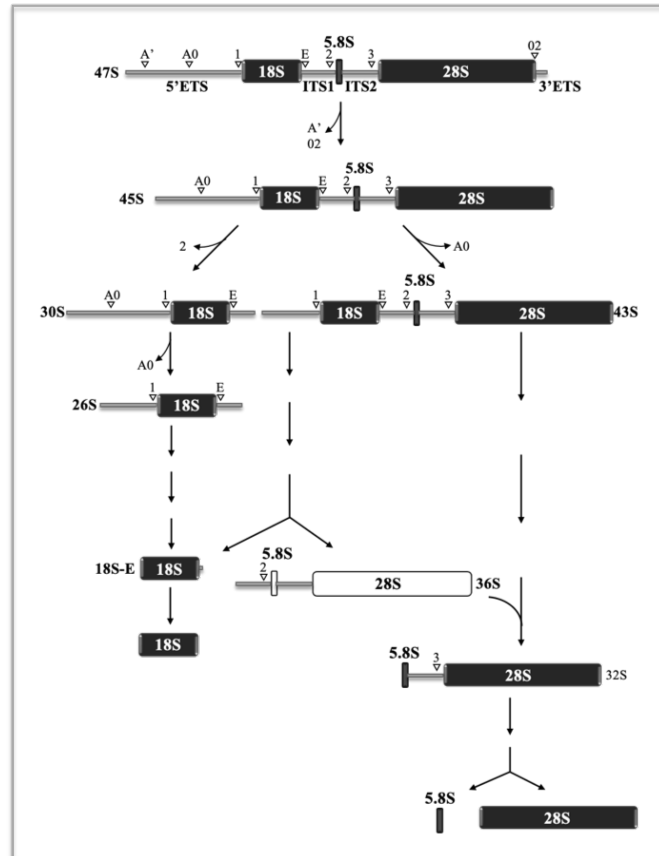
B

Figure 6. Alteration of expression levels of uL3 impairs rRNA processing. (A) Schematic representation of rRNA maturation process. Cleavage sites are indicated with white arrows. Within the nucleolus, ribosomal genes are transcribed by RNA Pol I to produce the 47S rRNA precursor, a single transcript that is then cleaved and processed to generate the mature 28S, 18S and 5.8S rRNAs. In the 47S rRNA precursor, the mature rRNAs are flanked by non-coding spacer sequences, which include the 5′ and 3′ external transcribed spacers (ETS) and internal transcribed spacers (ITS) 1 and 2. These transcribed spacers contain several cleavage sites and are gradually eliminated by the sequential action of endo- and exo-ribonucleases. (B) Total RNA from HCT 116$^{p53-/-}$ cells transfected or not with 1 μg of pHA-uL3 and uL3ΔHCT 116$^{p53-/-}$ cells was subjected to RT-qPCR with primers specific for intermediates and mature rRNAs (Table 1). Quantification of signals is shown. Bars represent the

mean of triplicate experiments; error bars represent the standard deviation. Untreated cells was set at 1. * $p < 0.05$, ** $p < 0.01$, *** $p < 0.001$ vs. HCT 116$^{p53-/-}$ cells set at 1.

In order to investigate whether the observed decrease of 47S pre-rRNA in condition of uL3 overexpression was due to the impairment in rRNA synthesis or to the enhancement of 47S pre-rRNA turnover, we firstly analyzed the rate of 47S pre-rRNA degradation in cells expressing normal levels of uL3 or stably silenced for uL3. To this aim, HCT 116$^{p53-/-}$ and uL3ΔHCT 116$^{p53-/-}$ cells were treated with Act D for 10, 30 and 60 min to block RNA Pol I-driven transcription. Then, total RNA was extracted from cell lysates and analyzed by RT-qPCR with specific primers for 47S pre-rRNA (Table 1). Analysis of rRNA amounts showed a decrease of 47S pre-rRNA levels of almost 10, 40 and 70% in both cell lines after 10, 30 and 60 min of treatment with Act D, respectively (Figure 7A). This result clearly indicated that the alteration of uL3 expression levels did not affect the rate of 47S pre-rRNA degradation.

In light of this result, we supposed that the observed reduction of 47S pre-rRNA levels in cells overexpressing uL3 might be due to the inhibition of RNA Pol I transcription. Thus, we performed a nuclear run-on assay to evaluate the rate of RNA Pol I-driven transcription initiation in condition of overexpression of uL3. As shown in Figure 7B, RNA Pol I mediated transcription activity was strongly reduced in cells overexpressing uL3. Furthermore, we analyzed the expression levels of RNA Pol I in HCT 116$^{p53-/-}$ overexpressing uL3 or treated with Act D. As shown in Figure 7C, RNA Pol I level did not changed significantly either in condition of uL3 over-expression then in condition of Act D treatment.

Overall, our results demonstrate that higher expression levels of uL3 are associated to the inhibition of RNA Pol I-driven transcription with consequent alteration in rRNA processing. This condition lead to the activation of uL3 mediated nucleolar stress response.
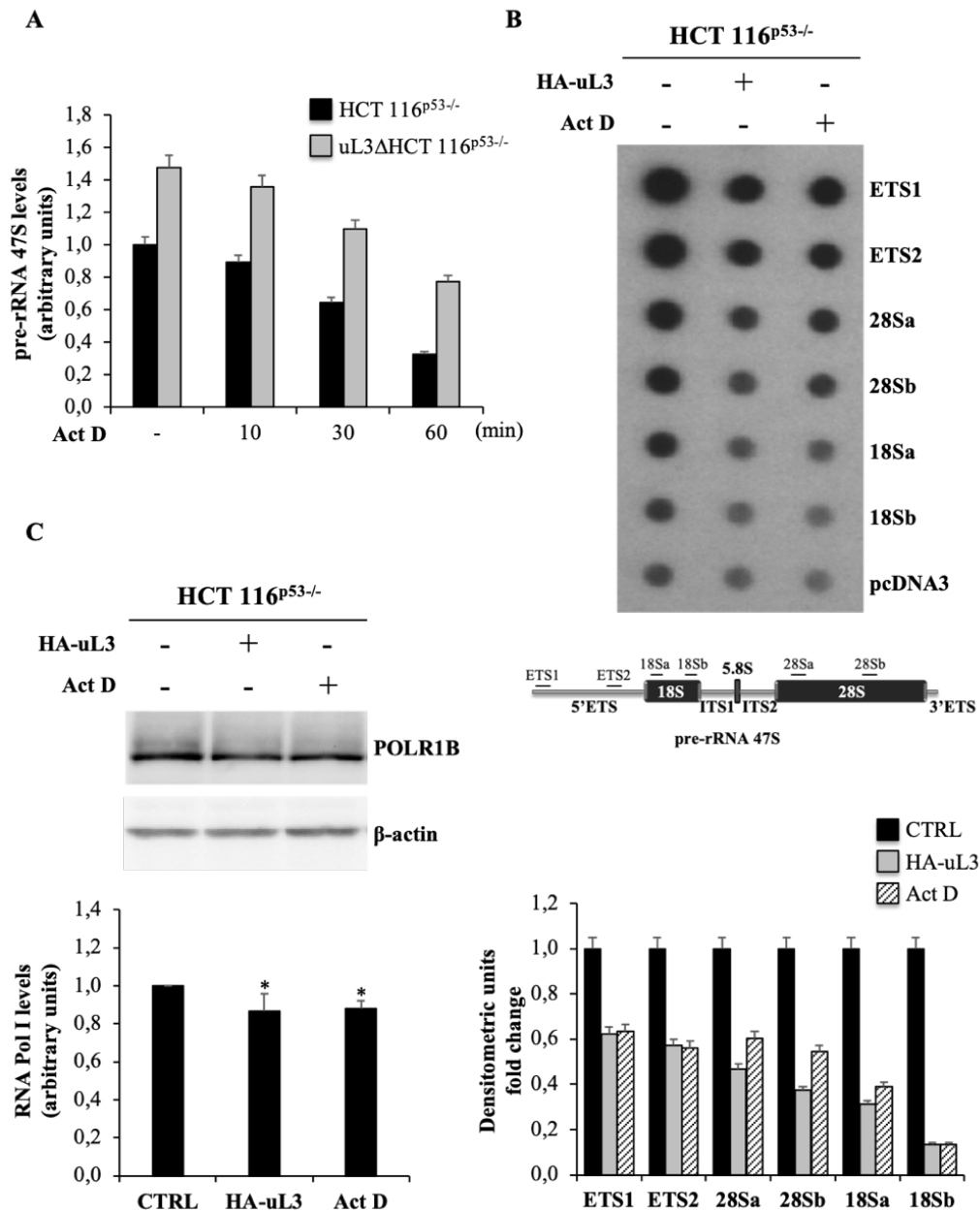
Figure 7. uL3 status affects 47S pre-rRNA synthesis and stability. (A) Total RNA from HCT 116[p53−/−] and uL3ΔHCT 116[p53−/−] cells, treated with Act D 5 nM for 0, 10, 30 and 60 min was subjected to RT-qPCR with primers specific for 5′ETS region of 47S pre-rRNA and β-actin mRNA (Table 1). Quantification of signals is shown. Bars represent the mean of triplicate experiments; error bars represent the standard deviation. (B) Nuclear run-on assay. 20 μg of plasmid DNA including sequences of two regions of 5′ETS, two regions of 28S, two regions of 18S and plasmid pcDNA3 were spotted on membrane and incubated with ^{32}P-labeled RNA from untreated HCT 116[p53−/−], HCT 116[p53−/−] cells transfected with 1 μg pHA-uL3 and HCT 116[p53−/−] cells treated with Act D. The average of two signals normalized for pHA-uL3 is reported in the bar graph in the lower panel. A schematic diagram of 47S pre-rRNA indicating the regions used in nuclear run-on assay is shown in the lower panel. (C) Total protein extracts from HCT 116[p53−/−] cells untransfected or transfected with 1μg pHA-uL3 and HCT 116[p53−/−] cells treated with Act D were analyzed by Western blot with the indicated antibodies. Full-length blots are shown in Figure S6. Quantification of signals is shown. Bars represent the mean of triplicate experiments; error bars represent the standard deviation. * p < 0.05 vs. HCT 116[p53−/−] cells set at 1.

3.2 uL3 localizes in the nucleoplasm upon Act D induced nucleolar stress

Previous data from our group have demonstrated that in condition of drug-induced nucleolar stress, uL3 protein can be found in the cells mainly as ribosome free form not associate to the ribosome (Esposito et al., 2014; Russo et al., 2016[b]). In light of this, we plan to evaluate the intracellular localization of ribosome-free uL3 in this experimental condition. To this aim, HCT 116$^{p53-/-}$ cells were transiently transfected with a plasmid expressing uL3 fused to GFP (Green Fluorescent Protein) and treated with 5 nM of Act D for 18 h. As expected, in untreated cells uL3 protein co-localizes in the nucleolus with Nucleolin, a well known marker of the nucleolus, according to its role as ribosome component (Figure 8C). Of interest, in Act D treated cells, uL3 protein re-distributes mainly in the nucleoplasm (Figure 8A,B).

Furthermore, as shown in Figure 8D, upon Act D treatment we observed also a decrease of pre-rRNA 47S levels, confirming the inhibition of RNA Pol I transcription, associated to an increase of uL3 mRNA levels. In light of this result, we cannot exclude that the re-localization of uL3 in the nucleoplasm upon Act D treatment might be due at least in part to an induction of uL3 expression.

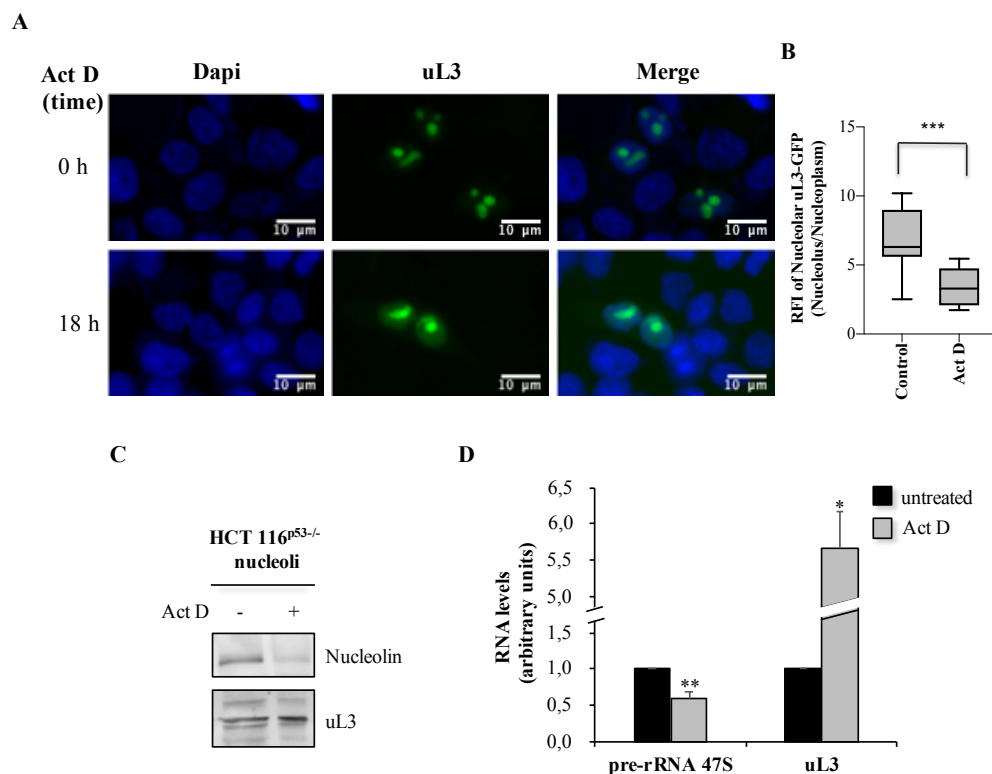**Figure 8.** uL3 localizes in the nucleoplasm upon Act D exposure. (A) Representative fluorescent microscopy images of HCT 116$^{p53-/-}$ cells transiently transfected with pGFP-uL3 and treated with Act D 5 nM for 18 h. DAPI is used as a nuclear stain and shown in blue; GFP-uL3 dependent fluorescence is shown in green. Scale bar: 10 μm. (B) Quantification of signal was shown. Nucleolar/nucleoplasmic

RFI ratio of uL3-GFP (n = 31) were displayed. Mean ± s.e.m. Unpaired t-test. ***P < 0.001. (C) HCT 116$^{p53-/-}$ cells were treated with 5nM Act D. 18 h later, cells were subjected to fractionation to isolate the nucleoli. Protein extracts from the samples were analyzed by western blotting with antibodies against uL3 and Nucleolin as marker of nucleolar fraction. (D) RT-qPCR of total RNA extracted from HCT 116$^{p53-/-}$ cells treated with Act D 5 nM for 18 h with primers specific for uL3 and 47 S pre-rRNA (Table 1). Bars represent the mean of triplicate experiments; error bars represent the standard deviation. *p < 0.05; **p < 0.01 vs. untreated cells set at 1.

3.3 uL3 status affects the expression profile of cell cycle and cell proliferation related genes

Starting from the notion that in condition of nucleolar stress uL3 localized mainly in the nucleoplasm where it can exert its extra-ribosomal function, we planned experiments to investigate the potential role of uL3 in regulating cell cycle progression. Firstly, we analyzed the expression levels of cell cycle-related genes upon Act D induced nucleolar stress. To this aim, HCT 116$^{p53-/-}$ and uL3ΔHCT 116$^{p53-/-}$ cells were treated with Act D 5 nM for 18 h. Then, total RNA extracted from cell lysates was analyzed by RT-qPCR with specific primers for the expression of cell cycle checkpoint proteins as Cyclin D1, Cyclin E1, Cyclin A and Cyclin B (Table 1). As shown in Figure 9A, Act D treatment in HCT 116$^{p53-/-}$ cells caused a strong reduction of Cyclin D1 associated to a lower reduction also in Cyclin E1; whereas, in this condition, the expression levels of Cyclin A and Cyclin B did not changed significantly indicating that these protein were not affect by Act D treatment. Published evidence indicated that the down-regulation of Cyclin D1 was associated with enhanced sensitivity of cancer cells to drug-induced apoptosis (Kothari et al., 2012); based on this, we analyzed the expression levels of pro-apoptotic protein Bax (Bcl-2-associated X protein) and anti-apoptotic Bcl-2 (B-cell lymphoma 2) by RT-qPCR. As expected, upon Act D induced nucleolar stress we observed a strong increase of Bax associated to a decrease of Bcl-2 in HCT 116$^{p53-/-}$ cells (Figure 9C).

Next, we investigated the expression levels of other proteins involved in cell cycle regulation. It is well known that the inactivation of the retinoblastoma protein (Rb) family and the consequent activation of transcription factor E2F1 is essential for G1 to the S phase transition (Bertoli et al., 2013). In particular, E2F1 controls the expression of many proteins including Cyclin D1 and MCM2-7, and constitutive activation of E2F1 is associated to G1 checkpoint activation and apoptosis preventing inappropriate re-initiation of DNA synthesis (Poppy Roworth et al., 2015).

Our data demonstrated that in HCT 116$^{p53-/-}$ cells, Act D treatment did not alter Rb expression but led to a significant decrease of E2F1 levels associated to a reduction of MCM6-7 levels (Figure 9C). These results strongly indicated a decrease in DNA synthesis upon Act D treatment.

To verify whether the observed changes in cell cycle-related gene expression could be correlated to uL3 status, we analyzed the expression profiles of tested genes in uL3 deleted cells. For this purpose, uL3ΔHCT 116$^{p53-/-}$ cells were treated with Act D for 18 h and total RNA extracted was analyzed with the same primers (Table 1). It is noteworthy that when uL3 expression was switched off, Act D treatment caused an increase of Cyclin D1 and E2F1 expression levels (Figure 9B,D). As in HCT 116$^{p53-/-}$ cells, the expression levels of other cyclins did not change significantly (Figure 9B). Moreover, in condition of uL3 silencing Act D treatment did not affect MCM6-7 expression and caused a strong increase of Bcl-2 expression (Figure 9C). These results clearly indicated that Act D failed to induce apoptosis in uL3 deleted cells.

All together our data suggest that Cyclin D1 and E2F1 play a crucial role in uL3-mediated nucleolar stress response in colon cancer cells devoid of p53.
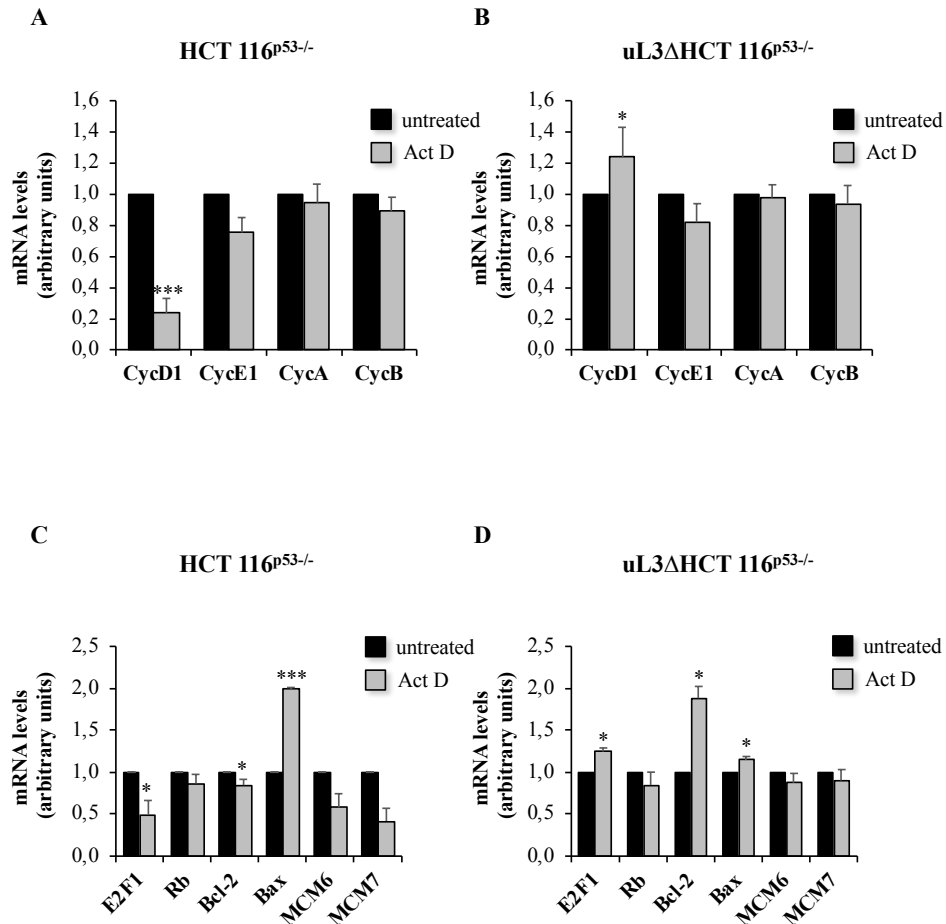
Figure 9. Act D treatment is associated to the uL3-mediated regulation of cell cycle and cell proliferation related genes. Total RNA from HCT 116$^{p53-/-}$ cells (A,C) and uL3ΔHCT 116$^{p53-/-}$ cells (B,D), untreated or treated with Act D 5 nM for 18 h, was subjected to RT-qPCR with primers specific for the indicated genes (Table 1). Quantification of signals is shown. Bars represent the mean of triplicate experiments; error bars represent the standard deviation. *p < 0.05; ***p < 0.001 vs. untreated cells set at 1.

3.4 uL3 negatively regulates Cyclin D1 mRNA and protein stability

Our previous results indicating that uL3 status affects Cyclin D1 expression levels in colon cancer cells, prompted us to investigate the molecular mechanism by which uL3 is involved in the regulation of Cyclin D1 expression.

Several studies have revealed that the regulation of Cyclin D1 expression occurs at multiple levels, including mRNA and protein stability (John et al., 2017). Therefore, we explored whether uL3 status could influence Cyclin D1 expression at mRNA and protein levels. To address this issue, HCT 116$^{p53-/-}$ and uL3ΔHCT 116$^{p53-/-}$ cells were treated with higher doses of Act D (2 μg/mL) to inhibit RNA Pol II-driven transcription for 2, 4 and 8 h. Then, total RNA was extracted from cell lysates and analyzed by RT-qPCR with specific primers for

Cyclin D1. As shown in Figure 10A, in uL3ΔHCT 116$^{p53-/-}$ cells the amount of Cyclin D1 mRNA was higher than in HCT 116$^{p53-/-}$ cells at all time points. Specifically, we observed an increase of about 40% in Cyclin D1 mRNA levels compared to parental cells after 8 h of Act D treatment (Figure 10A). These data indicate that the reduction of Cyclin D1 mRNA levels observed in HCT 116$^{p53-/-}$ upon Act D treatment might be due in part to a decrease in Cyclin D1 mRNA stability mediated by uL3.

Next, we have investigated a potential role of uL3 in the control of Cyclin D1 protein stability. For this purpose, HCT 116$^{p53-/-}$ and uL3ΔHCT 116$^{p53-/-}$ cells were incubated with cycloheximide (CHX) at different time points (10, 20, 30, 60 and 90 min). Then, the expression levels of Cyclin D1 protein was assessed by Western blotting. Analysis of the rate of disappearance of the Cyclin D1 protein upon CHX treatment highlighted that the down-regulation of uL3 was associated to an increase of Cyclin D1 stability (Figure 10B).

Altogether these results indicate that uL3 plays a crucial role in the tight regulation of Cyclin D1 expression by affecting Cyclin D1 stability either at mRNA than at protein levels.
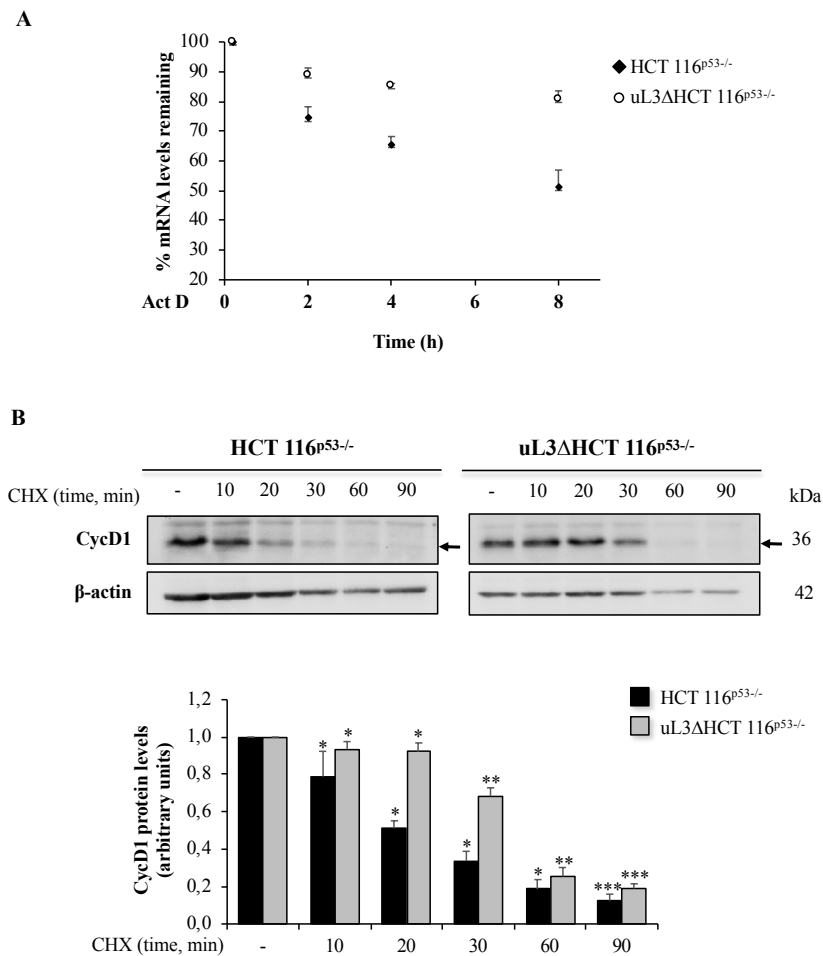

Figure 10. Effects of uL3 on Cyclin D1 mRNA and protein stability. (A) HCT 116$^{p53-/-}$ and uL3ΔHCT 116$^{p53-/-}$ cells were treated with Act D (2 μg/mL) for 8 h. At the indicated time points (0, 2, 4 and 8 h), total RNA was isolated and the mRNA levels of Cyclin D1 and β-actin were determined by

RT-qPCR. The relative amount of Cyclin D1 mRNA in untreated cells was set to 100% and the percentage of Cyclin D1 mRNA in cells treated with Act D was calculated accordingly. (B) HCT 116$^{p53-/-}$ and uL3ΔHCT 116$^{p53-/-}$ cells were treated with CHX (100 μg/mL) for 10, 20, 30, 60 and 90 min. Then, cell lysates were immunoblotted with anti-Cyclin D1 and anti-β-actin antibodies. Quantification of signals is shown. Bars represent the mean of triplicate experiments; error bars represent the standard deviation. ***$P < 0.001$, **$P < 0.01$, *$P < 0.05$ vs. untreated cells set at 1.

3.5 uL3 status affects E2F1 protein levels and transcription activity of E2F1 gene

Since E2F1 plays a central role in the regulation of cell cycle progression, its activity is subject to complex control mechanisms. In late G1 phase, hyperphosphorylation of Rb (pRb) by CDKs lead to the release of E2F1 resulting in the transactivation of the expression of E2F1-target genes (Bertoli et al., 2013). We have evaluated the expression of E2F1 and pRb in condition of drug induced nucleolar stress. To this aim, HCT 116$^{p53-/-}$ cells and uL3ΔHCT 116$^{p53-/-}$ cells were treated with Act D 5 nM for 18 h; then, proteins were extracted and analyzed by Western blotting. As expected, in cells expressing uL3 Act D treatment caused an increase of B23 (also known as nucleophosmin) and p21 levels confirming the induction of nucleolar stress (Figure 11A). Notably, in this condition the intracellular amounts of pRb-Ser612 were not altered,whereas the E2F1 and Cyclin D1 levels decreased significantly compared to the levels of unstressed cells (Figure 11B). In cells stably silenced of uL3, we observed a reduction of B23 and p21 levels (Figure 11A). As in parental cell line, the amounts of pRb-Ser612 did not changed, while we observed a slight decrease of E2F1 expression associated to a strong up-regulation of Cyclin D1 (Figure 11B). Interestingly, in condition of uL3 silencing and in absence of drug treatment the E2F1 and Cyclin D1 levels resulted extensively up-regulated (Figure 11B). These data clearly suggest that uL3 plays a key role in cell response to Act D induced nucleolar stress through the activation of a new uL3/E2F1/Cyclin D1 pathway that is independent from Rb status.

In order to better understand the effect of uL3 on the expression of E2F1, we investigate the ability of uL3 to influence the activity of E2F1 promoter by using a reporter luciferase assay. For this purpose, HCT 116$^{p53-/-}$ and uL3ΔHCT 116$^{p53-/-}$ cells were transiently transfected with a plasmid carrying E2F1 full length promoter. 24 h later, cell lysates were subjected to luciferase assay. As shown in Figure 11C, E2F1 promoter activity was strongly increased in uL3 deleted cells. As a control, HCT 116$^{p53-/-}$ cells were transiently transfected with siRNA specific for uL3 and 48 h later luciferase activity in cell lysates was analyzed. We found that transient uL3 silencing led to an effect similar to that observed with stable depletion of uL3 demonstrating that the alteration of E2F1 promoter activity specifically depends on uL3 status

(Figure 11C). Of interest, the effect on E2F1 promoter activity, observed in condition of uL3 silencing was rescue by uL3 transfection (Figure 11C). These data strongly indicated that uL3 is involved in the regulation of E2F1 transcriptional activity acting as a specific repressor of E2F1 promoter.

To further assess this issue, we performed luciferase assay in condition of uL3 overexpression. To this aim, HCT 116$^{p53-/-}$ cells were transiently transfected with increasing amount of pHA-uL3. 24 h later, luciferase activity in cell lysates was analyzed. Results showed in Figure 11D demonstrated that the overexpression of uL3 was associated to the reduction of E2F1 promoter activity in a dose-dependent manner.
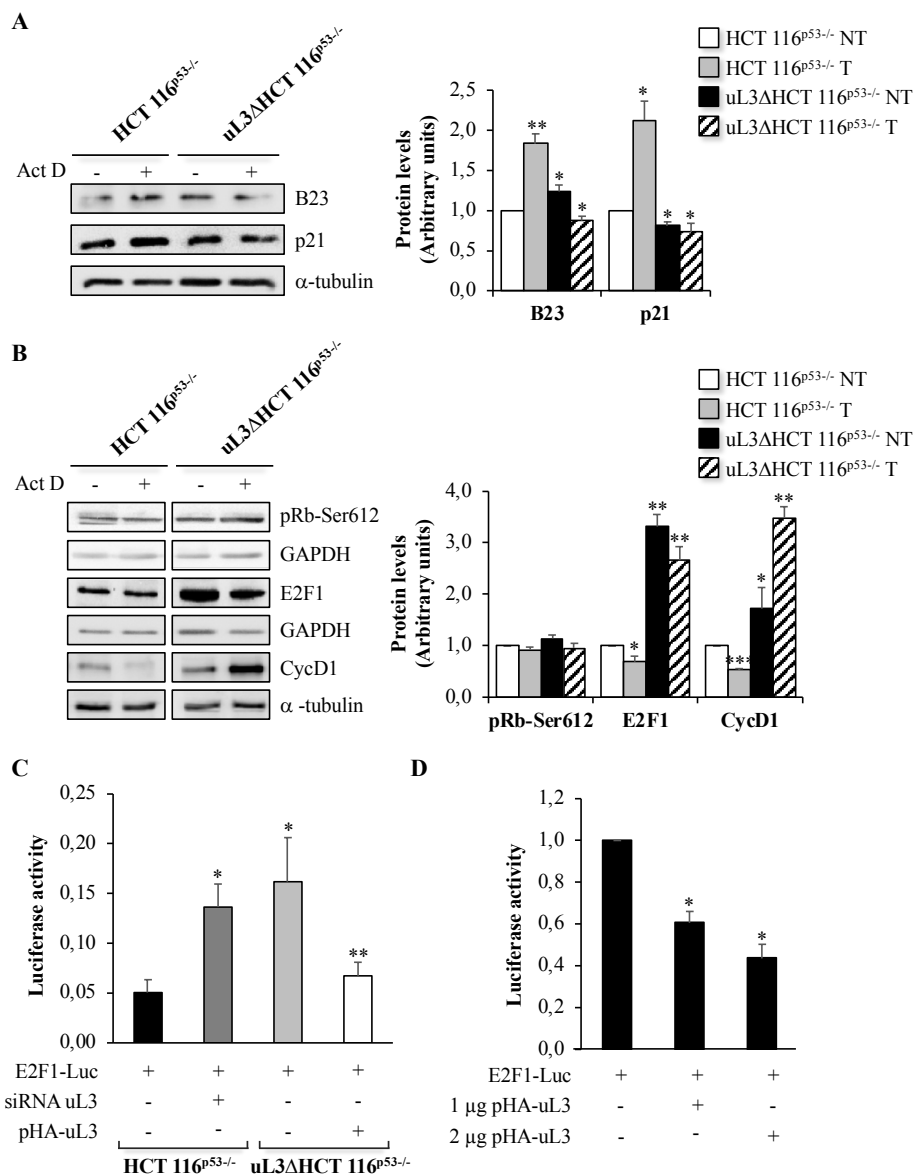

Figure 11. Effects of uL3 on cell cycle related gene expression and E2F1 promoter activity. (A) Representative western blotting of B23 and p21, (B) pRb-Ser612, E2F1 and CycD1. HCT 116$^{p53-/-}$ and uL3ΔHCT 116$^{p53-/-}$ cells were treated with Act D 5 nM for 18 h. After the treatment, protein extracts

from the samples were analyzed by western blotting with antibodies against indicated proteins. α-tubulin and GAPDH were used as loading controls. Quantification of signals is shown. Bars represent the mean of triplicate experiments; error bars represent the standard deviation. $**P < 0.01$, $*P < 0.05$ vs. untreated HCT $116^{p53-/-}$ cells set at 1. (C) HCT $116^{p53-/-}$ were transiently co-transfected with E2F1 promoter-driven reporter construct pGL2-AN (E2F1-Luc) and uL3 siRNA, uL3ΔHCT $116^{p53-/-}$ cells were transiently co-transfected with E2F1-Luc and pHA-uL3. Luciferase activities were measured after 24 h. Data are presented after normalizing transfection efficiency using the Renilla luciferase reporter gene. Bars represent the mean of triplicate experiments; error bars represent the standard deviation. $**P < 0.01$, $*P < 0.05$ vs. E2F1-Luc transfected cells. (D) HCT $116^{p53-/-}$ cells were transiently transfected with E2F1-Luc alone or with 1 μg or 2 μg of pHA-uL3. Luciferase activities were measured after 24 h. Data are presented after normalizing transfection efficiency using the Renilla luciferase reporter gene. Bars represent the mean of triplicate experiments; error bars represent the standard deviation. $*P < 0.05$ vs. E2F1-Luc transfected cells set at 1.

3.6 uL3 is a novel PARP-1-interacting protein and regulates PARP-1 mediated E2F1 promoter activation

In order to get a deeper insight into the molecular mechanism by which uL3 affects E2F1 promoter transactivation, we wondered whether uL3 physically interacts with Poly(ADP-ribose) polymerase 1 (PARP-1), the main E2F1 positive regulator in cells (Simbulan-Rosenthal et al., 2003). To approach this issue, we performed co-immunoprecipitation experiments in cell extracts by using antibodies against the endogenous proteins. Immunoprecipitated proteins were separated by SDS–PAGE and the presence of uL3 and PARP-1 was evaluated by Western blotting in the reciprocally immunoprecipitated complexes.

Results shown in Figure 12A demonstrated that uL3 and PARP-1 were co-immunoprecipitated indicating that they can interact in cells.

Next, we proceed in attempt to characterize the influence of the protein complex uL3-PARP-1 in the transactivation of E2F1 promoter. For this purpose, we performed reporter luciferase assays. Specifically, HCT $116^{p53-/-}$ cells were transiently co-transfected with the E2F1 reporter plasmid and increasing amounts of expression plasmids coding for uL3 and/or PARP-1. 24 h later, cell lysates were analyzed for luciferase activity. Predictably, we observed a strong increase of E2F1 promoter activity in condition of PARP-1 overexpression. In contrast, the enforced expression of uL3 negatively regulates E2F1 promoter activity. Interestingly, in condition of uL3 overexpression PARP-1 fails to transactivate E2F1 promoter (Figure 12B). These results strongly suggest that uL3 is involved in PARP-1 mediated activation of E2F1 promoter.

A

B

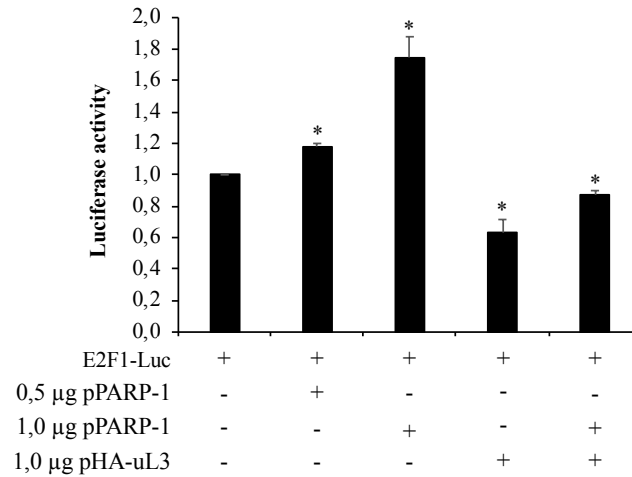|				
E2F1-Luc	+	+	+	+	+
0,5 µg pPARP-1	-	+	-	-	-
1,0 µg pPARP-1	-	-	+	-	+
1,0 µg pHA-uL3	-	-	-	+	+
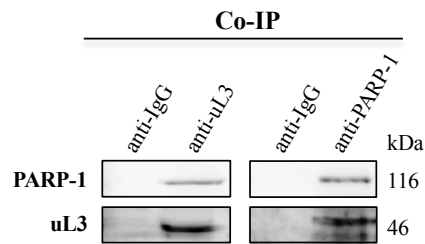
Figure 12. uL3 binds PARP-1 and regulates PARP-1 mediated E2F1 promoter activation. (A) *In vivo* binding of uL3 and PARP-1. uL3 and PARP-1 were specifically immunoprecipitated from HCT 116$^{p53-/-}$ cell extracts with antibodies against the endogenous uL3 and PARP-1. Immunoprecipitates were separated by SDS–PAGE and immunoblotted with antibodies versus PARP-1 and uL3 respectively. Note the absence of signal in IgG immunocomplex. (B) HCT 116$^{p53-/-}$ cells were transiently transfected with E2F1 promoter-driven reporter construct pGL2-AN (E2F1-Luc) alone or co-transfected with 0.5 or 1 µg of pPARP-1 plasmid or 1 µg of pHA-uL3 alone or in combination with 1 µg of pPARP-1 plasmid. Luciferase activities were measured after 24 h. Data are presented after normalizing transfection efficiency using the Renilla luciferase reporter gene. Bars represent the mean of triplicate experiments; error bars represent the standard deviation. *P < 0.05 vs. E2F1-Luc transfected cells set at 1.

In conclusion, our results led us to propose a model in which upon drug induced nucleolar stress, ribosome free uL3 accumulates in the nucleolus and translocates into the nucleoplasm where it can exert extra-ribosomal functions. In particular, our data strongly indicated that uL3 acts a specific repressor of E2F1 promoter activity. This effect could be explained considering that uL3 interacts with PARP-1 and it could prevent its binding to the E2F1 promoter with consequent inhibition of E2F1 promoter transactivation. In addition, we demonstrated that uL3 negatively affects Cyclin D1 expression at mRNA and protein levels.

Interestingly, previous studies reported that E2F1 plays a crucial role in the regulation of Cyclin D1 expression. In fact, it has been demonstrated that the human Cyclin D1 promoter contains an E2F1 consensus site and E2F1 positively affects Cyclin D1 gene expression (Klein et al., 2008).

Based on this, we speculate that uL3 could also regulate Cyclin D1 expression levels indirectly via inhibition of E2F1 promoter transactivation that, in turn, lead to a reduction of E2F1 protein. Thus, the inhibition of E2F1 promoter activity mediated by uL3 could be partially responsible of the lower levels of Cyclin D1 observed in condition of nucleolar stress.

All together our data reveal the existence of a novel uL3 mediated nucleolar stress response that involves two important regulators of cell cycle progression, E2F1 and Cyclin D1 (Figure 13).
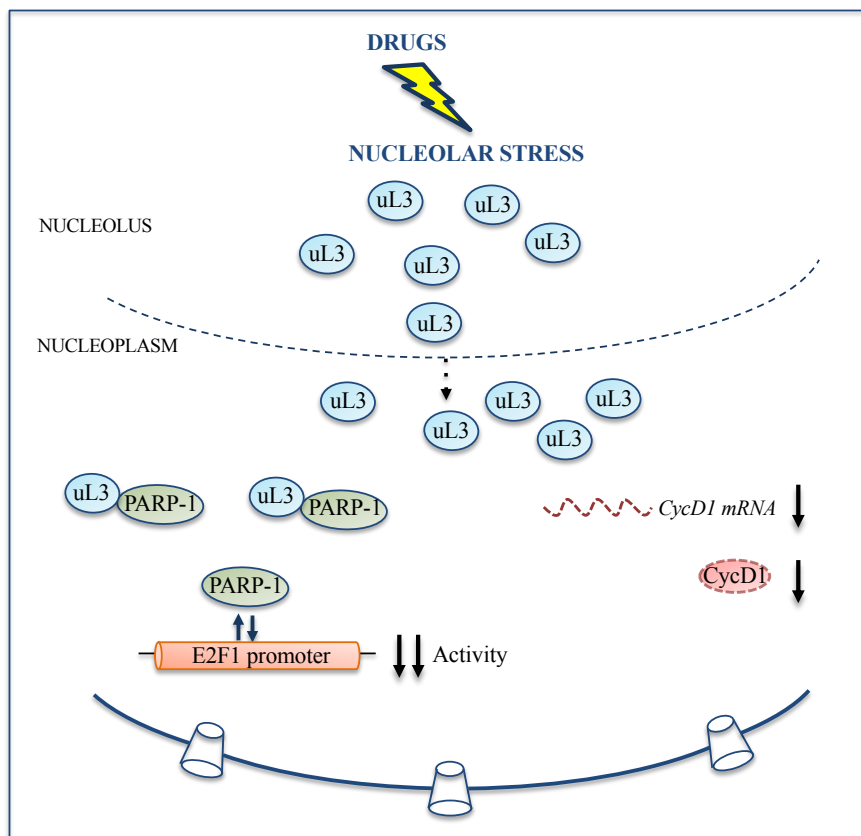

Figure 13. Schematic representation of proposed model. Upon drug induced nucleolar stress, ribosome free uL3 accumulates in the nucleolus and translocates into the nucleoplasm. Here, uL3 acts as a negative regulator of E2F1 promoter activity. In addition, uL3 inhibits Cyclin D1 protein half-life. These effects contribute to uL3 mediated cell response to nucleolar stress.

SECTION II

uL3 status influences drug sensitivity of colon cancer cells lacking functional p53

Several studies indicated that RPs are also involved in the molecular mechanisms activated in drug resistance in cancer cells lacking functional p53 (Russo et al., 2017[a]). We have recently identified a strictly correlation between uL3 expression levels and drug sensitivity in colon and lung cancer cells devoid of p53. The comparison of human lung and colon cancer specimens with normal tissues reveals a selective down-regulation of uL3 in the cancer tissues; uL3 mRNA amount decreases with malignant progression and the intensity of its expression is inversely related to tumor grade and tumor proliferation (Russo et al., 2016[a]). Data from our laboratory indicated that the loss of uL3 makes chemotherapeutic drugs, such as 5-FU, OHP, Act D, and cisplatin, ineffective in colon and lung cancer cells (Russo et al. 2016[a]; Russo et al., 2016[b]; Pagliara et al., 2016; Russo et al., 2016[d]). According to this, in a recent study we demonstrated that in a p53-mutated lung cancer cell line resistant to 5-FU (rCalu-6), uL3 expression is down-regulated and its restoration re-sensitized the cells to 5-FU through the regulation of reactive oxygen species (ROS) levels, glutathione (GSH) content, glutamate release, and cystine uptake. Specifically, uL3 functions as a transcriptional regulator of solute carrier family 7 member 11 (xCT) and glutathione S-transferase α1 (GST-α1) (Russo et al., 2017[b]).

All together, these findings imply that there is a mechanistic link between the response pathway to drug-induced nucleolar stress and the development of drug resistance. Based on this, the aim of this study is to examine the role of uL3 in chemoresistance in colon cancer cells lacking functional p53.

3.7 uL3 status influences cell migration and EMT program in colon cancer cells

We first investigated the effect of low levels of uL3 on cell motility and EMT. EMT is a complex cellular process that occurs both in physiological conditions and in pathological states leading to a cellular trans-differentiation continuum (Dongre et al., 2019). During EMT epithelial cells gradually lose their typical morphological characteristics as cell polarity, membrane adhesion and cell-to-cell contacts, and acquire a mesenchymal phenotype with the typical cellular stellate morphology and different propensity for intercellular signaling associated to an increase in cell motility, matrix remodeling properties, and a propensity for

invasiveness. These evident cellular alterations reflect the changes in the expression profiles of many genes. In particular, the activation of specific transcription factors results in the down-regulation of epithelial surface markers associated to an up-regulation of mesenchymal markers (Dongre et al., 2019).

Firstly, we evaluated the cell migration ability of HCT 116$^{p53-/-}$ and uL3ΔHCT 116$^{p53-/-}$ cells by using a wound healing assay. As shown in Figure 14A, upon uL3 silencing the wound healing ability of cells was markedly increased in time dependent manner compared to the wound healing ability observed in HCT 116$^{p53-/-}$ cells. Quantitative analysis showed that after 30 h, cells expressing normal levels of uL3 filled about 50% of the wound area while cells stably silenced of uL3 filled about 80% of the wound area, indicating that when uL3 expression was switched off cells closed the wound faster than parental cells. We also observed that the higher ability of uL3-deleted cells to migration was correlated to typical morphological changes of EMT; in particular, we observed a shift from compact adherent cells to elongated phenotype and a consistent reduction of cell-cell contacts (Figure 14B). Based on this, we analyzed the expression levels of EMT-related markers by Western blotting. We found that in condition of uL3 silencing there is a significant decrease of the epithelial marker E-cadherin and an increase of the mesenchymal marker vimentin (Figure 14C).

These data clearly indicated that uL3ΔHCT 116$^{p53-/-}$ cells displayed an enhancement in cell motility and a characteristic EMT phenotype compered to colon cancer cells expressing uL3.

Based on these results and considering that EMT is a cellular process involved in chemoresistance and evasion of apoptosis (Dongre et al., 2019), we speculated that the decrease chemosensitivity observed in cells stably deleted of uL3 could be at least in part due to the induction of EMT program.
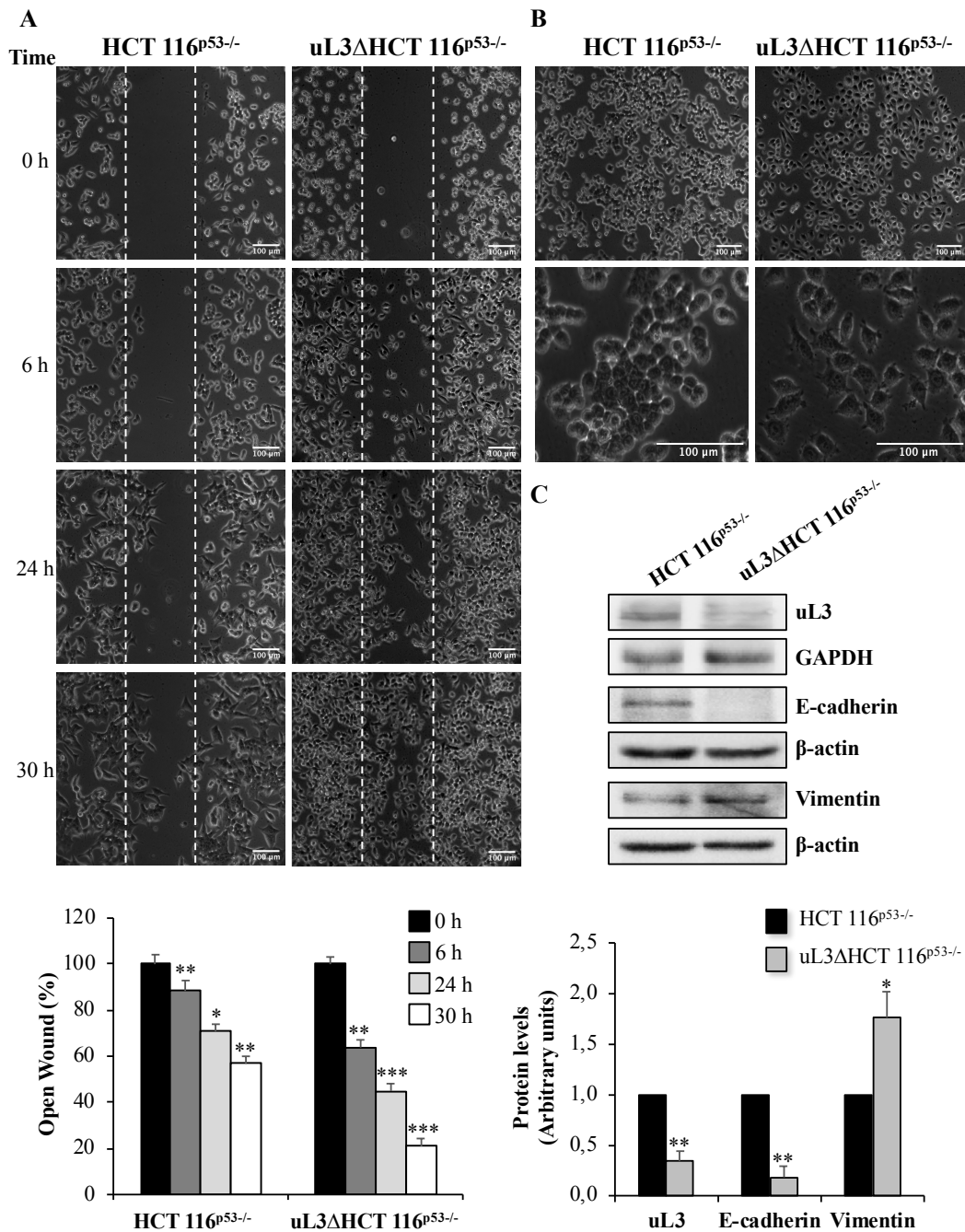
Figure 14. Effects of uL3 on cell migration and EMT program. (A) Wound widths in HCT 116[p53−/−] and uL3ΔHCT 116[p53−/−] cells were measured at 0, 6, 24 and 30 h on 3 fields per well and averaged. Data are expressed as the fold-decrease of area respect to control (time 0) set as 100%. (B) Representative bright-field microscope images of HCT 116[p53−/−] and uL3ΔHCT 116[p53−/−] cell lines. Scale bar: 100 µm. (C) Representative western blot analysis of uL3 and EMT markers. Protein extracts from HCT 116[p53−/−] and uL3ΔHCT 116[p53−/−] cells were analyzed by western blotting with the indicated antibodies. GAPDH and β-actin were used as loading controls. Quantification of signals is shown. Bars represent the mean of triplicate experiments; error bars represent the standard deviation. *$p < 0.05$; **$p < 0.01$ vs. HCT 116[p53−/−] cells set at 1.

3.8 Identification of genes and pathways differentially expressed in colon cancer cells in presence or absence of uL3

In order to further investigate the role of uL3 in drug resistance, we proceeded in attempt to identify the transcripts showing differential expression levels between HCT $116^{p53-/-}$ and uL3ΔHCT $116^{p53-/-}$ cells. We collected RNA samples from HCT $116^{p53-/-}$ and uL3ΔHCT $116^{p53-/-}$ cells treated or not with Act D (5 nM) and 24 h later transcriptomic RNA-seq analysis was performed. Briefly, libraries were prepared starting from 4 μg of total RNA and sequenced by a paired-end chemistry on an NovaSeq6000 platform in collaboration with the Next Generation Sequencing (NGS) Facility at TIGEM. Each library was loaded at a concentration of 8 pM, which was previously established as optimal. An average yield of ~4.5 Mb was obtained per sample. The data have been deposited in NCBIs Gene Expression Omnibus (GEO) (Edgar et al., 2002). GEO accession number is GSE145807. A data analysis was performed using the pipeline already established at the Bioinformatics and Statistics Core Facility at TIGEM (Pinelli et al., 2016).

Results shown in Figure 15A indicated that the differentially expressed genes (DEGs) between HCT $116^{p53-/-}$ and uL3ΔHCT $116^{p53-/-}$ cells were 11268 (5735 down-regulated and 5533 up-regulated). Furthermore, a total of 1724 genes resulted up-regulated and 2204 down-regulated in HCT $116^{p53-/-}$ cells, whereas 950 genes were strongly up-regulated and 1670 down-regulated by Act D treatment in uL3ΔHCT $116^{p53-/-}$ cells compared to untreated cells (Figure 15A).

Gene set enrichment analysis (GSEA) displayed a remarkable up-regulation of 10 gene set and a significant down-regulation of 1 gene set in uL3-deleted cells in comparison to parental cells (Figure 15B). Furthermore, GSEA revealed a significant up-regulation of four gene sets in Act D-treated uL3ΔHCT $116^{p53-/-}$ cells in comparison to treated parental cells. Among them we pointed out 2 gene sets that are strictly related to tumor aggressiveness: Hallmark_Epithelial_Mesenkymal_Transition, Hallmark _Angiogenesis (Figure 15B).

Moreover, GSEA indicated that a considerable number of gene sets were found strongly down-regulated (n = 13) and only two gene sets resulted significatively up-regulated in uL3ΔHCT $116^{p53-/-}$ upon Act D treatment compared to untreated cells. Interestingly, the most negatively enriched pathways were related to autophagy activation: Hallmark_P13K_AKT_mTOR_Signaling, Hallmark_mTORC1_Signaling, Hallmark_Wnt_Beta_Catenin_Signaling (Figure 15C).

These data strongly suggest that the observed drug resistance in condition of uL3 silencing could be in part due to the activation of autophagy.

Notably, upon Act D treatment in HCT 116$^{p53-/-}$ cells, a condition that is associated to induction of nucleolar stress and activation of extra-ribosomal functions of uL3, the most positively enriched pathways are represented by mTORC1 and IL6_JAK_STAT3 together with pathways related to the activation of apoptosis (Figure 15C). These data confirm the pro-apoptotic role for uL3 in condition of nucleolar stress, whereas the up-regulation of mTORC1 and IL6_JAK_STAT3 might be associated to inhibition of autophagic flux.

In conclusion, data from RNA-seq analysis strongly suggest that the different cellular response to drug treatment observed in HCT 116$^{p53-/-}$ and uL3ΔHCT 116$^{p53-/-}$ cells could be correlated to a differential expression of genes involved in the activation of autophagic pathway.
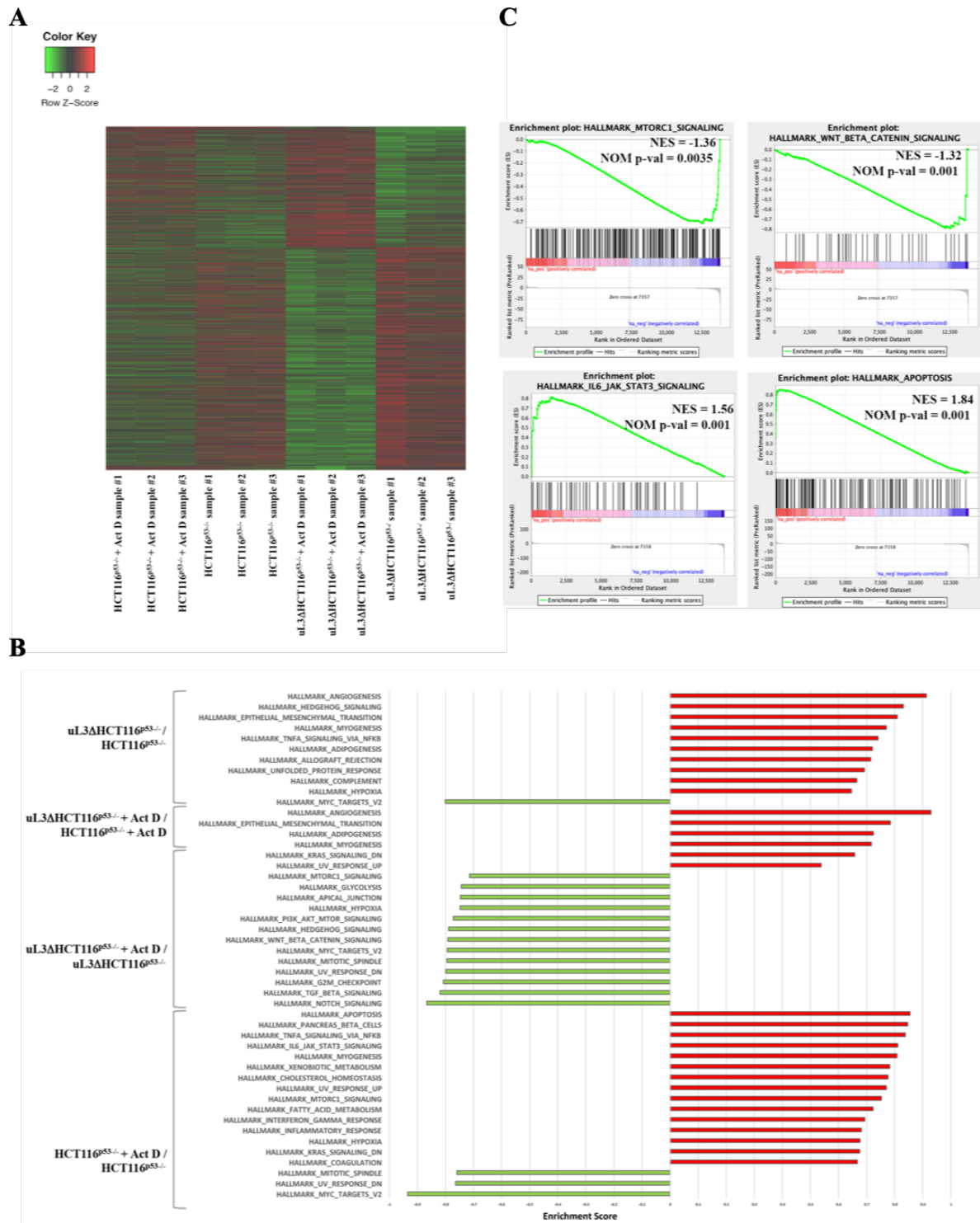
Figure 15. Key genes and pathways regulated by Act D treatment in HCT 116$^{p53-/-}$ cells and uL3ΔHCT 116$^{p53-/-}$ cells. (A) Unsupervised hierarchical Z-Score clustering. Clustering analyses revealed differentially expressed genes (DEGs) between the experimental groups. The color scale means the gene expression standard deviations from the mean, with green for low expression and red for the high expression levels. (B) GSEA querying hallmark genes depicting significant enrichment of signaling pathway genes as cell metabolism, apoptosis, autophagy, cell growth, as well as cancer-related pathways. (C) Enrichment plots for gene sets related to IL6/JAK/STAT3 and apoptosis pathways significantly enriched in Act D-treated HCT 116$^{p53-/-}$ cells versus untreated HCT 116$^{p53-/-}$ cells and for the most negatively enriched pathways mTORC 1 and WNT_Beta_Catenin in uL3ΔHCT

116[p53−/−] cells after Act D treatment compared to deleted untreated cells. The top portion of each panel shows the normalized enrichment scores (NES) for each gene; the bottom portion of the plot indicates the value of the ranking metric moving down the list of ranked genes. Location of the gene set members are indicated by black lines in the center of the plot. The gray plot at the bottom represents the ranked list of all differentially expressed genes. Genes which are more highly expressed are in red whereas genes more highly expressed in blue. GSEA, Gene set enrichment analysis; NES, normalized enrichment score; FDR, false discovery rate.

3.9 uL3 status affects the autophagic flux in colon cancer cells

Autophagy is a self-degradative system involved in keeping cellular homeostasis and survival. It consists of many sequential steps that culminate with the formation of subcellular double-membrane-bound structures known as autophagosomes containing degradable materials and their fusion with lysosomes to form autolysosomes whose contents are degraded by lysosomal enzymes (Chun et al., 2018). Autophagy exerts a dynamic and controversial role in cancer. In fact, in normal cells autophagy functions as tumor suppressor since it allows the physiologic degradation and recycling system of proteins and organelles; however, it has been reported that autophagy can support cancer cells survival allowing them to overcame environmental stress and satisfying their high metabolic demand. Moreover, recent studies revealed that autophagy can also induce cancer cell migration and invasion promoting chemotherapy resistance (Li et al., 2017).

Based on our previous findings, we supposed that uL3 could mitigate cancer response to drug treatment through the modulation of autophagic process. To verify this issue, we proceeded in attempt to characterize the role of uL3 in autophagic flux by different assays.

Since the fusion of the autophagosomes with lysosomes is a crucial step of autophagic flux, we firstly evaluated the cellular distribution of autophagic marker LC3B (microtubule-associated protein 1 light chain 3β) and lysosomal marker LAMP1 (lysosome associated membrane protein-1). To this purpose, HCT 116[p53−/−] and uL3ΔHCT 116[p53−/−] cells were subjected to confocal microscopy after immunofluorescence staining. In particular, green fluorescence is associated to LC3B making autophagosomes visible as green puncta, whereas red fluorescence is associated to LAMP1 allowing the visualization of acidic vesicles, lysosomes, as red puncta. The co-localization of green and red fluorescence signal indicates the presence of autolysosomes. Autophagic flux is enhanced when both green and red puncta are increased in cells, while autophagic flux is blocked when yellow puncta are increased and localised in perinuclear regions.

In order to investigate how the expression levels of uL3 affect autophagic flux, HCT 116[p53−/−] cells were transiently transfected with pHA-uL3 plasmid and 24 h later the levels of

endogenous LC3B and LAMP1 were analyzed by confocal microscopy. As shown in Figure 16, in condition of uL3 overexpression we observed an increase of yellow punctate structures around the nucleus compared to control cells indicating a role of uL3 in the inhibition of autophagic flux. Specifically, the enforced expression of uL3 was correlated with an increase in autophagic vacuoles content (red puncta).

These data are consistent with the above reported transcriptome analysis and indicate that uL3 might act as inhibitory factor of autophagic process.

Next, we further explored the effect caused by uL3 on autophagic flux in presence of Rapamycin (RAPA), a well known inducer of autophagy through inhibition of oncogene mTOR (Benjamin et al., 2011), and Chloroquine (CQ), which inhibits autophagy by blocking autophagosome-lysosome fusion (Mauthe et al., 2018). We found that in condition of uL3 overexpression, the number of yellow puncta increased compared to control and to cells treated with RAPA alone (Figure 16). These results indicated that the enforced expression of uL3 hampers the effect of RAPA. Interestingly, in HCT 116$^{p53-/-}$ cells overexpressing uL3 and treated with CQ we observed an increase of autophagy inhibition (Figure 16).

In cells stably silenced for uL3, we noticed an increase of LC3B puncta (green) and LAMP1 puncta (red) compared to parental cells which reflect an enhancement in autophagosome and lysosome formation, respectively (Figure 17). Thus, the silencing of uL3 was associated to an increase of autophagic flux. Of note, when uL3 expression was switched off, CQ treatment did not lead to an increase of yellow puncta demonstrating that CQ failed to exert its effect. These findings clearly suggest a role of uL3 in the mechanism of action of CQ. Interestingly, the restoration of uL3 in uL3ΔHCT 116$^{p53-/-}$ cells caused an increase of yellow punctate structures (LC3B-LAMP1) in perinuclear regions indicating the inhibition of autophagic flux (Figure 17).

In uL3 deleted cells transfected with pHA-uL3 and treated with CQ we did not observed significant difference compared to parental cells. Furthermore, the rescue of uL3 in uL3ΔHCT 116$^{p53-/-}$ cells hindered the induction of autophagy by RAPA (Figure 17).

All together these data demonstrated that uL3 acts as repressor of autophagic flux.
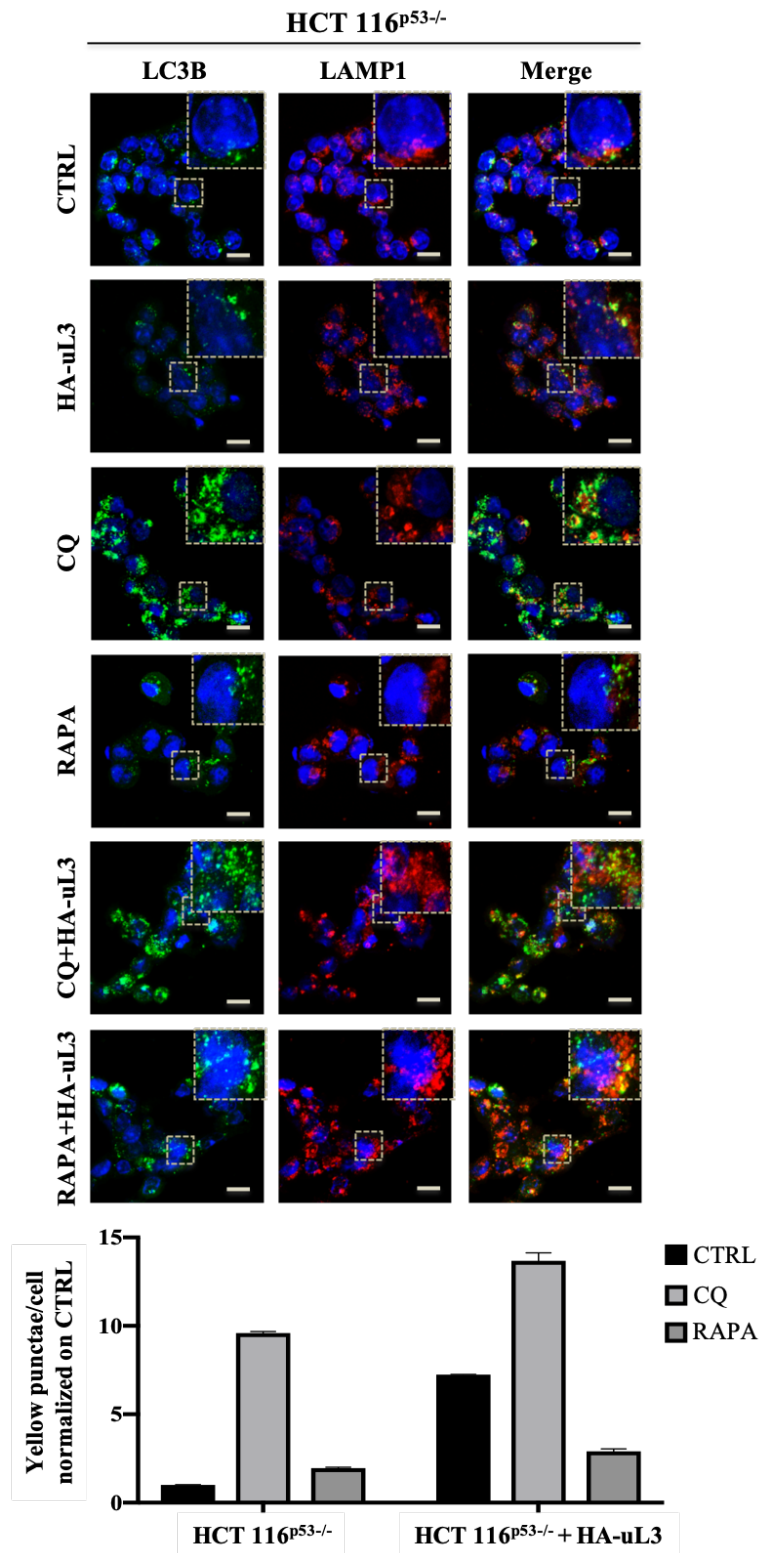
Figure 16. Enforced expression of uL3 inhibits autophagic flux in HCT 116[p53−/−] cells. Representative z-stack images of HCT 116[p53−/−] cells treated with 25 μM CQ or 1 μM RAPA or transiently transfected with 1 μg of pHA-uL3 for 24 h, alone or in combination. Cells were fixed and double stained with LC3B and LAMP1 antibodies. Nuclei were counterstained with Hoechst. Single-color fluorescence images of LC3B positive autophagosomes (green) and LAMP1 positive endosomes and/or lysosomes (red) are presented in the 1st and 2nd columns, respectively, and a merged view of these 2 proteins is shown in the 3rd column. Higher magnification views of the boxed area from the merged images are shown. Scal bar, 10 μm.
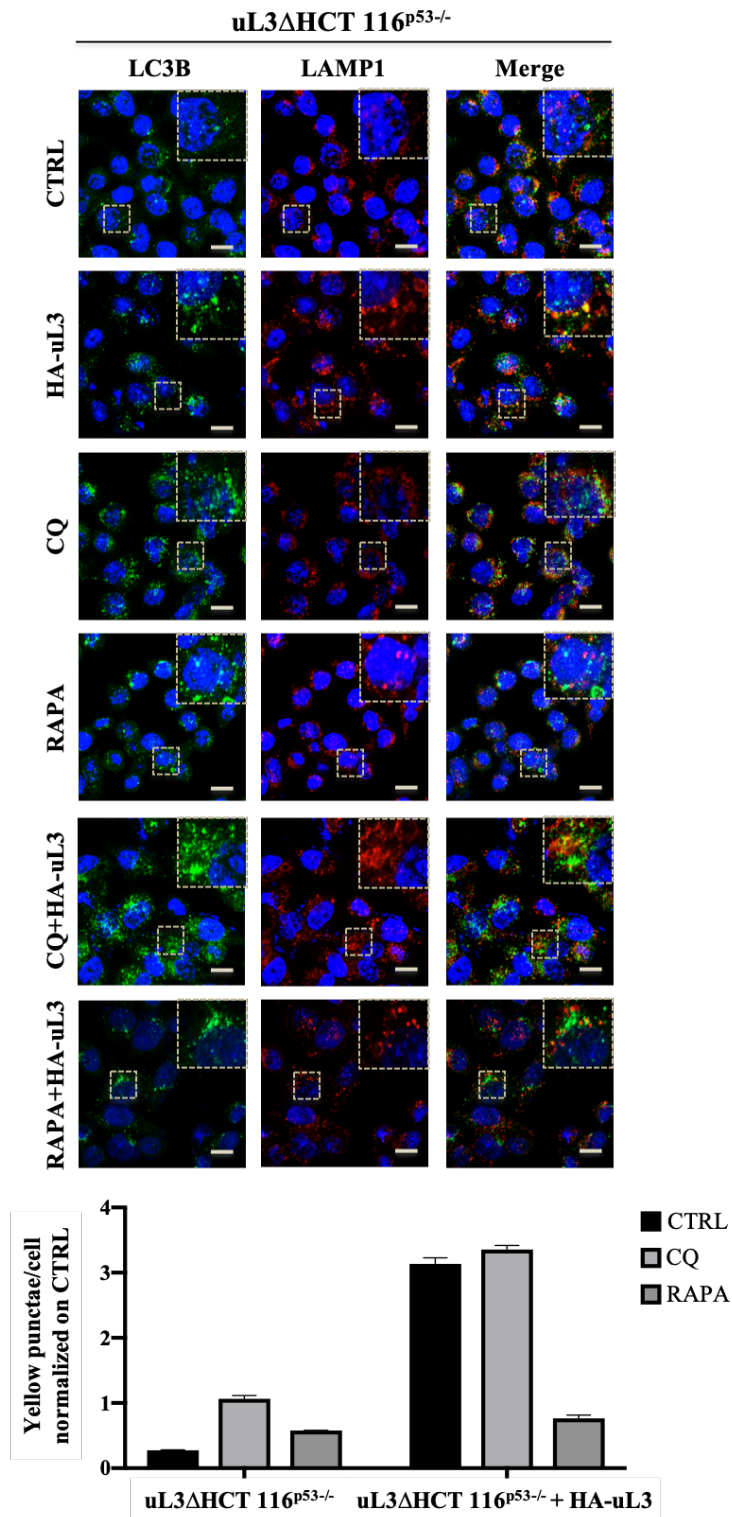
Figure 17. Depletion of uL3 enhances autophagic flux in HCT 116$^{p53-/-}$ cells and the restoration of uL3 in uL3ΔHCT 116$^{p53-/-}$ cells rescues this effect. Representative z-stack images of uL3ΔHCT 116$^{p53-/-}$ treated with 25 µM CQ or 1 µM RAPA for 4 h or transiently transfected with 1 µg of pHA-uL3 for 24 h, alone or in combination. Cells were fixed and double stained with LC3B and LAMP1 antibodies. Nuclei were counterstained with Hoechst. Single-color fluorescence images of LC3B positive autophagosomes (green) and LAMP1 positive endosomes and/or lysosomes (red) are presented in the 1st and 2nd columns, respectively, and a merged view of these 2 proteins is shown in

the 3rd column. Higher magnification views of the boxed area from the merged images are shown. Scal bar, 10 μm.

Next, we proceed in attempt to evaluate the autophagic flux by analyzing the expression of LC3B and p62 proteins through Western blotting. In cells, after translation the unprocessed form of LC3B is proteolytically cleaved resulting in the LC3B-I form. Upon autophagy induction, LC3B-I is conjugated to phosphatidylethanolamine (PE) generating LC3B-II form that specifically localized into lipid membranes at autophagosomes and is commonly used as autophagosome marker (Galluzzi et al., 2017). The p62 protein, also known as sequestosome 1 (SQSTM1), is a selective autophagy receptor which sequesters ubiquitinated proteins into autophagosomes by interacting with LC3B-II. In this process p62 is itself degraded; therefore, p62 levels are negatively correlated with autophagic flux (Galluzzi et al., 2017). In fact, when autophagy is activated, p62 levels decreased; whereas, when autophagy is inhibited p62 accumulates in the cell.

More specifically, we evaluated the abundance of LC3B-I, LC3B-II, LC3B-II/I ratio and p62 by Western blotting in HCT $116^{p53-/-}$ and uL3ΔHCT $116^{p53-/-}$ cells in condition of uL3 overexpression or CQ treatment.

As expected, in HCT $116^{p53-/-}$ cells CQ treatment caused a significant increase of LC3-II expression as well as the LC3B-II/I ratio associated to the up-regulation of p62 levels compared to control cells (Figure 18A,C). In fact, CQ inhibits autophagy flux by preventing autophagosome-lysosome fusion with consequent accumulation of autophagosomes. In condition of uL3 overexpression, the decrease of the LC3B-II/I ratio was associated to the a substantial increase in the amount of p62 (Figure 18A,C). Notably, in condition of uL3 silencing we observed a strong increase of LC3B-II and a reduction of p62 compared to parental cells confirming that autophagic flux is enhanced in uL3ΔHCT $116^{p53-/-}$ cells. Moreover, in these cells CQ treatment failed to exert its effect as demonstrated by reduction of the LC3B-II/I ratio and p62 levels (Figure 18B,D). Interestingly, the restoration of uL3 in uL3ΔHCT $116^{p53-/-}$ cells led to a decrease of the LC3B-II/I ratio associated to a strong increase of p62 amount (Figure 18B,D).

All together, these findings are in line with the results of immunofluorescence experiments indicating the inhibitory role of uL3 on autophagic flux.

To further investigate the role of uL3 on autophagy we analyzed the transcript levels of some pivotal autophagy related genes including ULK1 (unc-51-like kinase 1), ATG13 (autophagy-related protein 13), ATG101 (autophagy-related protein 101) and Transcription factor EB (TFEB), a major regulator of autophagy and lysosomal biogenesis (Chun et al., 2018). To this purpose, total RNA was extracted from HCT $116^{p53-/-}$ and uL3ΔHCT $116^{p53-/-}$ cells

transfected or not with pHA-uL3 and analyzed by RT-qPCR with primers specific for ATG13, ATG101, ULK1 and TFEB (Table 1).

As shown in Figure 18E, we found that the enforced expression of uL3 in HCT 116$^{p53-/-}$ cells was associated to the down-regulation of all these genes; in contrast, in uL3 deleted cells we observed an increase in the expression levels of all the tested genes. Of note, the restoration of uL3 in these cells rescued the effect on autophagy observed in condition of uL3 silencing indicating that the presence uL3 is associated to a negative regulation of the autophagic flux. These data strongly support the idea that the enhanced autophagic flux observed in uL3ΔHCT 116$^{p53-/-}$ cells is associated to chemoresistance and can be rescued by transfecting cells with a plasmid expressing uL3.
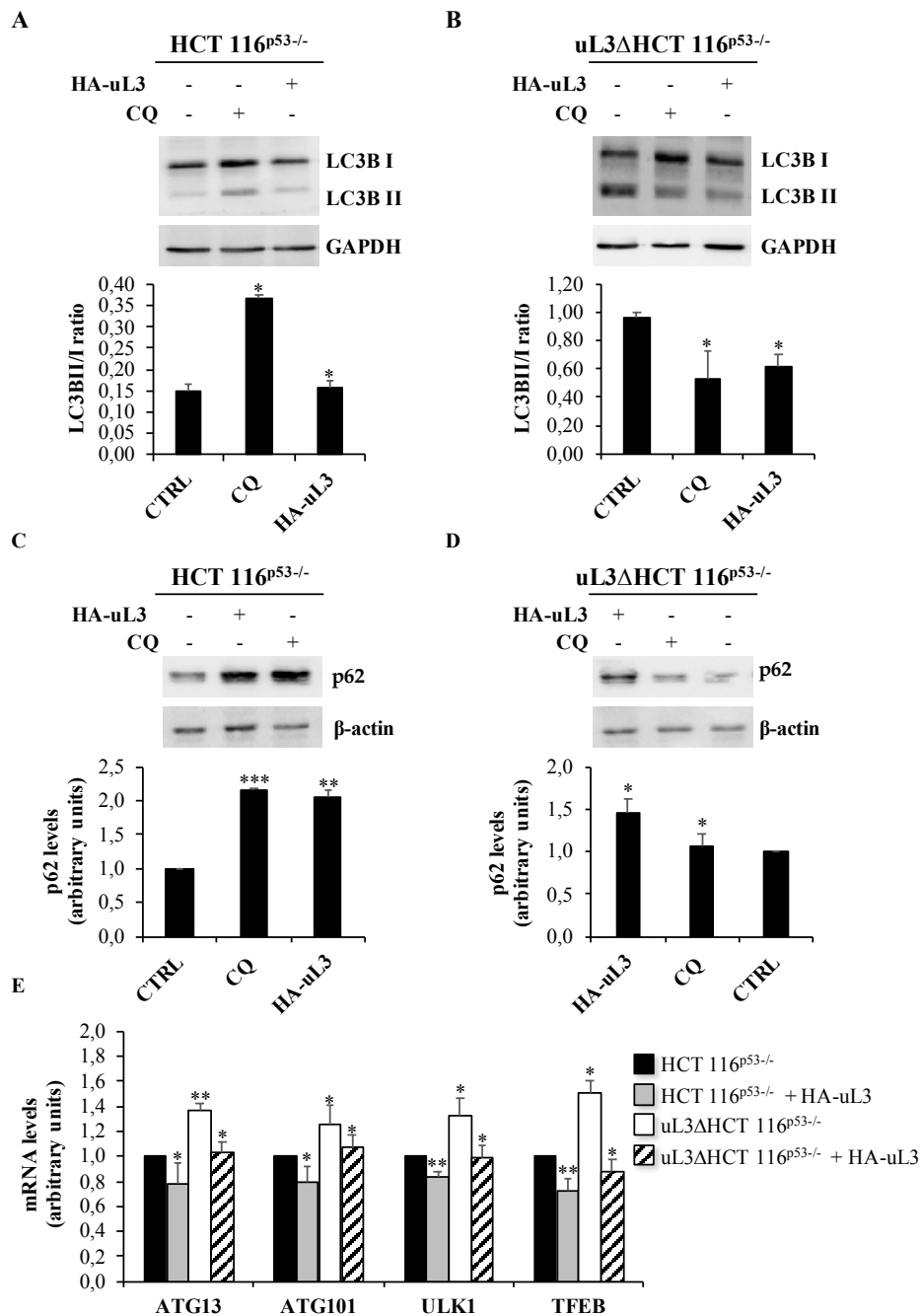
Figure 18. Effect of uL3 status on the conversion of LC3B and on the expression of autophagy-related genes. Representative immunoblotting showing LC3B protein conversion (A) and p62 protein levels (C) in HCT 116$^{p53-/-}$ cells and LC3B protein conversion (B) and p62 protein levels (D) in uL3ΔHCT 116$^{p53-/-}$ cells treated or not with 25 μM CQ or transiently transfected with 1 μg of pHA-uL3. 24 h later, protein extracts from the samples were analyzed by Western blotting with antibodies against indicated proteins. GAPDH and β-actin were used as loading controls. Quantification of LC3B-II/I ratio is shown. Full-length blots are shown in Figures S7 and S8. (E) Total RNA from HCT 116$^{p53-/-}$ and uL3ΔHCT 116$^{p53-/-}$ cells, transfected or not with 1 μg of pHA-uL3, was subjected to RT-qPCR with primers specific for the indicated genes (Table 1). Quantification of signals is shown. Bars represent the mean of triplicate experiments; error bars represent the standard deviation. * $p < 0.05$, ** $p < 0.01$ vs. untreated cells set at 1.

3.10 uL3 restoration is associated to G1 cell cycle arrest and apoptosis in uL3 deleted colon cancer cells

Based on our previous results, we proceed in attempt to further investigate the effect of uL3 restoration in uL3ΔHCT 116$^{p53-/-}$ cells. For this purpose, we analyzed the cell cycle distribution by flow cytometry in HCT 116$^{p53-/-}$ and uL3ΔHCT 116$^{p53-/-}$ cells transfected with pHA-uL3 or treated with CQ. Results shown in Figure 19A demonstrated that in HCT 116$^{p53-/-}$ cells CQ treatment significantly increased the percentage of cells in G1 phase (79%) compared to control cells, whereas in uL3ΔHCT 116$^{p53-/-}$ cells CQ failed to exert its effects. These data are in accordance with our previous results from confocal microscopy and Western blotting analysis.

Predictably, the enforced uL3 expression in HCT 116$^{p53-/-}$ cells caused G1 phase arrest (78%) (Russo et al., 2013). Interestingly, the ectopic expression of uL3 in uL3 deleted cells resulted in an increase of the percentage of cells in G1 phase (70%) compared to control cells (Figure 19A).

Furthermore, in the same experimental conditions we analyzed apoptosis by Annexin V-Alexa Fluor 488/PI dual staining (Figure 19B). Not surprisingly, in HCT 116$^{p53-/-}$ cells uL3 overexpression caused a strong increase of the percentage of late apoptotic cells (Annexin V$^+$ and PI$^+$) of approximately 30% compared to the untransfected cells (Russo et al., 2013). Moreover, we found that pHA-uL3 transfection in uL3 deleted cells led to an increase of apoptotic cells from 2.8% in control cells to 26.4% in cells transfected with pHA-uL3 (Figure 19B).

Overall these data firmly suggest that the ectopic expression of uL3 in colon cancer cells devoid of uL3 and lacking of functional p53 leads to G1 cell cycle arrest associated to the activation of apoptotic cell death. In addition, these results corroborate the crucial role of uL3 in the mechanism of action of CQ.

A

B
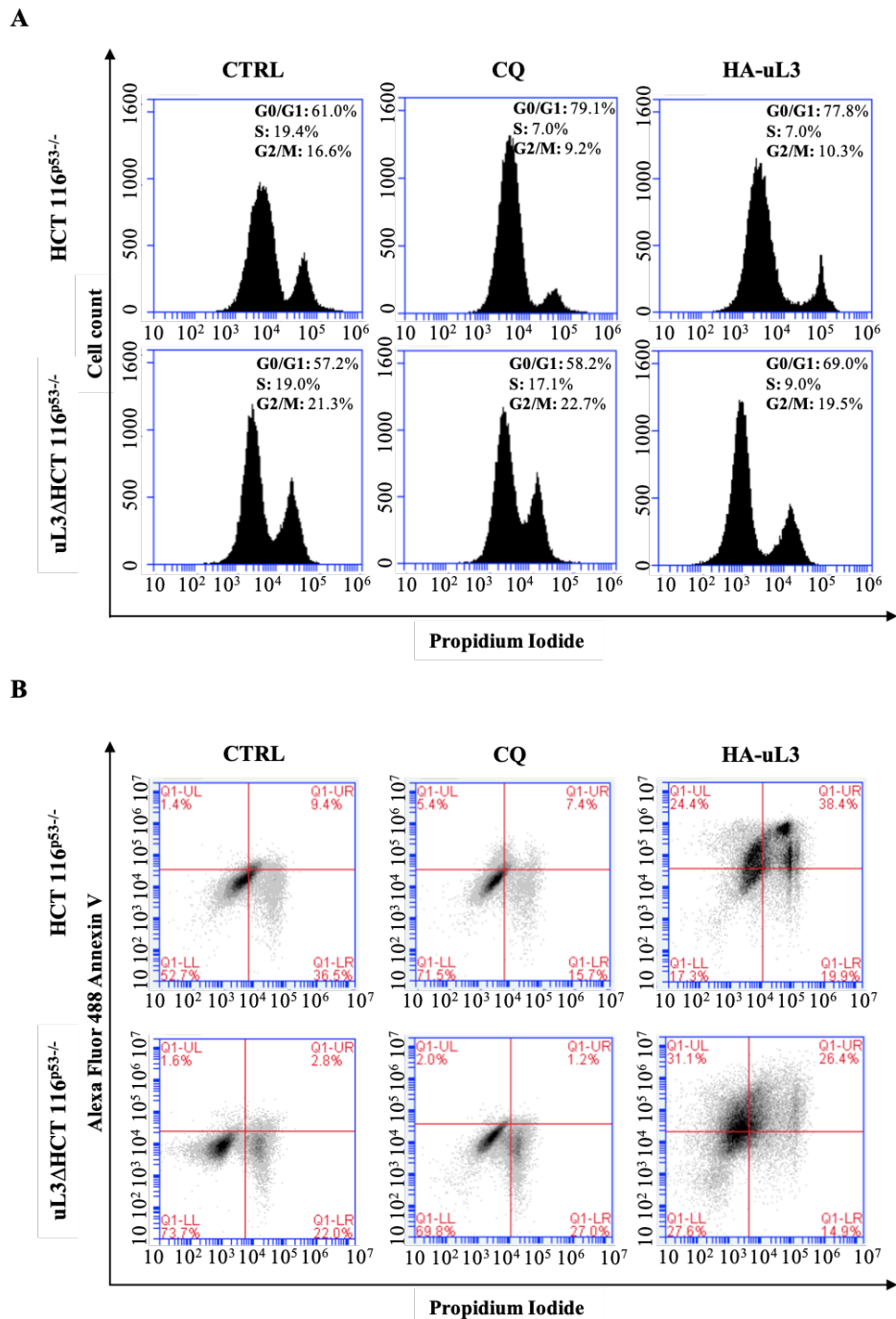
Figure 19. Effect of uL3 restoration in uL3ΔHCT 116$^{p53-/-}$ cells on cell cycle and apoptosis. (A) HCT 116$^{p53-/-}$ and uL3ΔHCT 116$^{p53-/-}$ cells were transiently transfected with 1 µg pHA-uL3 or treated with 25 µM CQ. 24 h later, cells were stained with PI and analysed using FACS. Peaks representing histograms of cell numbers and percentages in G1, S, and G2/M phases are shown. (B) Representative flow cytometry dot blots with double Annexin V-Alexa Fluor 488/PI staining for HCT 116$^{p53-/-}$ and uL3ΔHCT 116$^{p53-/-}$ transiently transfected with pHA-uL3 or treated with CQ for 24 h.

In conclusion, our findings strongly indicate that nucleolar stress and autophagy are strictly interconnected in our model of colon cancer. In particular, we demonstrate that silencing of uL3 in colon cancer cells triggers autophagy associated to Act D resistance, whereas the

restoration of uL3 is associated to the inhibition of autophagy resulting in re-sensitization of cancer cells to drug treatment (Figure 20).
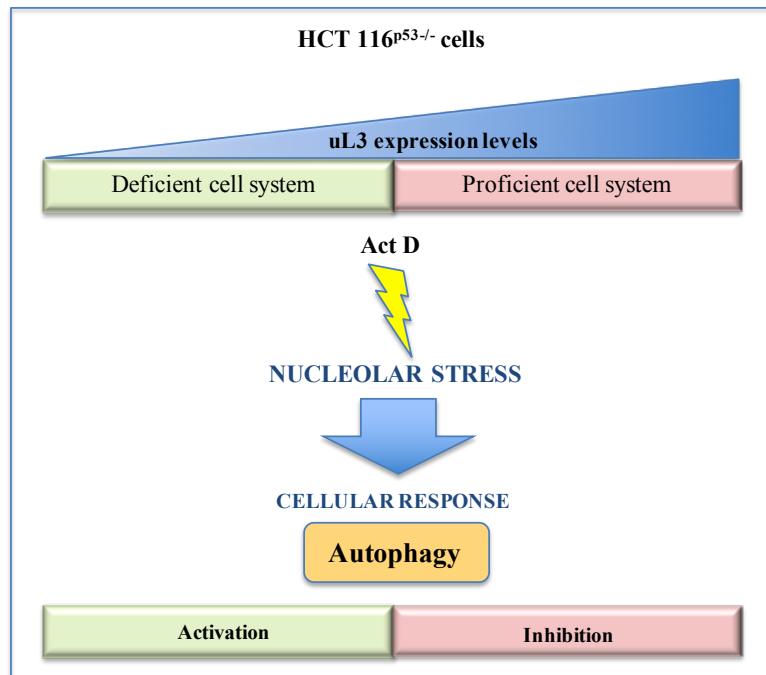
Figure 20. Effect of uL3 status on autophagy in colon cancer cells devoid of p53. The nucleolar stress response upon Act D treatment depends on uL3 status. Reduced uL3 levels cause a cellular response employing autophagy induction, while increased uL3 amounts inhibit this process. (Image adapted from Pecoraro et al., 2020[(b)])

In the light of these data, we conclude that uL3 can increase the cytotoxic effects of many drugs as a result of its pro-apoptotic and anti-autophagic activity. Therefore, this study provides a potential therapeutic strategy for the management of tumors characterizing by lack of functional p53 and reduced levels of uL3.

SECTION III

S-Adenosyl-l-Methionine: a strategy for overcoming uL3-mediated drug resistance in p53 deleted colon cancer cells

Published evidence from our group demonstrate that the down-regulation of uL3 protein in p53 deleted cancer cells resulted in being resistant to different chemotherapeutic agents including 5-FU, OHP, and Act D (Esposito et al., 2014; Russo et al., 2016[b]; Pagliara et al., 2016; Russo et al., 2016[d]). As extensively discussed in the previous paragraphs, the chemoresistance observed in colon cancer cells stably silenced for uL3 is associated to autophagy activation and EMT phenotype, two cellular processes strictly interconnected with tumor development and metastasis (Pecoraro et al., 2019; Pecoraro et al., 2020[a]).

Nowadays, considerable efforts are being made to overcome drug resistance in cancer treatment. In this context, emerging evidence are accumulating regarding the application of natural compounds as a promising source of new anticancer drugs. In the last decades, several *in vivo* and *in vitro* studies have highlighted the antiproliferative, anti-metastatic and pro-apoptotic effects of S-Adenosyl-L-methionine in cancer cells (Mosca et al., 2020[b]). Hence, the growing scientific interest is focused on identifying the biological mechanisms and the signal transduction pathways related to the chemopreventive activities of this natural compound. S-Adenosyl-L-methionine (AdoMet, also known as SAM or SAMe), is an ubiquitous and naturally occurring sulfonium compound exerting a variety of well-documented biological functions. It represents the main methyl donor required in numerous methylation reactions, and also the precursor of the decarboxylated S-adenosylmethionine, the propylamine group donor in polyamine biosynthesis. The peculiar AdoMet reactivity is inherent to its sulfonium pole that makes the three carbon atoms (bound to the sulfur atom) highly susceptible to nucleophilic substitution; this characteristic renders the molecule able to donate the methyl group, the aminopropyl group and the adenosyl group (Fontecave et al., 2004). In addition, AdoMet is an approved nutritional supplement thus lending itself to be used for therapeutic purposes without the common contraindications of chemotherapy drugs (Mosca et al., 2020[b]).

In order to study novel therapeutic approaches taking advantage from anticancer and anti-proliferative effects of natural compounds, we focused our interest on AdoMet and its potential in overcoming chemoresistance observed in our model of colon cancer cells lacking of functional p53 and characterized by low expression levels of uL3.

3.11 AdoMet inhibits proliferation in colon cancer cells

In order to examine the role of AdoMet in uL3-mediated drug resistance, we firstly analyzed its cytotoxic activity in our model of colon cancer cells deleted of p53. For this purpose, sensitive HCT116$^{p53-/-}$ cells and drug-resistant uL3ΔHCT116$^{p53-/-}$ cells were treated with different concentrations (from 72 to 1000 µM) of AdoMet. Then, cell viability was evaluated by the 3-(4,5-dimethylthiazol-2-yl)-2,5-diphenyltetrazolium bromide (MTT) assay at indicated time points (24, 48, and 72 h). Results shown in Figure 21A demonstrated that HCT 116$^{p53-/-}$ was sensitivity to AdoMet treatment and cell viability was strongly reduced in a dose- and time-dependent manner indicating that AdoMet is able to exert its cytotoxic activity in these cells. It is noteworthy that in resistant uL3ΔHCT 116$^{p53-/-}$ cells AdoMet treatment also caused a reduction in cell viability (Figure 21B); however, in uL3 deleted cells we found an IC50 value of 750 µM compared to an IC50 value of 500 µM in parental cells at 72 h.

Next, uL3ΔHCT 116$^{p53-/-}$ cells were incubated with different concentration of AdoMet (from 125 to 1000 µM), 5-FU (from 12.5 to 100 µM), or with a combination of AdoMet and 5-FU for 72 h. Then, cell viability was assessed by MTT assay. As expected, AdoMet treatment caused a reduction in cell viability whereas 5-FU treatment failed to exert its cytotoxic activity. Interestingly, the combination of 5-FU with AdoMet led to a strongly decrease in cell viability compared to that cells treated with AdoMet alone (Figure 21C). All together, these results clearly indicate that AdoMet restores sensitivity of uL3 deleted cells to 5-FU treatment.
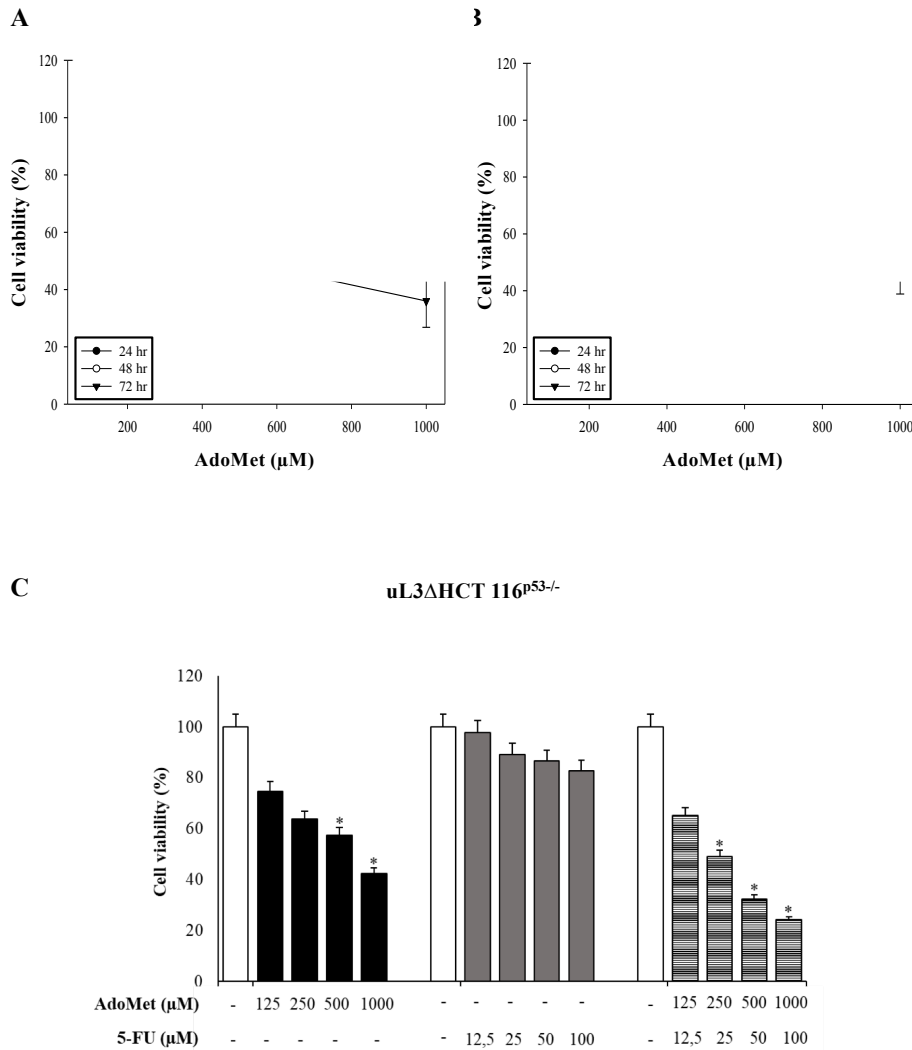
Figure 21. Cytotoxic effect of AdoMet on HCT 116$^{p53-/-}$ and uL3ΔHCT 116$^{p53-/-}$ colon cancer cells. HCT 116$^{p53-/-}$ (A) and uL3ΔHCT 116$^{p53-/-}$ cells (B) were treated with increasing amounts of AdoMet (72–1000 μM) from 24 to 72 h, then cell viability was measured by the MTT assay. Results are presented as a percentage of the control cells. * $p < 0.05$ versus untreated cells (C) uL3ΔHCT 116$^{p53-/-}$ were treated with AdoMet (from 125 to 1000 μM), and 5-FU (from 12.5 to 100 μM), alone or in combination, for 72 h. Cell viability was assayed using the MTT assay. Data represent the average of three independent experiments; error bars represent the standard deviation. * $p < 0.05$ versus untreated cells.

3.12 AdoMet causes cell cycle arrest in S phase in uL3 deleted colon cancer cells

In order to examine the mechanism by which AdoMet exerts its cytotoxic activity in colon cancer cells lacking functional p53, we analyzed cell cycle distribution in HCT 116$^{p53-/-}$ and uL3ΔHCT 116$^{p53-/-}$ cells treated with 500 μM of AdoMet for 72 h. We found that AdoMet treatment did not affect the cell cycle distribution in HCT 116$^{p53-/-}$ cells (Figure 22A,C). In contrast, in uL3 deleted cells AdoMet treatment induced an increase in percentage of cells in

the S phase (from about 13% to about 40%) associated with a slightly decrease of cells in the G2/M phase (from about 20% to about 11%) and G1 phase (from about 65% to about 41%) (Figure 22B,C). Furthermore, in the same experimental conditions we evaluated the expression profile of Cyclins, that are key regulatory proteins of cell cycle progression. Western blot analysis revealed that in HCT 116[p53−/−] cells the expression levels of Cyclin B, D, and E were not significantly altered upon AdoMet treatment; whereas we observed an increase in expression levels of Cyclin A (Figure 23A).

In uL3ΔHCT 116[p53−/−] cells AdoMet treatment was associated to overexpression of the G1 phase-related protein as Cyclin E and G2/M phase-related Cyclin B; as in parental cells, we found that Cyclin A amount was significantly up-regulated upon AdoMet treatment (Figure 23B). It is particularly important to note that the treatment of uL3ΔHCT 116[p53−/−] cells with AdoMet caused a strongly down-regulation of Cyclin D that is over expressed in this cells upon uL3 silencing (Pecoraro et al., 2019).

Altogether, these findings demonstrate that the cytotoxic activity of AdoMet on uL3ΔHCT 116[p53−/−] cells was correlated to alteration in cell cycle progression, reduced expression of Cyclin D, and enhanced expression of Cyclin A.
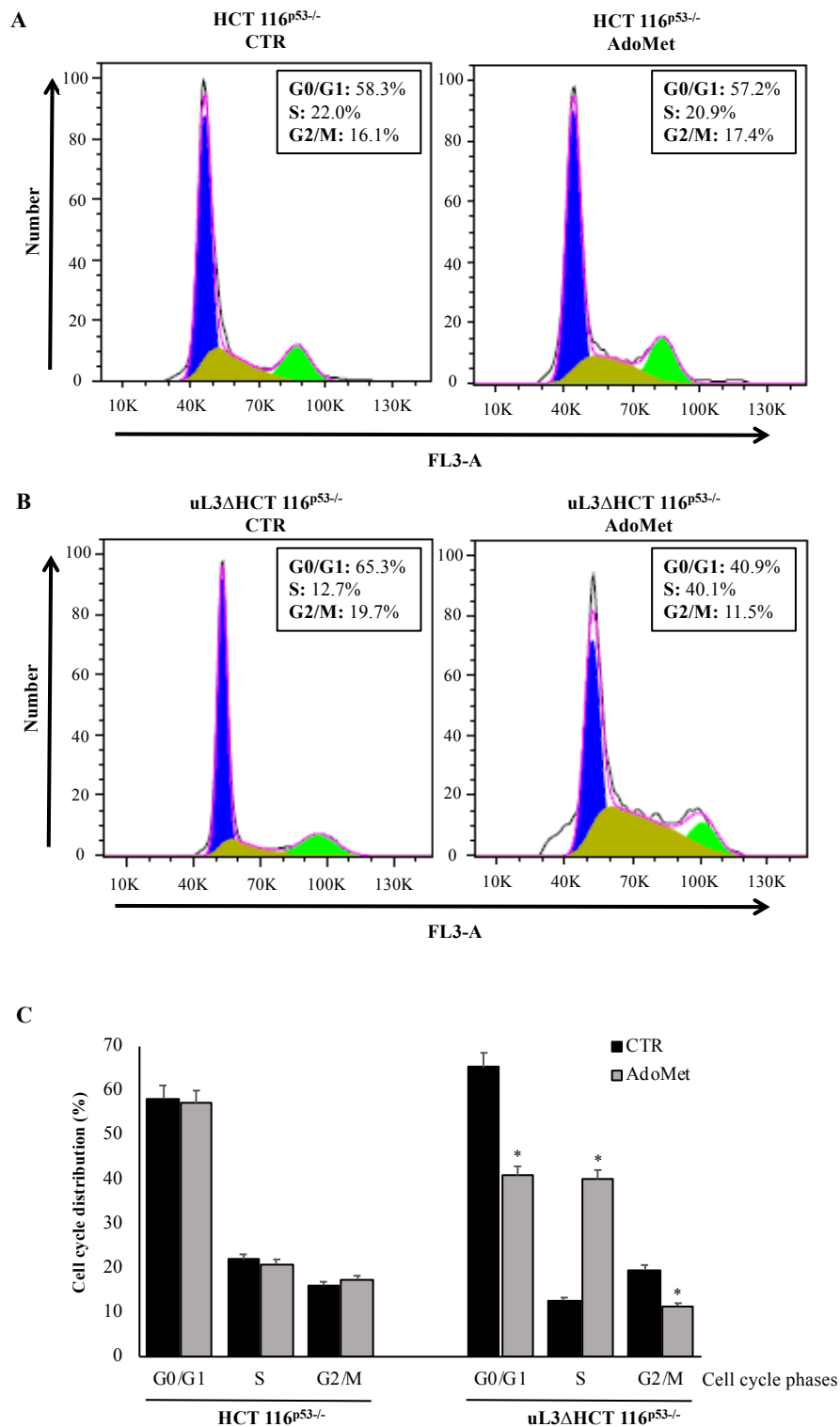
Figure 22. Effect of AdoMet on cell cycle in HCT 116$^{p53-/-}$ and uL3ΔHCT 116$^{p53-/-}$ colon cancer cells. Representative FACS histograms of propidium iodide (PI)-stained of HCT 116$^{p53-/-}$ (A) and uL3ΔHCT 116$^{p53-/-}$ (B) cells treated or not (CTR) with 500 μM AdoMet for 72 h. (C) The bar diagram shows the percentage of cells in each phase of the cell cycle. Each bar represents the mean of triplicate experiments; error bars represent the standard deviation. For each sample, at least 2×10^4 events were analyzed. * $p < 0.05$ versus untreated cells.
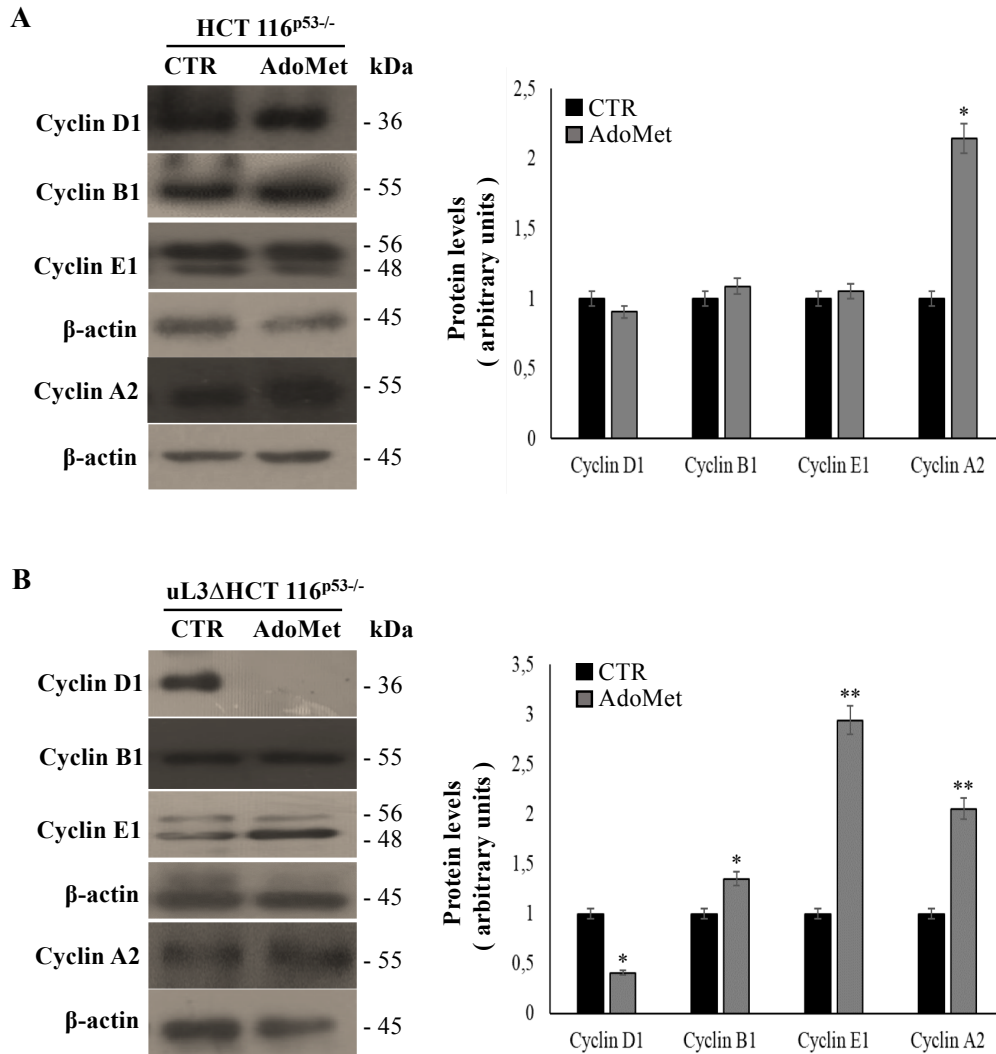
Figure 23. Effect of AdoMet on cell cycle regulatory proteins in HCT 116$^{p53-/-}$ and uL3ΔHCT 116$^{p53-/-}$ colon cancer cells. The level of cell cycle-regulatory proteins in HCT 116$^{p53-/-}$ (A) and uL3ΔHCT 116$^{p53-/-}$ cells (B) was measured by western blot analysis. The housekeeping protein β-actin was used as a loading control. The relative densitometric analysis is reported in the corresponding graphs, expressed as arbitrary units. Bars represent the mean of triplicate experiments; error bars represent the standard deviation. * $p < 0.05$, ** $p < 0.01$ vs. untreated cells set at 1. The images are representative of three immunoblotting analyses obtained from three independent experiments.

3.13 AdoMet induces apoptosis in colon cancer cells

With the aim of further examining the mechanism by which AdoMet inhibits cell growth in our model of colon cancer cells, we proceed in attempt to establish whether AdoMet exerts its cytotoxic effect by triggering apoptosis. To this purpose, HCT 116$^{p53-/-}$ cells and uL3ΔHCT 116$^{p53-/-}$ cells were incubated with 500 μM AdoMet for 72 h. Then, apoptosis was analyzed by Annexin V-FITC/PI double staining.

We found that AdoMet treatment caused an increase of the apoptotic cells proportion in both cell lines (Figure 24A). In particular, in HCT 116$^{p53-/-}$ cells the percentage of late apoptotic cells (Annexin V+ and PI+) raised from 6% in the untreated cells to 13% in the treated cells; while, in uL3ΔHCT 116$^{p53-/-}$ apoptotic cells proportion increased from 3 to 17% upon AdoMet treatment (Figure 24A). Next, we evaluated the expression levels of caspases and PARP-1, proteins playing a crucial role in the initiation and execution of apoptotic process (Kiraz et al., 2016). To this aim, both cell lines were treated with 500 μM AdoMet. 72 later, the expression of these proteins was assessed by Western blotting. Consistently, we found that in both cell lines AdoMet treatment caused a decrease of full-length PARP-1, pro-caspase 3, 9, 8, associated to an increase in the ratio between pro-apoptotic Bad and anti-apoptotic Bcl-2.
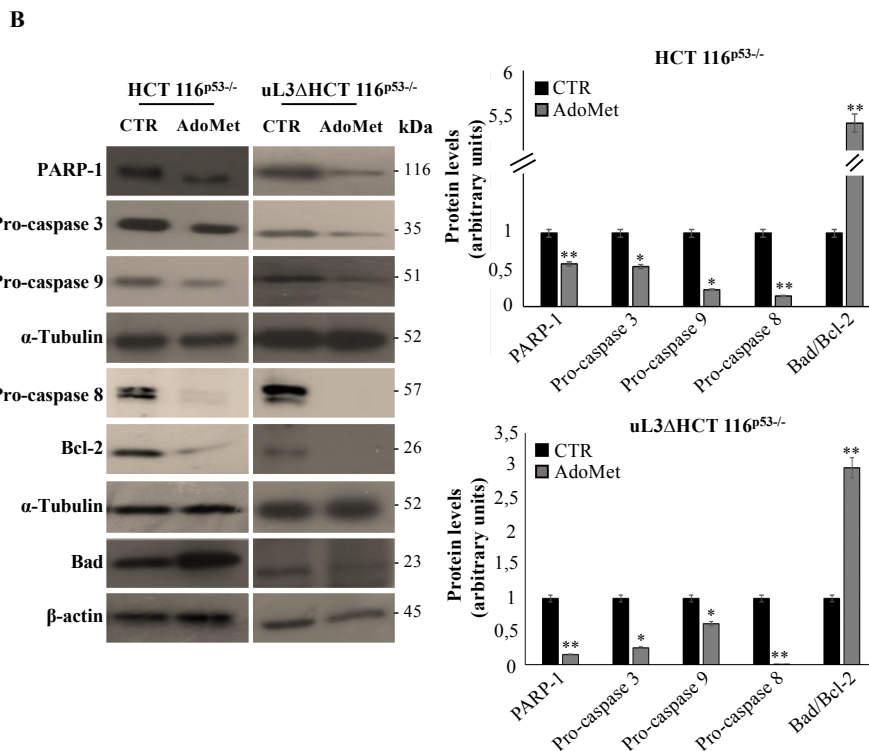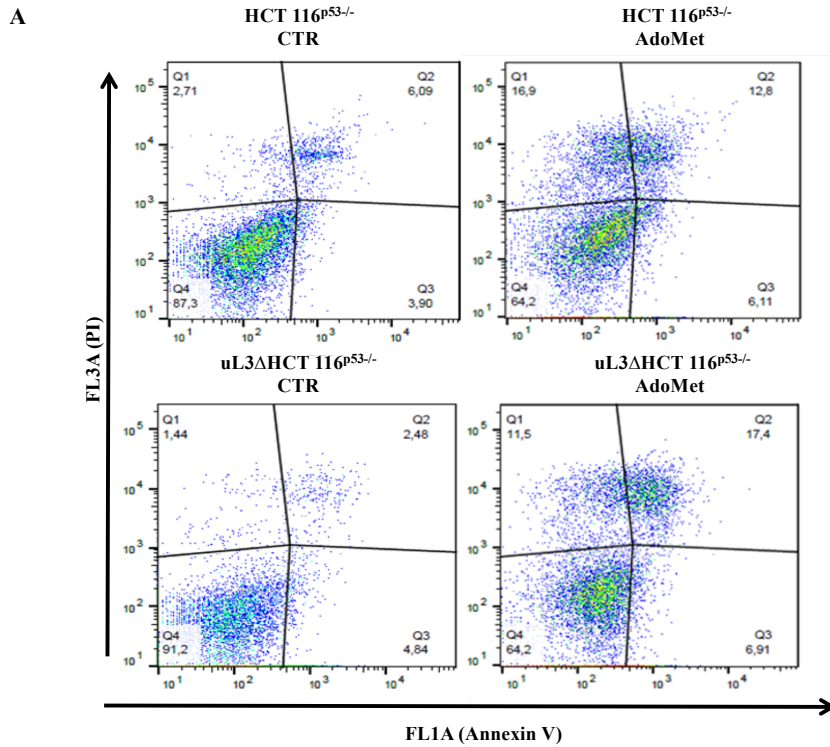
Figure 24. Effect of AdoMet on apoptosis in HCT 116$^{p53-/-}$ and uL3ΔHCT 116$^{p53-/-}$ colon cancer cells. (A) Representative dot plots of Annexin V-FITC and PI-stained HCT 116$^{p53-/-}$ and uL3ΔHCT 116$^{p53-/-}$ cells incubated with 500 μM AdoMet for 72 h. The experiments were repeated three times. (B) Immunoblots of HCT 116$^{p53-/-}$ and uL3ΔHCT 116$^{p53-/-}$ for PARP-1, pro-caspase 3, pro-caspase 8, pro-caspase 9, Bad, and Bcl-2; the housekeeping proteins α-tubulin and β-actin were used as loading control. Graphs show the relative densitometric analyses, expressed as arbitrary units. Bars represent the mean of triplicate experiments; error bars represent the standard deviation. * p < 0.05, ** p < 0.01

vs. untreated cells set at 1. The images are representative of three immunoblotting analyses obtained from three independent experiments.

3.14 AdoMet increases ROS production in colon cancer cells

Starting from the notion that in cancer cells the pro-apoptotic effect of several natural compounds is mediated by their pro-oxidant activity, we hypothesized that AdoMet treatment could affect the generation of reactive oxygen species (ROS). To this purpose, HCT $116^{p53-/-}$ cells and uL3ΔHCT 116p53$^{-/-}$ cells were incubated with 500 μM AdoMet for 72 h. Then, the intracellular ROS levels were quantitatively evaluated by the 2′,7′-dichlorofluorescein diacetate (DCF-DA) flow cytometric assay. As shown in Figure 25, AdoMet treatment led to an enhancement in ROS production in both cell lines. In particular, we observed an increase of 2- and 3-fold in ROS levels in treated uL3ΔHCT $116^{p53-/-}$ and HCT $116^{p53-/-}$ cells, respectively, compared to untreated cells.

All together these findings demonstrate that the induction of ROS production might constitute one of the mechanisms by which AdoMet induces apoptotic cell death in our model of colon cancer cells deleted of p53.
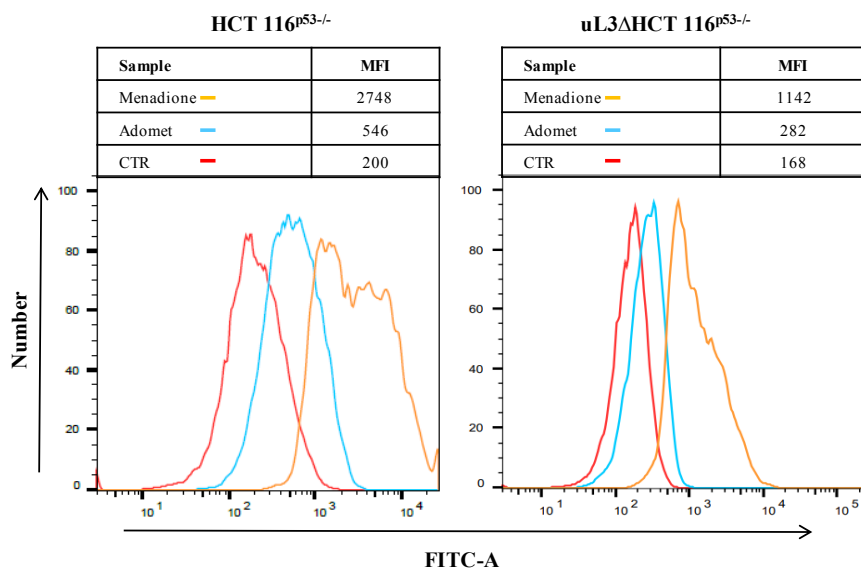
Figure 25. Effect of AdoMet on ROS accumulation in HCT $116^{p53-/-}$ and uL3ΔHCT $116^{p53-/-}$ colon cancer cells. HCT $116^{p53-/-}$ and uL3ΔHCT $116^{p53-/-}$ cells were treated or not (CTR) with 500 μM AdoMet for 72 h and then subjected to flow cytometry to measure ROS levels. FACS analysis was performed using 2′,7′-dichlorofluorescein diacetate (DCF-DA) as a substrate. For the quantitative evaluation of ROS, FlowJo software was used to calculate median fluorescence intensities (MFI) by the formula (MFI-treated/MFI-control). Analysis was carried out by triplicate determination on three separate experiments.

3.15 AdoMet inhibits autophagy in colon cancer cells

Data from the literature largely demonstrate that autophagy represents also a tumor pro-survival mechanism closely connected to chemoresistance (Pecoraro et al., 2020[b]). On the basis of our previous findings indicating that drug resistance observed in uL3ΔHCT 116$^{p53-/-}$ cells is associated to enhanced autophagic flux (Pecoraro et al., 2020[a]), we wondered whether AdoMet treatment could modulate autophagic process in these cells. To this purpose, HCT 116$^{p53-/-}$ and uL3ΔHCT 116$^{p53-/-}$ cells were incubated with 500 μM AdoMet. 48 h later, cells were stained with LysoTracker (LTR), a vital fluorescent dye for labeling and tracking cellular acidic organelles, such as lysosomes and autophagolysosomes, and analyzed by fluorescent microscopy. Upon AdoMet treatment we found a reduction in formation of red dotted acidic vacuoles compared to control cells, demonstrating that AdoMet inhibits autophagic flux in both cell lines (Figure 26A). This result was confirmed by flow cytometry analysis, in fact the measure of median fluorescence indicated a decrease in acidic vesicles upon AdoMet treatment in both cell lines (Figure 26B).

A

HCT 116$^{p53-/-}$ uL3ΔHCT 116$^{p53-/-}$

CTR

AdoMet

CQ

100 μm   100 μm

B

HCT 116$^{p53-/-}$

Sample		MFI
Adomet	—	210
CTR	—	300

uL3ΔHCT 116$^{p53-/-}$

Sample		MFI
Adomet	—	443
CTR	—	569

Number
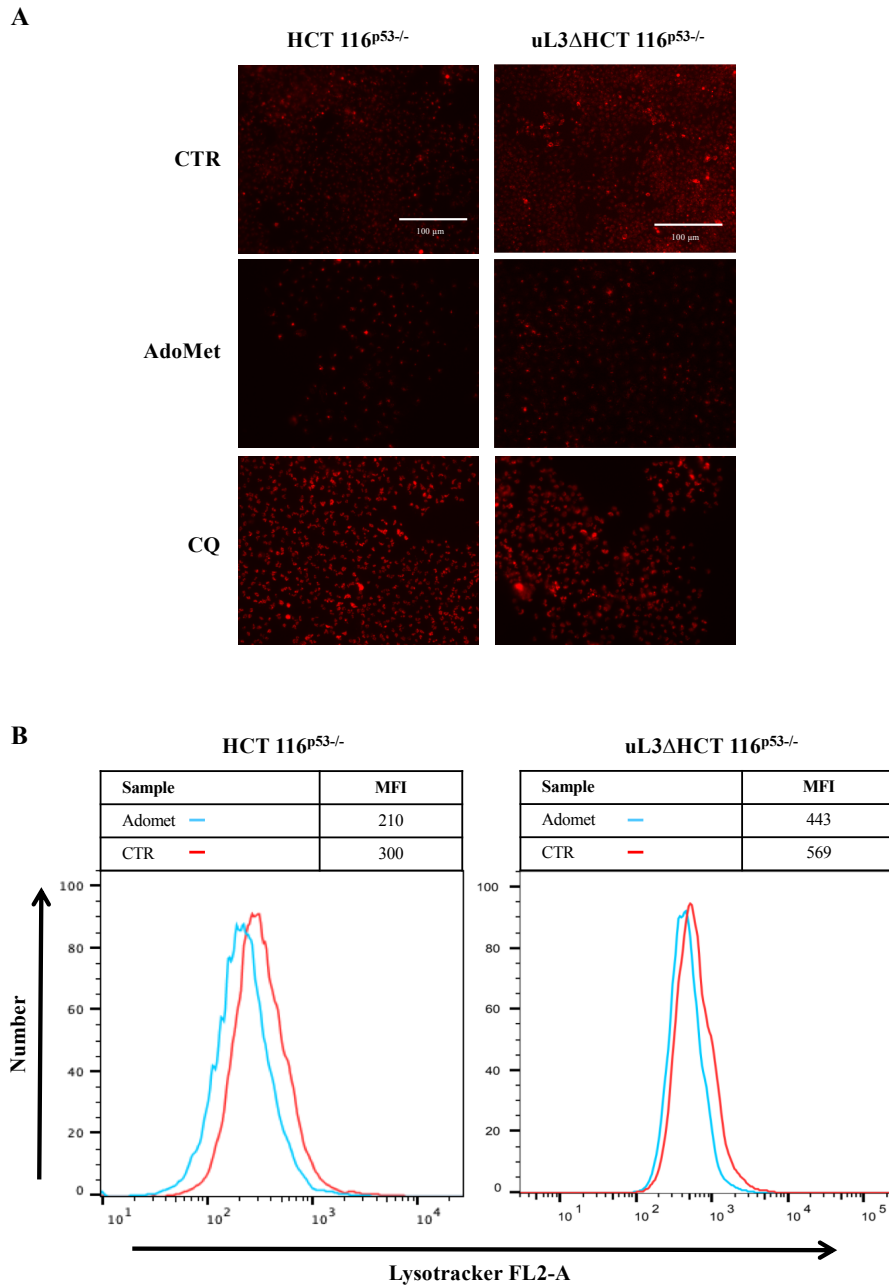
Lysotracker FL2-A

Figure 26. Effect of AdoMet on autophagic flux in HCT 116$^{p53-/-}$ and uL3ΔHCT 116$^{p53-/-}$ colon cancer cells. (A) Representative images of vital dye LysoTracker (LTR) staining of HCT 116$^{p53-/-}$ and uL3ΔHCT 116$^{p53-/-}$ cells treated or not (CTR) with 500 μM of AdoMet for 48 h analyzed by fluorescence microscopy. Chloroquine (CQ) was used as a positive control. (B) Flow cytometry analysis of HCT 116$^{p53-/-}$ and uL3ΔHCT 116$^{p53-/-}$ labeled with LTR. Median fluorescence values are shown in the graphs. At least 2×10^4 events were acquired in log mode. For the quantitative evaluation of LTR, FlowJo software was used to calculate median fluorescence intensities (MFI) by the formula (MFI-treated/MFI-control). The experiments were repeated three times.

Based on these results, we proceed in attempt to further characterize the effect of AdoMet on autophagic flux by analyzing the expression levels of some crucial autophagy-related proteins as LC3BI/II, Atg7 and p62, through Western blotting. These proteins are essential during autophagy activation, when LC3BI is cleaved and lapidated by the coordinated activity of

several proteins including Atg7 with consequent formation of LC3BII that is incorporated into the autophagosome membranes. Hence, p62 binds to and sequesters ubiquitinated proteins into autophagosomes; in this process p62 is itself degraded (Galluzzi et al., 2017). Western blot analysis revealed that in both cell lines AdoMet treatment led to a decrease of Atg7 and a significant increase of p62 (Figure 27A,B), which was associated to a reduction in the ratio between LC3BII and LC3BI (Figure 27C,D). These data clearly indicate that AdoMet exerts an inhibitory effect on autophagic flux in both cell lines.
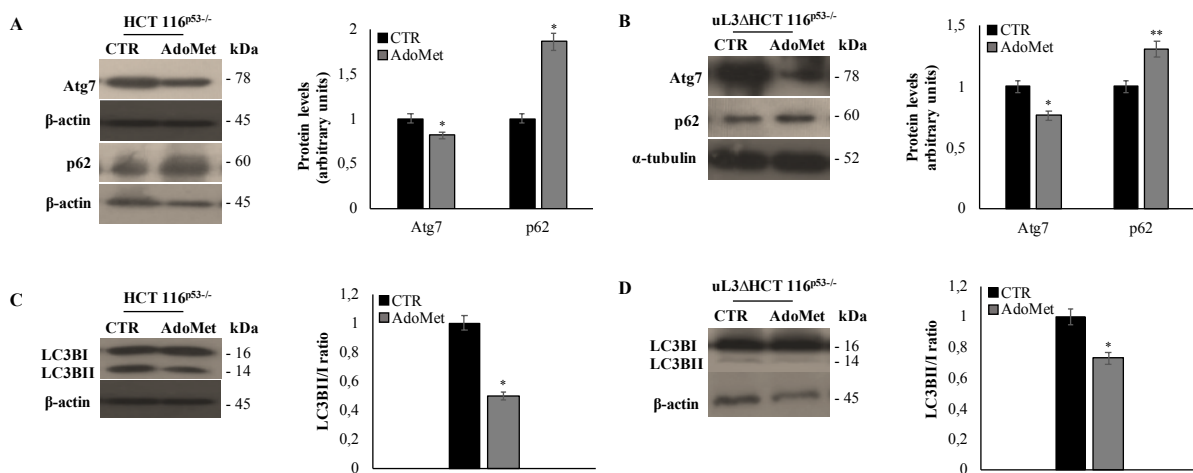

Figure 27. Effect of AdoMet on the autophagy related markers in HCT 116$^{p53-/-}$ and uL3ΔHCT 116$^{p53-/-}$ colon cancer cells. Representative immunoblotting of ATG7, p62, and LC3BI/II in HCT 116$^{p53-/-}$ cells (A,C) and uL3ΔHCT 116$^{p53-/-}$ cells (B,D) treated or not with 500 µM AdoMet for 48 h. The housekeeping protein β-actin was used as a loading control; graphs show the relative densitometric analyses, expressed as arbitrary units. Quantification of the LC3B-II/I ratio is shown in the graphs. Bars represent the mean of triplicate experiments; error bars represent the standard deviation. * p < 0.05, ** p < 0.01 vs. untreated cells set at 1.

In conclusion, our findings led us to propose a model on the mechanisms underlying AdoMet anticancer activity in colon cancer cells deleted of p53 and expressing low levels of uL3. Specifically, AdoMet arrests cell cycle at the S phase, suppresses autophagic flux, increases ROS generation, and ultimately induces apoptotic cell death. Consistently, AdoMet leads to a strong reduction of Cyclin D1 levels and a significant increase of pro-apoptotic caspase 3/8/9 activation and PARP-1 cleavage (Figure 28).

To our knowledge, results reported in this study provides, for the first time, a new exploratory perspective to consider AdoMet, a naturally-occurring multifunctional sulfonium compound, as a promising agent for overcoming the drug resistance of colon cancer cells showing p53 and uL3 lower levels.
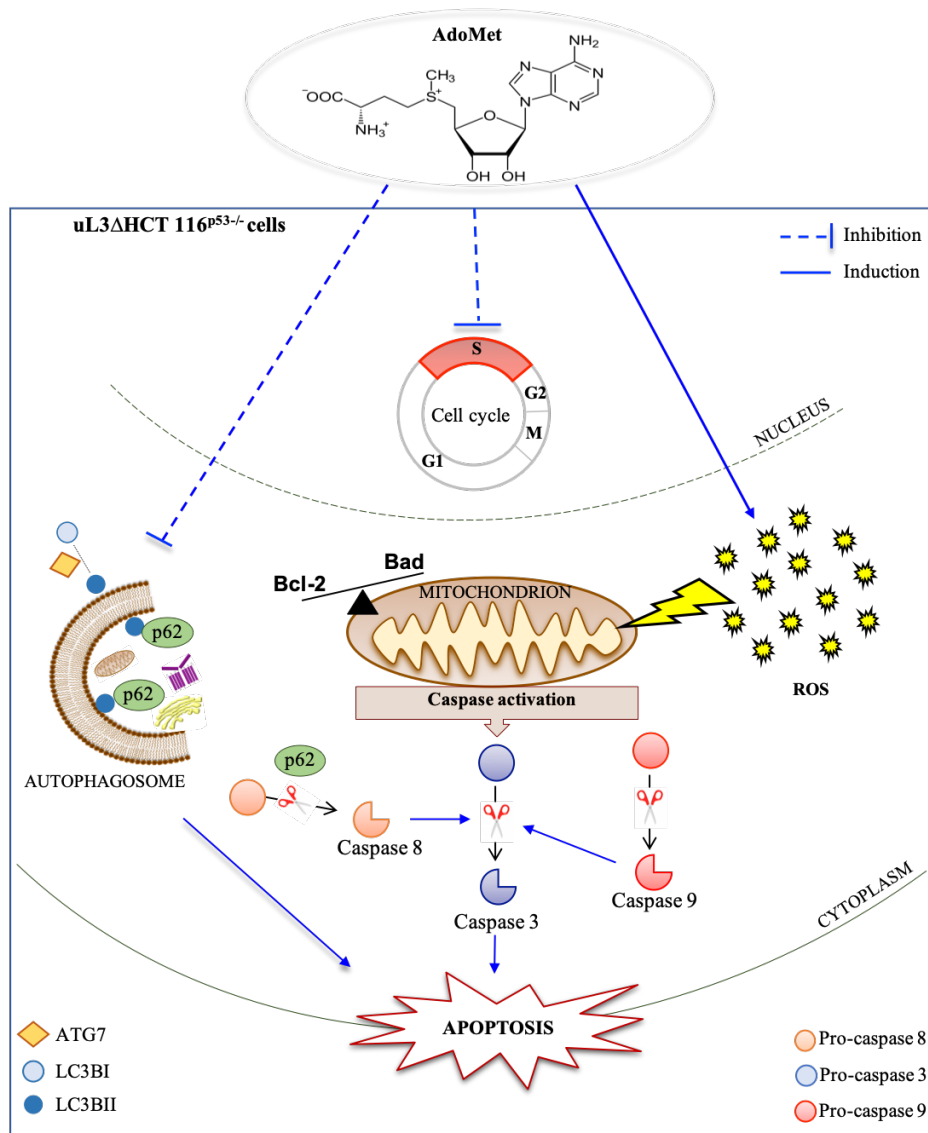
Figure 28. Schematic representation of the proposed model of AdoMet effects in uL3ΔHCT 116$^{p53-/-}$ colon cancer cells. AdoMet treatment affected cell proliferation causing cell cycle arrest in the S phase. The inhibition of the autophagic process and induction of ROS upon exposure to AdoMet led to activation of the caspase cascade, triggering the apoptotic pathway.

SECTION IV

uL3 is a key mediator of stress response pathway activated by a specific G-quadruplex TBA derivative

The pathogenesis of cancer is very complex, and finding novel anti-cancer drugs with high selectivity and few adverse effects is still one of the major challenges in the field of the anti-cancer drug research.

Nucleic acid aptamers are relatively short single-stranded DNA and RNA oligonucleotides showing high affinity and specificity for a given target molecule (Zhou et al., 2017). Generally, they are discovered by SELEX technology, an *in vitro* iterative selection procedure that starts from random oligonucleotide sequences and through selection and amplification steps, leads to the identification of ligands able to adopt peculiar tridimensional structures. During the SELEX process, one of the most important characteristic of aptamers is their ability to fold in properly stable secondary structures (Wu et al., 2016). In particular, typical structural motives found in aptamers are hairpins, pseudoknots, and loops. Of note, a considerable number of aptamers selected against biologically relevant protein targets are characterized by G-rich sequences, that can fold into G-quadruplex structures, which are among the most stable nucleic acid conformations (Roxo et al., 2019). The core unit of a G-quadruplex is constituted by a planar squared arrangement of four guanines (G-tetrad) interconnected by eight Hoogsteen hydrogen bonds. Two or more G-tetrads can stack on each other, originating the G-quadruplex structure, which is further stabilized by cations accommodated in its cavity. The outstanding polymorphism of the G-quadruplex structures is the key feature that grants to the G4-aptamers the ability to interact with several different targets (Roxo et al., 2019).

Recently, G-quadruplex-based aptamers (G4-aptamers) have attracted ever-growing attention because of their ability to activate potent antiproliferative effects in a variety of cancer cell lines (Ogloblina et al., 2018). In this context, the thrombin binding aptamer (TBA), formerly developed as an anticoagulant agent, has lately aroused great interest as a potential anticancer agent by virtue of its remarkable antiproliferative activity, relatively reduced size and its ability to fold in a well-defined antiparallel chair-like right-handed G-quadruplex structure (Virgilio et al., 2020). In particular, TBA adopted structure is characterized by two stacked G-tetrads connected through three loops, specifically two small TT and one large TGT loops (Figure 29). However, TBA has been undergone to several chemical modifications in order to

improve its antiproliferative activity, thermal stability and resistance to enzymes in physiological conditions (Esposito et al., 2018[a]; Virgilio et al., 2020).
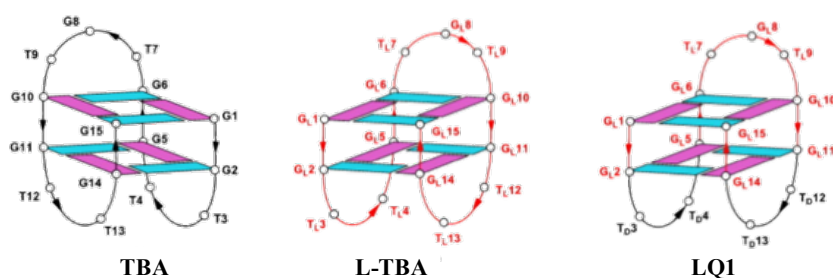

Figure 29. Proposed G-quadruplex structures for the TBA and its derivatives, L-TBA and LQ1 (Table 2). *Anti* and *syn* guanosines are indicated in light blue and purple, respectively. Arrows indicate the 5′–3′ orientation. D- and L-residues are labelled in black and red, respectively. (Image adapted from Esposito et al., 2017)

Published data from our group reported the antiproliferative activity of many TBA derivatives on two different cancer cell lines, Calu-6 and HCT 116$^{p53-/-}$ (Esposito et al., 2017). Among these previously investigated TBA derivatives, L-TBA and LQ1 (formerly D13) aroused our interest since they are characterized by no anticoagulant activity and remarkable resistance to nucleases. Specifically, L-TBA is composed exclusively by L-residues, whereas LQ1 is constituted by L-nucleosides except for those ones in the small loops (Figure 29 and Table 2).

Table 2. Sequences of TBA and its derivatives.

Name	Sequence
TBA	5'-GGTTGGTGTGGTTGG-3'
L-TBA	5'-ggttggtgtggttgg-3'
LQ1	5'-ggTTggtgtggTTgg-3'
LQ2	5'-ggTtgggtgtggTtgg-3'
LQ3	5'-ggtTgggtgtggtTgg-3'

D and L residues are indicated in upper and lower case, respectively.
The residues in the small loops are highlighted in red.

The aim of the present study is to investigate the molecular mechanism of L-TBA and LQ1 cytotoxic activity in p53-deleted colon cancer cells. In addition, we analyze the antiproliferative activity of two further G-quadruplex aptamer TBA derivatives, namely LQ2 and LQ3, differing from LQ1 only by the D/L-residues composition of the small loops and specifically designed to maintain thymidines T4 and T13, important for structural stability (Table 2).

3.16 uL3 is essential to mediate cell response to LQ1 treatment in colon cancer cells

Firstly, we proceed in attempt to evaluate the cytotoxic activity of the new G-quadruplex oligodeoxynucleotides (ODNs), LQ2 and LQ3 compared to that of TBA, L-TBA and LQ1 recently published (Esposito et al., 2017). To this aim, HCT 116$^{p53-/-}$ cells were treated with 10 and 50 μM of these ODNs and cell cytotoxicity was assessed at 24, 48, and 72 h of treatment by the 3-(4,5-dimethylthiazol-2-yl)-2,5-diphenyltetrazolium bromide (MTT) assay. As shown in Figure 30A, we observed that upon LQ2 and LQ3 treatment cells showed an higher viability compared to that of the same cells treated with the others ODNs at both concentrations and all time points. Specifically, HCT 116$^{p53-/-}$ cells retained about 60% of viability compared to control cells upon 48 h of treatment at 50 μM with LQ2 and LQ3; while, the viability of cells treated with TBA, L-TBA, and LQ1 in the same experimental conditions was about 20%–30%. Furthermore, we evaluated the cytotoxic activity of all ODNs in uL3ΔHCT 116$^{p53-/-}$ cells. Results shown in Figure 30B demonstrate that in condition of uL3 silencing the cytotoxic activity of TBA, L-TBA, LQ2, and LQ3 did not changed significantly compared to that observed in parental cells at both concentrations and all time points.

These findings clearly indicate that the cytotoxicity activity of these ODNs was independent of uL3 status. Interestingly, uL3 silencing completely abrogated the cytotoxicity effect of LQ1. In fact, in uL3ΔHCT 116$^{p53-/-}$ cells treated with LQ1 we found an higher viability compared to that obtained in cells expressing uL3 at both concentrations and all time points (Figure 30B).

These results strongly indicate that uL3 plays a crucial role in mediating cell response to LQ1 treatment in colon cancer cells devoid of p53.
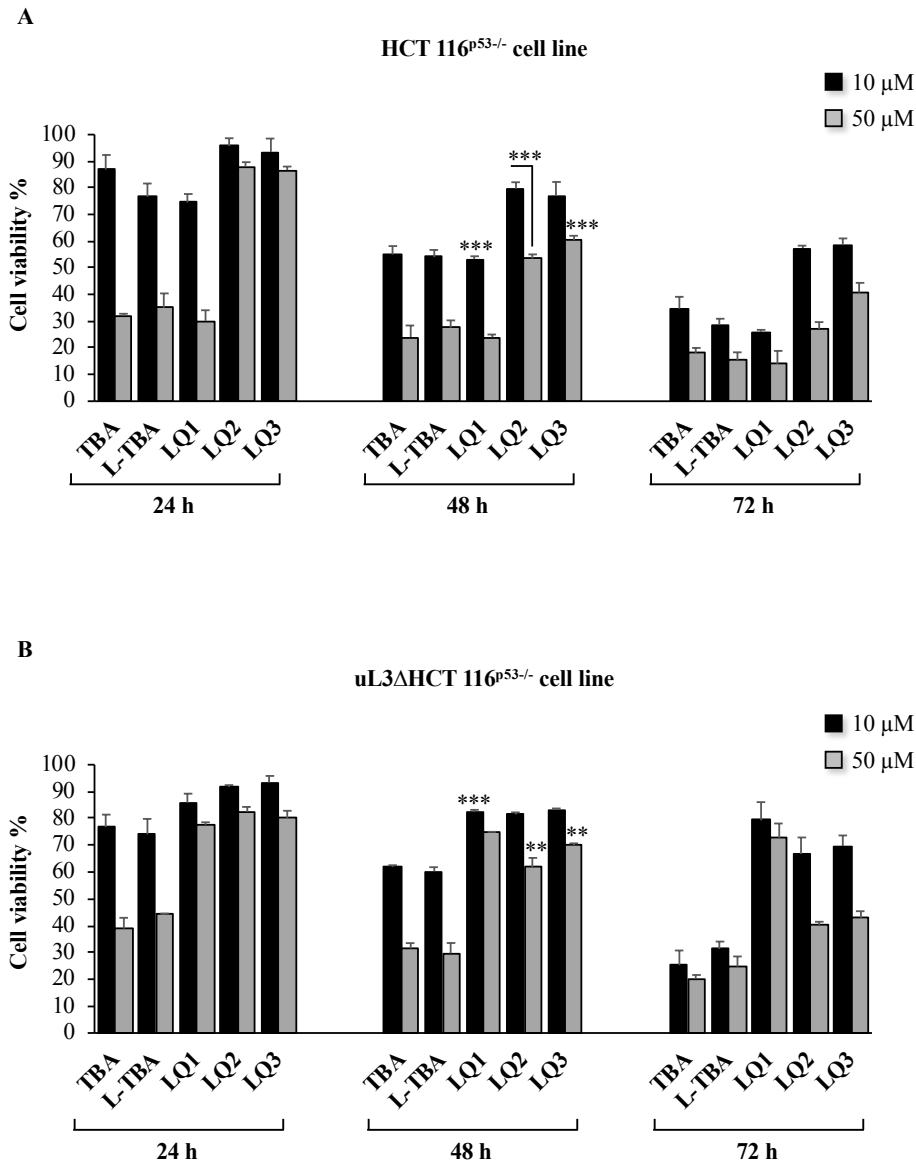
Figure 30. Cytotoxic activity of L-TBA and its derivatives on HCT 116$^{p53-/-}$ (A) and uL3ΔHCT 116$^{p53-/-}$ (B) cells. Cells have been treated with 10 and 50 μM of ODNs from 24 to 72 h. Cell viability was assayed using the MTT assay. Results are presented as percentage of the untreated cells. Bars represent the mean of triplicate experiments; error bars represent the standard deviation. ** $p < 0.01$, *** $p < 0.001$ vs. untreated cells set at 100%.

3.17 LQ1 causes nucleolar stress and impairs rRNA processing

As previously reported, our findings demonstrate that uL3 is an essential mediator of p53-independent pathways activated in response to nucleolar stress. In this light and based on the results of previously described MTT assays, suggesting a role of uL3 in the cytotoxic activity of LQ1, we suppose that the cytotoxic effect of this ODN might be mediated by a nucleolar stress pathway involving uL3. To explore this hypothesis, we evaluated the expression levels of uL3 and other RPs, uL5(RPL11), uL11(RPL12), uL18(RPL5), uS12(RPS23), that are well

known to be involved in the nucleolar stress response, along with the nucleolar marker B23 (Nucleophosmin). For this purpose, HCT 116$^{p53-/-}$ and uL3ΔHCT 116$^{p53-/-}$ cells were incubated with 10 μM of LQ1 for 48 h. Then, the mRNAs levels of indicated proteins were assessed by RT–qPCR with specific primers (Table 1). As shown in Figure 31A, in HCT 116$^{p53-/-}$ cells LQ1 treatment led to a strong increase of uL3, uL5, uL11, and uL18 expression levels associated to a reduction in B23 transcript levels. Of note, the observed deregulation in the expression profile of these proteins upon LQ1 treatment is a peculiar characteristic of the activation of nucleolar stress response pathway (Russo et al., 2017[a]). In cells stably silenced of uL3, LQ1 treatment did not cause any significant alteration in the mRNA levels of all tested proteins (Figure 31B).

All together these results clearly indicate that LQ1 treatment is associated to the induction of nucleolar stress response depending on uL3 status.

Starting from the notion that the deregulated expression of some RPs observed during nucleolar stress is strictly interconnected with unbalance in the amount of rRNAs (Russo et al, 2017[a]), we evaluated also the amount of pre-rRNA 47S, a single long transcript that is then cleaved and processed to generate the mature 28S, 18S, and 5.8S rRNAs (Aubert et al., 2018). In cells expressing normal levels of uL3, LQ1 treatment led to an accumulation of about 40% of the 47S pre-rRNA (Figure 31A); whereas in uL3 deleted cells, LQ1 failed to cause this effect since the production of the 47S pre-rRNA appeared to be unchanged compared to untreated cells (Figure 31B).

Next, we wondered whether LQ1 treatment could impair pre-rRNA processing (schematically reported in Figure 31C). To this aim, both cell lines were treated with 10 μM of LQ1. 48 h later, total RNA was extracted from cell lysates and the relative abundance of precursors and mature rRNAs was determined by RT–qPCR with specific primers (Table 1). The 47S pre-rRNA is cleaved at sites A' and 02 (located in the 5'-ETS and 3'-ETS, respectively) with consequent generation of 45S pre-rRNA (Figure 31C). Results shown in Figure 31D indicated that in parental cells LQ1 treatment caused an increase of 45S transcript associated to a marked accumulation of 36S pre-rRNA. It has been reported that the 36S pre-rRNA is normally expressed at low levels in normal cells and its presence is a consequence of the inhibition of processing at site 2 within ITS1 (Figure 31C). Interestingly, the accumulation of this characteristic precursor could not impair the subsequent processing steps leading to 5.8S and 28S rRNAs (O'Donohue et al., 2010). In fact, upon LQ1 treatment the levels of 32S pre-rRNA, 28S, and 5.8S rRNAs were comparable with untreated cells (Figure 31D). It is noteworthy that in cells stably silenced for uL3 LQ1 treatment did not cause a significant

alteration in the expression levels of 45S and 36S pre-rRNAs (Figure 31E). These findings demonstrate that uL3 plays a pivotal role in the activation of this characteristic alternative maturation pathway that, in turn, triggers nucleolar stress pathway. Furthermore, in cells expressing uL3 LQ1 treatment also caused an increase of about 30% of 30S pre-rRNA, the precursor of 18S rRNA, due to the inhibition of processing within 5′ETS leading to a significant decrease (about 50%) of 18S rRNA, as shown in Figure 31D.

All together these data demonstrate that the mechanism of action of LQ1 is strictly correlated to the inhibition of pre-rRNA processing.
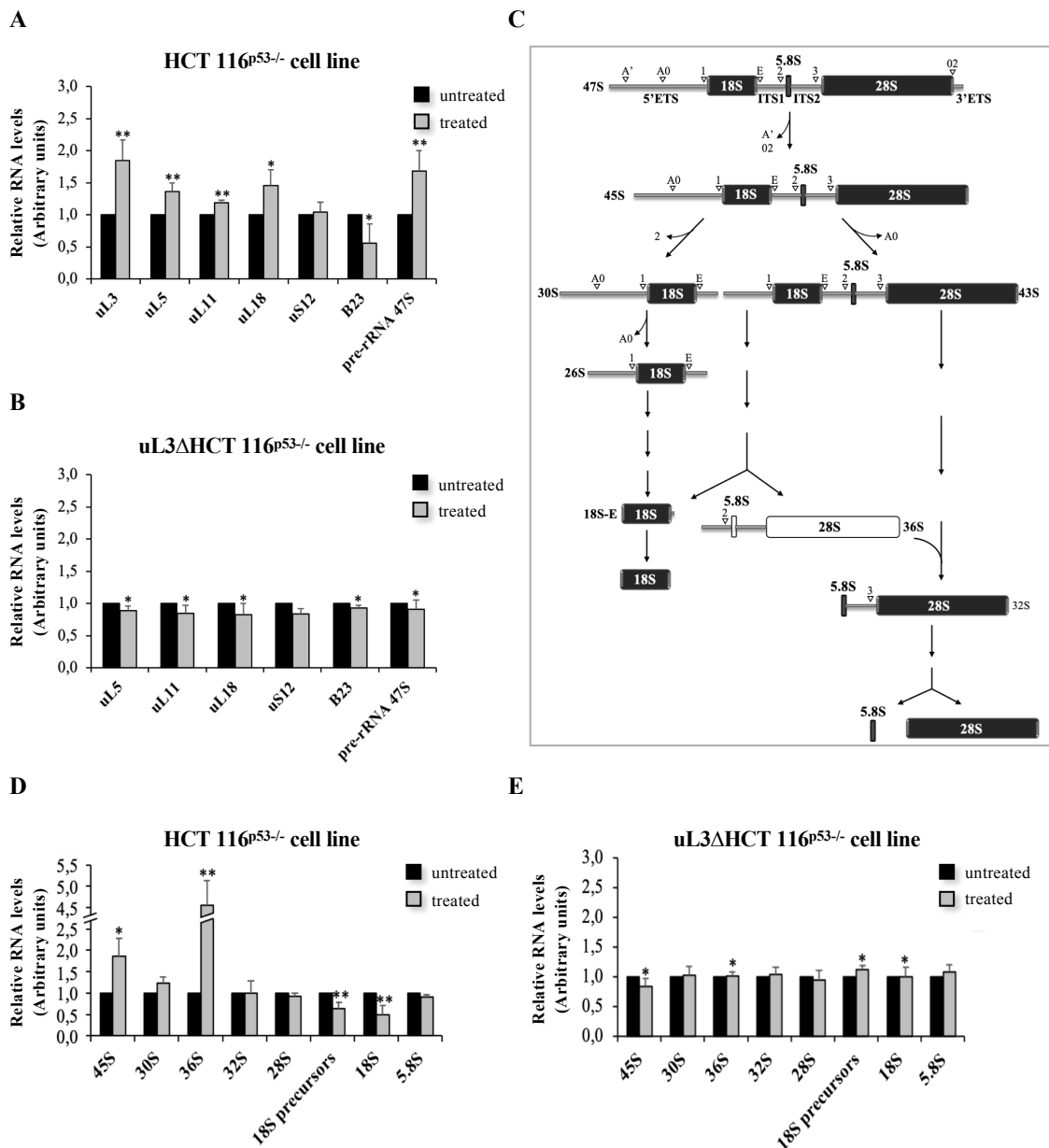
Figure 31. LQ1 treatment induces nucleolar stress and impairs rRNA processing. Total RNA from HCT 116$^{p53-/-}$ (A) and uL3ΔHCT 116$^{p53-/-}$ (B) cells, untreated or treated with 10 μM of LQ1 for 48 h, was subjected to RT–qPCR with primers specific for indicated genes (Table 1). Quantification of signals is shown. Bars represent the mean of triplicate experiments; error bars represent the standard deviation. * p < 0.05, ** p < 0.01 vs. untreated cells set at 1. (C) Schematic representation of

ribosomal gene processing. Relative expression levels of rRNAs, from HCT 116$^{p53-/-}$ (D) and uL3ΔHCT 116$^{p53-/-}$ (E) cells, untreated or treated with 10 μM of LQ1 for 48 h analyzed by RT–qPCR with primers specific for intermediates and mature rRNAs (Table 1). Bars represent the mean of triplicate experiments; error bars represent the standard deviation. * p < 0.05, ** p < 0.01 vs. untreated cells set at 1

3.18 LQ1 treatment leads to cell cycle arrest and induces early apoptosis

Several studies have been reported that the activation of nucleolar stress pathways ultimately lead to cell cycle arrest and/or induction of apoptosis (Russo et al., 2017[a]). Hence, to further investigate the mechanism by which LQ1 is able to activate nucleolar stress, we analyzed cell cycle distribution in HCT 116$^{p53-/-}$ and uL3ΔHCT 116$^{p53-/-}$ cells treated with 10 μM of LQ1 for 48 h. Then, cell cycle analysis was performed by flow cytometry. As shown in Figure 32A, upon LQ1 treatment, we observed an increase in the percentage of cells in the G2/M phase (from about 13% to about 29%) associated to a decrease in that in the G0/G1 phase (from about 74% to about 48%), whereas the percentage of cells in the S phase was unchanged. These data demonstrate that LQ1 induces a delay in cell cycle progression by inducing G2/M arrest in cells expressing uL3. Interestingly, LQ1 treatment resulted ineffective in cells stably silenced for uL3. In fact, upon LQ1 exposure the cell cycle distribution was not affect (Figure 32B) suggesting that uL3 is essential to mediate cell cycle arrest caused by LQ1 treatment.

To confirm this hypothesis, we analyzed the expression levels of crucial regulator of the G2/M transition, as Cyclin B1, CDK1, and Cyclin A (Kousholt et al., 2012). To this purpose, both cell lines were incubated with LQ1 at 10 μM for 48 h. Then, total RNA was extracted from cells and analyzed for the expression of these cell cycle-related genes (Table 1). In HCT 116$^{p53-/-}$ cells, LQ1 led to a decrease of Cyclin A (CycA) levels associated to a remarkable reduction of Cyclin B1 (CycB1) levels. These results are consistent with those obtained from cell cycle analysis indicating that LQ1 treatment caused G2/M arrest (Figure 32C). On the other hand, CDK1 mRNA levels were not significant altered upon LQ1 exposure, revealing that CDK1 was not involved in G2/M arrest induced by LQ1.

In addition, we also evaluated the expression levels of p21, a well-known cyclin-dependent kinases inhibitor. As shown in Figure 32C, we found an increase of p21 in LQ1 treated cells compared to control cells. Of note, these effects were abolished in condition of uL3 silencing (Figure 32D).

Furthermore, cell cycle analysis revealed that in HCT 116$^{p53-/-}$ cells LQ1 treatment is associated with the presence of a sub G0/G1 population that is representative of apoptotic

cells (Figure 32A), while in cells stably silenced for uL3 we did not observe the sub G0/G1 population (Figure 32B). Based on these findings, we assessed the expression levels of the pro-apoptotic protein Bax and the anti-apoptotic protein Bcl-2. As expected, LQ1 treatment led to a strong induction of Bax associated to a decrease of Bcl-2 in parental cells (Figure 32C). In contrast, When uL3 was switched off, LQ1 exposure induced a strong increase of anti-apoptotic Bcl-2 (Figure 32D), suggesting the activation of mechanisms of resistance to the apoptosis caused by LQ1 (Willis et al., 2003).

With the aim to confirm that LQ1 exerts its cytotoxic activity through the induction of apoptosis, we carried out Annexin V-Alexa Fluor 488/PI dual staining. To this purpose, HCT 116$^{p53-/-}$ cells and uL3ΔHCT 116$^{p53-/-}$ cells were incubated with 10 μM of LQ1. 48 h later, apoptosis was analyzed by Annexin V-Alexa Fluor 488. We found that LQ1 treatment caused a strong increase of the percentage of early apoptotic cells (from 1% in the untreated cells to 30% in treated cells) in HCT 116$^{p53-/-}$ cells (Figure 32E), indicating that the induction of apoptosis plays an essential role in the antiproliferative activity of LQ1. In contrast, when uL3 was switched off, LQ1 failed to induce apoptosis (Figure 32F), demonstrating that uL3 is necessary for the activation of apoptosis induced by LQ1.

Overall, these findings strongly indicate that LQ1 effects on cell cycle progression and on apoptosis depends on uL3 status.
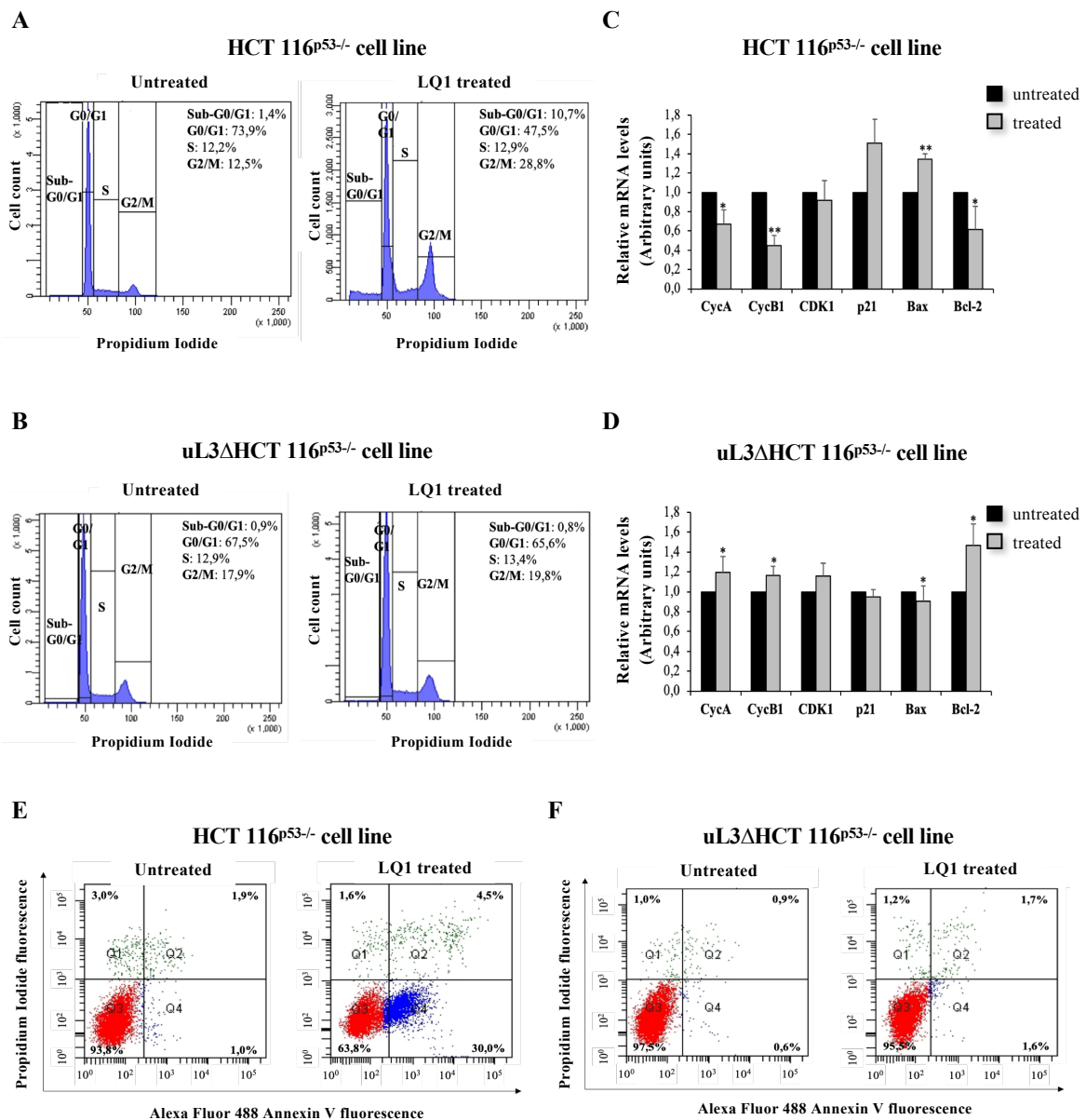
Figure 32. LQ1 treatment leads to cell cycle arrest and induces early apoptosis in colon cancer cells. HCT 116$^{p53-/-}$ (A) and uL3ΔHCT 116$^{p53-/-}$ (B) cells were incubated with 10 μM of LQ1 for 48 h, and the cell cycle distribution was evaluated using PI staining and flow cytometry analysis. Total RNA from HCT 116$^{p53-/-}$ (C) and uL3ΔHCT 116$^{p53-/-}$ (D) cells, untreated or treated with 10 μM of LQ1 for 48 h, was subjected to RT–qPCR with primers specific for indicated genes (Table 1). Quantification of signals is shown. Bars represent the mean of triplicate experiments; error bars represent the standard deviation. * $p < 0.05$, ** $p < 0.01$ vs. untreated cells set at 1. HCT 116$^{p53-/-}$ (E) and uL3ΔHCT 116$^{p53-/-}$ (F) cells were incubated with 10 μM of LQ1 for 48 h. Then, cell death was assessed by FACS analysis of Annexin V and PI staining. Representative dot plots are shown.

All together our data led us to propose a model on the mechanism of action of the G4-aptamer LQ1 in colon cancer cells devoid of p53. Specifically, LQ1 impairs rRNA processing leading to the activation of nucleolar stress response that, in turn, causes cell cycle arrest in the G2/M phase and induces apoptotic cell death (Figure 33). Importantly, all these effects are abolished

in cells stably silencing for uL3. Therefore, we identify a novel p53-independent and uL3-dependent nucleolar stress response pathway activated by a specific G-quadruplex TBA derivative.

To best of our knowledge, our study provides the first evidence of a connection between the antiproliferative activity of G4-aptamers and alteration of the nucleolar function leading to the activation of the nucleolar stress pathway. Several reports indicate that cancer cells are characterized by higher production of ribosomes, thus resulting more sensitive to drugs that impair nucleolar functions and induce the nucleolar stress (Carotenuto et al., 2019). In this light, our data might have a considerable value in the development of new targeted anticancer therapies for colorectal tumors lacking functional p53 and showing low expression levels of uL3 protein.
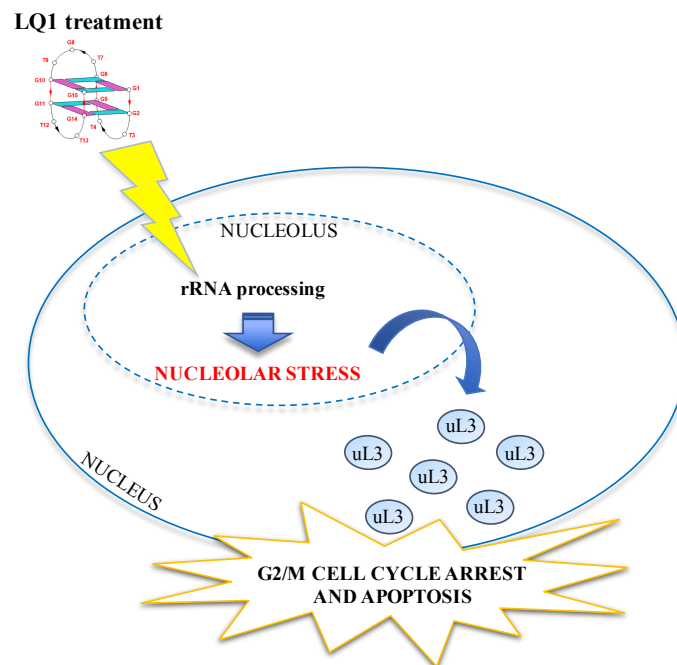

Figure 33. Schematic representation of the proposed model of LQ1 effects in colon cancer cells devoid of p53. LQ1 treatment impairs rRNA processing leading to the activation of nucleolar stress response that, in turn, causes cell cycle arrest in the G2/M phase and induces apoptotic cell death.

4. DISCUSSION

Over the past decades, a plethora of research work has investigate more in details the mechanisms underlying the tumor biology with the aim to identify novel targeted therapeutic approaches improving the current treatment outcome for cancer patients. In this light, different studies have focused on the specific molecular alterations of cancer cells highlighted the functional link between the nucleolus and cancer (Carotenuto et al., 2019). In fact, large and abnormal nucleoli are observed in most cancer cells as a direct consequence of the over-activation of ribosome biogenesis necessary to sustain uncontrolled proliferation. In addition, the nucleolus as the main stress sensor in cells has started to be considered as an emerging hallmark of cancer and many therapeutic interventions targeting nucleolus have been developed (Carotenuto et al., 2019). Specifically, a growing amount of evidence have indicated that the perturbation in pre-rRNA processing or alteration in the RPs content hindering ribosome biogenesis induce the nucleolar stress response. In this condition a sub set of RPs translocates to the nucleoplasm where can exert their extra-ribosomal function leading to cell cycle arrest and/or apoptosis (Russo et al. 2017[a]). Among these RPs, our group have extensively investigated the extra-ribosomal functions of ribosomal protein uL3 in lung and colon cancer cells. Specifically, our previous studies have indicated uL3 is a key mediator of nucleolar stress pathway induced by chemotherapeutics as 5-FU, Act D, and OHP independently from p53 status (Russo et al. 2017[a]).

In this context, the studies presented in this thesis allowed us to go more in depth in understanding the mechanism by which uL3 is able to activate nucleolar stress pathway and the role of this protein in chemoresistance. More specifically, our findings demonstrated that uL3 inhibits RNA Pol I function with consequent reduction of 47S pre-rRNA production. Moreover, analysis of rRNA processing indicated that uL3 over-expression is associated to defects in the processing of 47S pre-rRNA with consequent accumulation of 45S, 30S pre-rRNAs and mature rRNAs (28S and 18S). On the other hand, the silencing of uL3 induced a strong accumulation of 36S and 45S pre-rRNAs whereas the levels of 28S, 18S, and 5,8S resulted only slightly affected. These results suggest that alteration in the expression levels of uL3 causes nucleolar stress by interfering with synthesis and maturation of pre-rRNAs (Pecoraro et al., 2020[a]).

Based on our previous results indicating that in condition of Act D-induced nucleolar stress uL3 protein accumulates as ribosome-free form (Russo et al., 2016[b]), we procced in an attempt to better characterize subcellular localization of ribosome-free uL3. Here, we show that ribosome-free uL3 traslocates from the nucleolus to the nucleoplasm where it can exert

its extra-ribosomal functions. Specifically, our findings demonstrate that in HCT 116$^{p53-/-}$ upon Act D treatment, uL3 is able to negatively regulate the expression of E2F1 which was associated to down-regulation of Cyclin D1 and up-regulation of proapoptotic gene Bax (Pecoraro et al., 2019). Of note, in colon cancer cells stably silenced of uL3 Act D treatment caused a strong increase of E2F1, Cyclin D1, and anti-apoptotic Bcl-2 gene expression. Overall, these results indicate that uL3 is a key mediator of Act D-induced cell cycle arrest through the regulation of crucial cell cycle and cell proliferation proteins. Remarkably, in both cell lines Act D treatment did not affect the phosphorylation status of Rb protein suggesting that uL3 mediated regulation of E2F1 differ from that generally reported (Bertoli et al., 2013).

Published studies indicate that increasing expression levels of E2F1 and Cyclin D1 are correlated with malignant progression in many types of tumor (Ma et al., 2013; John et al., 2017). In particular, Cyclin D1 is involved in the transcriptional regulation of genes necessary for cell migration (Li et al., 2006). According to this, in condition of uL3 silencing we found that hyperactivation of E2F1 promoter and the up-regulation of Cyclin D1 was associated to a marked increase in cell motility and EMT transition. Based on the concept that EMT is a tissue remodeling process reactivated during tumor progression, we infer that the low expression of uL3 results in a more aggressive and invasive cancer phenotype in colon cancer cells devoid of p53. Notably, the increased amount of Cyclin D1 also represents a mechanism of drug resistance in different types of cancers (Kothari et al., 2012). For all these reason, it is not surprising that Cyclin D1 expression is finely regulated at multiple levels (Klein et al., 2008). Here, we have demonstrated that uL3 plays a central role in the regulation of Cyclin D1 intracellular amounts. In fact, when uL3 expression was switched off we observed an increase in the stability of Cyclin D1 at mRNA and protein levels compared with those in parental cells. Based on these results, we speculate that uL3 might control Cyclin D1 expression acting on the stability of mRNA and protein (Pecoraro et al., 2019).

With regards to the molecular mechanisms by which uL3 regulates E2F1 promoter activity, we found that uL3 specifically co-immunoprecipitate with PARP-1, a nuclear enzyme required for genomic stability and chromatin remodeling and well known as the main positive regulator of E2F1 promoter activity in cells (Simbulan-Rosenthal et al., 2003). Furthermore, data from luciferase assay upon uL3 and PARP-1 co-expression demonstrate that uL3 acts as repressor of E2F1 promoter activity suggesting that uL3 may bind PARP-1 and sequester it from the E2F1 promoter. These findings lead us to propose PARP-1 as a new molecular target of uL3 (Pecoraro et al., 2019).

Data from RNA-seq analysis in HCT 116$^{p53-/-}$ cells in presence or absence of uL3 and in condition of nucleolar stress activated by Act D have revealed that several processes underwent dramatic changes in dependence of the uL3 status. Interestingly, in HCT 116$^{p53-/-}$ cells treated with Act D we observed an up-regulation of mTORC1, IL6_JAK_STAT3 compared to untreated cells whereas in uL3ΔHCT 116$^{p53-/-}$ we found a down-regulation of mTORC1, PI3K_AKT_mTORC1 and WNT_Beta_Catenin (Pecoraro et al., 2020[a]).

It is well known that mTORC1 (mTOR complex 1) is considered as a master regulator of autophagy machinery that is constituted by more than 30 autophagy-related (ATG) proteins (Chun et al., 2018). Specifically, mTORC1 inhibition was necessary for the induction of the autophagic process (Dossou et al., 2019). According to this, our results strongly indicate a role of uL3 as inhibitor of autophagy.

Autophagy is a self-degradative system involved in keeping cellular homeostasis and survival (Chun et al., 2018). It has been reported that a variety of cellular stressors can induce either autophagic response than nucleolar stress including lack of nutrients, hypoxia, low energy, UV exposure, chemical compounds and different anticancer agents (Pecoraro et al., 2020[b]). Therefore, it is not surprising that the alteration of autophagy process is associated with the development of different disease including cancer. However, there are different examples of tumor types in which autophagy plays a tumor suppressive role and others in which autophagy support cancer cells growth. Hence, the role of autophagy in cancer is complex and strictly dependent on cell context representing a double-edge sword in tumor progression (Pecoraro et al., 2020[b]).

Analysis of the autophagic flux by confocal microscopy indicated that the ectopic expression of uL3 in HCT 116$^{p53-/-}$ cells was associated to a marked suppression of autophagic flux. Moreover, in this condition the treatment with RAPA, a well known inducer of autophagic flux (Benjamin et al., 2011), failed to exert its positive effect on autophagy whereas the treatment with CQ, an inhibitor of autophagy (Mauthe et al., 2018), hampered autophagic process. Notably, in uL3 deleted cells the autophagic flux was significantly enhanced and CQ failed to exert its inhibitor role on autophagy. In addition, the restoration of uL3 in uL3ΔHCT 116$^{p53-/-}$ cells interfered with the induction of autophagy by RAPA. These results were also confirmed by RT-qPCR experiments aimed to evaluate the expression levels of mRNAs coding for protein components of autophagy initiating ULK complex.

Altogether, these data clearly identify uL3 as an inhibitor of autophagic flux in colon cancer cells lacking p53 (Pecoraro et al., 2020[a]).

Recent studies unveiled a complex relationship between autophagy and EMT in cancer (Chen et al., 2019). Intriguingly, the effect of autophagy on EMT seems to be presumably dependent on the cellular type and on the stimulus that induces or inhibits the autophagic process. Of note, in our experimental model, the lower expression of uL3 is associated to enhancement of autophagic flux and EMT phenotype (Pecoraro et al., 2019; Pecoraro et al., 2020[a]). These observations imply a possibility that silencing of uL3 might increase the resistance of p53-deleted colon cancer cells to drug treatment through autophagy activation, enhancement in cell motility and EMT phenotype.

In the field of anticancer therapy, re-sensitizing tumor cells to the drugs by exploiting novel strategies is a promising approach to overcome the drug resistance with consequent improvement in clinical treatment (Bukowski et al., 2020). Nowadays, a growing amount of evidence have indicate that simultaneous inhibition of different signaling pathways by natural compounds might constitute a more suitable therapeutic approach than that of individual inhibitors. In this light, we have become interested in exploring the potential anticancer and anti-proliferative effects of the natural compound AdoMet to overcome drug resistance in the uL3ΔHCT 116$^{p53-/-}$ cell line.

In last decades, numerous *in vitro* and *in vivo* studies have revealed the AdoMet is able to impair the development and the progression of different types of human tumors through its pleiotropic effects on many biological pathways (Mosca et al., 2020[b]). Based on this, the natural compound AdoMet represents an useful strategy to overcome uL3-mediated drug resistance.

In this thesis we have reported results demonstrating that AdoMet induced cell death in uL3 deleted cells in a dose- and time-dependent manner. Of note, the combined treatment with AdoMet plus 5-FU was able to rescue the cytotoxic effects of 5-FU in uL3ΔHCT 116$^{p53-/-}$ cells. These results support the possibility that AdoMet could be a potential therapeutic agent for treatment of resistant colon cancer cells characterized by a low expression profile of uL3 and lacking functional p53.

In particular, in uL3ΔHCT 116$^{p53-/-}$ cells, AdoMet exposure impaired cell cycle progression inducing a remarkable cell cycle arrest at the S phase, which was associated to a significant increase of Cyclin E and a decrease of Cyclin D. Interestingly, our previous data indicated that the up-regulation of Cyclin D in uL3 deleted cells was associated to drug resistance displayed by this cell population (Pecoraro et al., 2019). Hence, we assume that the reduction of Cyclin D levels observed upon AdoMet treatment in uL3ΔHCT 116$^{p53-/-}$ cells is responsible for the re-sensitizing of these cells to drug treatment.

Besides its role in regulating cell cycle progression, Cyclin D plays also a key role in the regulation of apoptosis (Roué et al., 2008). According to this, analysis of apoptosis in uL3ΔHCT 116[p53−/−] cells showed that AdoMet treatment increased the apoptotic cells proportion as in parental cell line (Mosca et al., 2020[(a)]). Furthermore, we found that AdoMet treatment is correlated with an increase in ROS production and a downregulation of Bcl-2 expression in both cell lines (Mosca et al., 2020[(a)]).

Published evidence have indicated that impairments in the autophagy process could be associated with an increase in ROS production that can induce the activation of the intrinsic apoptotic pathway (Kongara et al., 2012). Moreover, recent studies have demonstrated a role of AdoMet in the regulation of autophagy. Specifically, in breast cancer cells AdoMet exhibited a synergistic effect with CQ in inhibiting autophagic flux by targeting the AKT/mTOR pathway (Cave et al., 2018). Consistent with this, we found that AdoMet treatment caused the inhibition of autophagy flux in both cell lines. This effect is particularly interesting in uL3 deleted cells, characterized by a high basal level of protective autophagy.

To best of our knowledge, the present study unveils, for the first time, the capability of AdoMet to re-sensitize drug resistant colon cancer cells indicating this natural compound as a potential therapeutic agent for colon cancer cells lacking of functional p53 and characterized by low expression levels of uL3 (Mosca et al., 2020[(a)]).

In cancer therapy, a considerable number of chemical compounds are attractive based on their antiproliferative activity in different cancer cell lines (Ogloblina et al., 2018). Recently, our group have investigated the antiproliferative activities of several G-quadruplex aptamers derived from the thrombin binding aptamer (TBA) (Esposito et al., 2017; Esposito et al., 2018[(b)]). One of the major challenges in the field of TBA derivatives as anticancer agents is to give a better comprehension on the molecular mechanisms by which these molecules target and kill tumor cells. Herein, we have investigated the molecular mechanism underlying antiproliferative effects of LQ1 in HCT 116[p53−/−] and uL3ΔHCT 116[p53−/−] cells. LQ1 is a previously investigated TBA derivative (Esposito et al., 2017) composed of L-nucleosides except for those in the small loops. Specifically, our findings demonstrate that LQ1 is able to activate a novel p53-independent and uL3-dependent nucleolar stress pathway (Pecoraro et al., 2020[(c)]). In fact, we found that LQ1 treatment is associated to the alteration of expression profile of a specific subset of RPs including uL3, uL5, and uL18, and of the nucleolar marker B23 in HCT 116[p53−/−] cells. Moreover, analysis of the rRNA processing highlighted that LQ1 treatment impairs the processing of 47S pre-rRNA with consequent accumulation of 45S, 36S, and 30S pre-rRNA. These data strongly support LQ1 treatment of HCT 116[p53-/-] cells

hinders ribosome biogenesis trough the inhibition of pre-rRNA processing, with consequent induction of the nucleolar stress response and stabilization of a subset of RPs that are the specific hallmark of this condition (Russo et al., 2017[a]). Of note, LQ1 failed to exert its effects in uL3 deleted cells demonstrating that LQ1 is able to activate a p53-independent but uL3-dependent nucleolar stress pathway. In addition, we have demonstrated that LQ1 treatment causes cell cycle arrest in G2/M and triggers early apoptosis in uL3 expressing cells. Consistently, we found a significant decrease of proteins regulating the cell cycle progression as Cyclin B1 and Cyclin A (Huang et al., 2013) associated to an increase in the expression levels of uL3 and p21. These effects are not present in uL3 deleted cells confirming the crucial role of uL3 in the anticancer activity of LQ1 (Pecoraro et al., 2020[c]). In view of these results, we suppose that LQ1 treatment induces the release of uL3, as ribosome form, and its accumulation in the nucleoplasm, where uL3 positively regulates p21 expression. It has been reported that p21 inhibits mitosis via the degradation of the mitotic cyclins contributing to cell cycle arrest at G2 phase (Shamloo et al., 2019). Hence, we speculate that increased p21 intracellular amount can downregulate Cyclin B1, a master mitotic regulator, that contribute to the induction of G2/M cell cycle arrest. Further research on the molecular mechanisms underlying LQ1 anticancer activity may provide novel therapeutic approaches for targeting tumor cells.

All these findings have extended the scenario of mechanisms of drugs such as 5-FU, OHP and Act D that specifically impairs ribosome biogenesis highlighting the essential role of human uL3 protein as a mediator of nucleolar cell response pathway. In particular, our results might have a significant value in the development of new targeted therapies for the treatment of cancers lacking functional p53 and characterized by low expression levels of uL3, which are often resistant to current therapies and have a poor prognosis.

5. PUBLICATIONS

During the course of my doctoral work I carried out a number of side projects developed in collaboration with my colleagues and other research group. The publications related to these project have been extensively discussed in the present thesis and are listed below.

1. Carotenuto P, **Pecoraro A**, Palma G, Russo G, Russo A. Therapeutic Approaches Targeting Nucleolus in Cancer. Cells. 2019 Sep 16;8(9):1090. doi: 10.3390/cells8091090.

2. **Pecoraro A**, Carotenuto P, Russo G, Russo A. Ribosomal protein uL3 targets E2F1 and Cyclin D1 in cancer cell response to nucleolar stress. Sci Rep. 2019 Oct 28;9(1):15431. doi: 10.1038/s41598-019-51723-7.

3. **Pecoraro A**, Carotenuto P, Franco B, De Cegli R, Russo G, Russo A. Role of uL3 in the Crosstalk between Nucleolar Stress and Autophagy in Colon Cancer Cells. Int J Mol Sci. 2020 Mar 20;21(6):2143. doi: 10.3390/ijms21062143.

4. **Pecoraro A**, Virgilio A, Esposito V, Galeone A, Russo G, Russo A. uL3 Mediated Nucleolar Stress Pathway as a New Mechanism of Action of Antiproliferative G-quadruplex TBA Derivatives in Colon Cancer Cells. Biomolecules. 2020 Apr 10;10(4):583. doi: 10.3390/biom10040583.

5. **Pecoraro A**, Pagano M, Russo G, Russo A. Role of Autophagy in Cancer Cell Response to Nucleolar and Endoplasmic Reticulum Stress. Int J Mol Sci. 2020 Oct 4;21(19):7334. doi: 10.3390/ijms21197334.

6. Virgilio A, Esposito V, **Pecoraro A**, Russo A, Vellecco V, Pepe A, Bucci M, Russo G, Galeone A. Structural properties and anticoagulant/cytotoxic activities of heterochiral enantiomeric thrombin binding aptamer (TBA) derivatives. Nucleic Acids Res. 2020 Dec 16;48(22):12556-12565. doi: 10.1093/nar/gkaa1109.

7. Mosca L, Pagano M, **Pecoraro A**, Borzacchiello L, Mele L, Cacciapuoti G, Porcelli M, Russo G, Russo A. S-Adenosyl-l-Methionine Overcomes uL3-Mediated Drug Resistance in p53 Deleted Colon Cancer Cells. Int J Mol Sci. 2020 Dec 24;22(1):103. doi: 10.3390/ijms22010103.

8. **Pecoraro A**, Pagano M, Russo G, Russo A. Ribosome biogenesis and cancer: overview on ribosomal proteins. Int J Mol Sci. Under revision (round 2).

6. BIBLIOGRAPHY

Al Bitar S, Gali-Muhtasib H. The Role of the Cyclin Dependent Kinase Inhibitor p21cip1/waf1 in Targeting Cancer: Molecular Mechanisms and Novel Therapeutics. Cancers (Basel). 2019 Sep 30;11(10):1475. doi: 10.3390/cancers11101475.

Al-Hadid Q, Roy K, Chanfreau G, Clarke SG. Methylation of yeast ribosomal protein Rpl3 promotes translational elongation fidelity. RNA. 2016 Apr;22(4):489-98. doi: 10.1261/rna.054569.115.

Andreeff M, Kelly KR, Yee K, Assouline S, Strair R, Popplewell L, Bowen D, Martinelli G, Drummond MW, Vyas P et al. Results of the Phase I Trial of RG7112, a Small-Molecule MDM2 Antagonist in Leukemia. Clin Cancer Res. 2016 Feb 15;22(4):868-76. doi: 10.1158/1078-0432.CCR-15-0481.

Aubert M, O'Donohue MF, Lebaron S, Gleizes PE. Pre-Ribosomal RNA Processing in Human Cells: From Mechanisms to Congenital Diseases. Biomolecules. 2018 Oct 24;8(4):123. doi: 10.3390/biom8040123.

Ayrault O, Andrique L, Fauvin D, Eymin B, Gazzeri S, Séité P. Human tumor suppressor p14ARF negatively regulates rRNA transcription and inhibits UBF1 transcription factor phosphorylation. Oncogene. 2006 Dec 7;25(58):7577-86. doi: 10.1038/sj.onc.1209743.

Benjamin D, Colombi M, Moroni C, Hall MN. Rapamycin passes the torch: a new generation of mTOR inhibitors. Nat Rev Drug Discov. 2011 Oct 31;10(11):868-80.

Bertoli C, Skotheim JM, de Bruin RA. Control of cell cycle transcription during G1 and S phases. Nat Rev Mol Cell Biol. 2013 Aug;14(8):518-28. doi: 10.1038/nrm3629.

Bukowski K, Kciuk M, Kontek R. Mechanisms of Multidrug Resistance in Cancer Chemotherapy. Int J Mol Sci. 2020 May 2;21(9):3233. doi: 10.3390/ijms21093233.

Burger K, Mühl B, Harasim T, Rohrmoser M, Malamoussi A, Orban M, Kellner M, Gruber-Eber A, Kremmer E, Hölzel M, Eick D. Chemotherapeutic drugs inhibit ribosome biogenesis at various levels. J Biol Chem. 2010 Apr 16;285(16):12416-25. doi: 10.1074/jbc.M109.074211.

Bywater MJ, Pearson RB, McArthur GA, Hannan RD. Dysregulation of the basal RNA polymerase transcription apparatus in cancer. Nat Rev Cancer. 2013 May;13(5):299-314. doi: 10.1038/nrc3496.

Bywater MJ, Poortinga G, Sanij E, Hein N, Peck A, Cullinane C, Wall M, Cluse L, Drygin D, Anderes K et al. Inhibition of RNA polymerase I as a therapeutic strategy to promote cancer-specific activation of p53. Cancer Cell. 2012 Jul 10;22(1):51-65. doi: 10.1016/j.ccr.2012.05.019.

Carotenuto P, Pecoraro A, Palma G, Russo G, Russo A. Therapeutic Approaches Targeting Nucleolus in Cancer. Cells. 2019 Sep 16;8(9):1090. doi: 10.3390/cells8091090.

Cave DD, Desiderio V, Mosca L, Ilisso CP, Mele L, Caraglia M, Cacciapuoti G, Porcelli M. S-Adenosylmethionine-mediated apoptosis is potentiated by autophagy inhibition induced by chloroquine in human breast cancer cells. J Cell Physiol. 2018 Feb;233(2):1370-1383. doi: 10.1002/jcp.26015.

Challagundla KB, Sun XX, Zhang X, DeVine T, Zhang Q, Sears RC, Dai MS. Ribosomal protein L11 recruits miR-24/miRISC to repress c-Myc expression in response to ribosomal stress. Mol Cell Biol. 2011 Oct;31(19):4007-21. doi: 10.1128/MCB.05810-11.

Chen HT, Liu H, Mao MJ, Tan Y, Mo XQ, Meng XJ, Cao MT, Zhong CY, Liu Y, Shan H, Jiang GM. Crosstalk between autophagy and epithelial-mesenchymal transition and its application in cancer therapy. Mol Cancer. 2019 May 24;18(1):101. doi: 10.1186/s12943-019-1030-2.

Chen M, von Mikecz A. Formation of nucleoplasmic protein aggregates impairs nuclear function in response to SiO2 nanoparticles. Exp Cell Res. 2005 Apr 15;305(1):51-62. doi: 10.1016/j.yexcr.2004.12.021.

Cheok CF, Verma CS, Baselga J, Lane DP. Translating p53 into the clinic. Nat Rev Clin Oncol. 2011 Jan;8(1):25-37. doi: 10.1038/nrclinonc.2010.174.

Chun Y, Kim J. Autophagy: An Essential Degradation Program for Cellular Homeostasis and Life. Cells. 2018 Dec 19;7(12):278. doi: 10.3390/cells7120278.

Cuccurese M, Russo G, Russo A, Pietropaolo C. Alternative splicing and nonsense-mediated mRNA decay regulate mammalian ribosomal gene expression. Nucleic Acids Res. 2005 Oct 27;33(18):5965-77. doi: 10.1093/nar/gki905.

d'Angelo I, Costabile G, Durantie E, Brocca P, Rondelli V, Russo A, Russo G, Miro A, Quaglia F, Petri-Fink A, Rothen-Rutishauser B, Ungaro F. Hybrid Lipid/Polymer Nanoparticles for Pulmonary Delivery of siRNA: Development and Fate Upon In Vitro Deposition on the Human Epithelial Airway Barrier. J Aerosol Med Pulm Drug Deliv. 2018 Jun;31(3):170-181. doi: 10.1089/jamp.2017.1364.

Dai MS, Sears R, Lu H. Feedback regulation of c-Myc by ribosomal protein L11. Cell Cycle. 2007 Nov 15;6(22):2735-41. doi: 10.4161/cc.6.22.4895.

Dang CV. c-Myc target genes involved in cell growth, apoptosis, and metabolism. Mol Cell Biol. 1999 Jan;19(1):1-11. doi: 10.1128/mcb.19.1.1.

De Keersmaecker K, Atak ZK, Li N, Vicente C, Patchett S, Girardi T, Gianfelici V, Geerdens E, Clappier E, Porcu M et al. Exome sequencing identifies mutation in CNOT3 and ribosomal genes RPL5 and RPL10 in T-cell acute lymphoblastic leukemia. Nat Genet. 2013 Feb;45(2):186-90. doi: 10.1038/ng.2508.

Donati G, Brighenti E, Vici M, Mazzini G, Treré D, Montanaro L, Derenzini M. Selective inhibition of rRNA transcription downregulates E2F-1: a new p53-independent mechanism linking cell growth to cell proliferation. J Cell Sci. 2011 Sep 1;124(Pt 17):3017-28. doi: 10.1242/jcs.086074.

Dongre A, Weinberg RA. New insights into the mechanisms of epithelial-mesenchymal transition and implications for cancer. Nat Rev Mol Cell Biol. 2019 Feb;20(2):69-84. doi: 10.1038/s41580-018-0080-4.

Dossou AS, Basu A. The Emerging Roles of mTORC1 in Macromanaging Autophagy. Cancers (Basel). 2019 Sep 24;11(10):1422. doi: 10.3390/cancers11101422.

Drygin D, Lin A, Bliesath J, Ho CB, O'Brien SE, Proffitt C, Omori M, Haddach M, Schwaebe MK, Siddiqui-Jain A et al. Targeting RNA polymerase I with an oral small molecule CX-5461 inhibits ribosomal RNA synthesis and solid tumor growth. Cancer Res. 2011 Feb 15;71(4):1418-30. doi: 10.1158/0008-5472.CAN-10-1728.

Drygin D, Siddiqui-Jain A, O'Brien S, Schwaebe M, Lin A, Bliesath J, Ho CB, Proffitt C, Trent K, Whitten JP, Lim JK, Von Hoff D, Anderes K, Rice WG. Anticancer activity of CX-3543: a direct inhibitor of rRNA biogenesis. Cancer Res. 2009 Oct 1;69(19):7653-61. doi: 10.1158/0008-5472.CAN-09-1304.

Edgar R, Domrachev M, Lash AE. Gene Expression Omnibus: NCBI gene expression and hybridization array data repository. Nucleic Acids Res. 2002 Jan 1;30(1):207-10. doi: 10.1093/nar/30.1.207.

Esposito D, Crescenzi E, Sagar V, Loreni F, Russo A, Russo G. Human rpL3 plays a crucial role in cell response to nucleolar stress induced by 5-FU and L-OHP. Oncotarget. 2014 Nov 30;5(22):11737-51. doi: 10.18632/oncotarget.2591.

Esposito V, Russo A, Amato T, Varra M, Vellecco V, Bucci M, Russo G, Virgilio A, Galeone A. Backbone modified TBA analogues endowed with antiproliferative activity. Biochim Biophys Acta Gen Subj. 2017 May;1861(5 Pt B):1213-1221. doi: 10.1016/j.bbagen.2016.09.019.

Esposito V, Russo A, Amato T, Vellecco V, Bucci M, Mayol L, Russo G, Virgilio A, Galeone A. The "Janus face" of the thrombin binding aptamer: Investigating the anticoagulant and antiproliferative properties through straightforward chemical modifications. Bioorg Chem. 2018 Feb;76:202-209. doi: 10.1016/j.bioorg.2017.11.005. (a)

Esposito V, Russo A, Vellecco V, Bucci M, Russo G, Mayol L, Virgilio A, Galeone A. Thrombin binding aptamer analogues containing inversion of polarity sites endowed with antiproliferative and anti-motility properties against Calu-6 cells. Biochim Biophys Acta Gen Subj. 2018 Dec;1862(12):2645-2650. doi: 10.1016/j.bbagen.2018.07.031. (b)

Evan GI, Vousden KH. Proliferation, cell cycle and apoptosis in cancer. Nature. 2001 May 17;411(6835):342-8. doi: 10.1038/35077213.

Fancello L, Kampen KR, Hofman IJ, Verbeeck J, De Keersmaecker K. The ribosomal protein gene RPL5 is a haploinsufficient tumor suppressor in multiple cancer types. Oncotarget. 2017 Feb 28;8(9):14462-14478. doi: 10.18632/oncotarget.14895.

Ferreira R, Schneekloth JS Jr, Panov KI, Hannan KM, Hannan RD. Targeting the RNA Polymerase I Transcription for Cancer Therapy Comes of Age. Cells. 2020 Jan 21;9(2):266. doi: 10.3390/cells9020266.

Fontecave M, Atta M, Mulliez E. S-adenosylmethionine: nothing goes to waste. Trends Biochem Sci. 2004 May;29(5):243-9. doi: 10.1016/j.tibs.2004.03.007.

Fumagalli S, Ivanenkov VV, Teng T, Thomas G. Suprainduction of p53 by disruption of 40S and 60S ribosome biogenesis leads to the activation of a novel G2/M checkpoint. Genes Dev. 2012 May 15;26(10):1028-40. doi: 10.1101/gad.189951.112.

Galluzzi L, Baehrecke EH, Ballabio A, Boya P, Bravo-San Pedro JM, Cecconi F, Choi AM, Chu CT, Codogno P, Colombo MI, et al. Molecular definitions of autophagy and related processes. EMBO J. 2017 Jul 3;36(13):1811-1836. doi: 10.15252/embj.201796697.

Gou Y, Shi Y, Zhang Y, Nie Y, Wang J, Song J, Jin H, He L, Gao L, Qiao L, Wu K, Fan D. Ribosomal protein L6 promotes growth and cell cycle progression through upregulating cyclin E in gastric cancer cells. Biochem Biophys Res Commun. 2010 Mar 19;393(4):788-93. doi: 10.1016/j.bbrc.2010.02.083.

Grummt I. The nucleolus—guardian of cellular homeostasis and genome integrity. Chromosoma. 2013 Dec;122(6):487-97. doi: 10.1007/s00412-013-0430-0.

Guo X, Shi Y, Gou Y, Li J, Han S, Zhang Y, Huo J, Ning X, Sun L, Chen Y, Sun S, Fan D. Human ribosomal protein S13 promotes gastric cancer growth through down-regulating p27(Kip1). J Cell Mol Med. 2011 Feb;15(2):296-306. doi: 10.1111/j.1582-4934.2009.00969.x.

Hamdane N, Herdman C, Mars JC, Stefanovsky V, Tremblay MG, Moss T. Depletion of the cisplatin targeted HMGB-box factor UBF selectively induces p53-independent apoptotic death in transformed cells. Oncotarget. 2015 Sep 29;6(29):27519-36. doi: 10.18632/oncotarget.4823.

Huang Y, Sramkoski RM, Jacobberger JW. The kinetics of G2 and M transitions regulated by B cyclins. PLoS One. 2013 Dec 4;8(12):e80861. doi: 10.1371/journal.pone.0080861.

Iizumi Y, Oishi M, Taniguchi T, Goi W, Sowa Y, Sakai T. The flavonoid apigenin downregulates CDK1 by directly targeting ribosomal protein S9. PLoS One. 2013 Aug 29;8(8):e73219. doi: 10.1371/journal.pone.0073219.

Issaeva N, Bozko P, Enge M, Protopopova M, Verhoef LG, Masucci M, Pramanik A, Selivanova G. Small molecule RITA binds to p53, blocks p53-HDM-2 interaction and activates p53 function in tumors. Nat Med. 2004 Dec;10(12):1321-8. doi: 10.1038/nm1146.

John RR, Malathi N, Ravindran C, Anandan S. Mini review: Multifaceted role played by cyclin D1 in tumor behavior. Indian J Dent Res. 2017 Mar-Apr;28(2):187-192. doi: 10.4103/ijdr.IJDR_697_16.

Juli G, Gismondi A, Monteleone V, Caldarola S, Iadevaia V, Aspesi A, Dianzani I, Proud CG, Loreni F. Depletion of ribosomal protein S19 causes a reduction of rRNA synthesis. Sci Rep. 2016 Oct 13;6:35026. doi: 10.1038/srep35026.

Kampen KR, Sulima SO, Vereecke S, De Keersmaecker K. Hallmarks of ribosomopathies. Nucleic Acids Res. 2020 Feb 20;48(3):1013-1028. doi: 10.1093/nar/gkz637.

Kiraz Y, Adan A, Kartal Yandim M, Baran Y. Major apoptotic mechanisms and genes involved in apoptosis. Tumour Biol. 2016 Jul;37(7):8471-86. doi: 10.1007/s13277-016-5035-9.

Klein EA, Assoian RK. Transcriptional regulation of the cyclin D1 gene at a glance. J Cell Sci. 2008 Dec 1;121(Pt 23):3853-7. doi: 10.1242/jcs.039131.

Kodiha M, Mahboubi H, Maysinger D, Stochaj U. Gold Nanoparticles Impinge on Nucleoli and the Stress Response in MCF7 Breast Cancer Cells. Nanobiomedicine (Rij). 2016 Jan 1;3:3. doi: 10.5772/62337.

Kongara S, Karantza V. The interplay between autophagy and ROS in tumorigenesis. Front Oncol. 2012 Nov 21;2:171. doi: 10.3389/fonc.2012.00171.

Kothari V, Mulherkar R. Inhibition of cyclin D1 by shRNA is associated with enhanced sensitivity to conventional therapies for head and neck squamous cell carcinoma. Anticancer Res. 2012 Jan;32(1):121-8.

Kousholt AN, Menzel T, Sørensen CS. Pathways for genome integrity in G2 phase of the cell cycle. Biomolecules. 2012 Nov 30;2(4):579-607. doi: 10.3390/biom2040579.

Li YJ, Lei YH, Yao N, Wang CR, Hu N, Ye WC, Zhang DM, Chen ZS. Autophagy and multidrug resistance in cancer. Chin J Cancer. 2017 Jun 24;36(1):52. doi: 10.1186/s40880-017-0219-2.

Li Z, Jiao X, Wang C, Ju X, Lu Y, Yuan L, Lisanti MP, Katiyar S, Pestell RG. Cyclin D1 induction of cellular migration requires p27(KIP1). Cancer Res. 2006 Oct 15;66(20):9986-94. doi: 10.1158/0008-5472.CAN-06-1596.

Liao JM, Zhou X, Gatignol A, Lu H. Ribosomal proteins L5 and L11 co-operatively inactivate c-Myc via RNA-induced silencing complex. Oncogene. 2014 Oct 9;33(41):4916-23. doi: 10.1038/onc.2013.430.

Ma X, Gao Y, Fan Y, Ni D, Zhang Y, Chen W, Zhang P, Song E, Huang Q, Ai Q, Li H, Wang B, Zheng T, Shi T, Zhang X. Overexpression of E2F1 promotes tumor malignancy and correlates with TNM stages in clear cell renal cell carcinoma. PLoS One. 2013 Sep 4;8(9):e73436. doi: 10.1371/journal.pone.0073436.

Mailliot J, Garreau de Loubresse N, Yusupova G, Meskauskas A, Dinman JD, Yusupov M. Crystal Structures of the uL3 Mutant Ribosome: Illustration of the Importance of Ribosomal Proteins for Translation Efficiency. J Mol Biol. 2016 May 22;428(10 Pt B):2195-202. doi: 10.1016/j.jmb.2016.02.013.

Mantovani F, Collavin L, Del Sal G. Mutant p53 as a guardian of the cancer cell. Cell Death Differ. 2019 Jan;26(2):199-212. doi: 10.1038/s41418-018-0246-9.

Mauthe M, Orhon I, Rocchi C, Zhou X, Luhr M, Hijlkema KJ, Coppes RP, Engedal N, Mari M, Reggiori F. Chloroquine inhibits autophagic flux by decreasing autophagosome-lysosome fusion. Autophagy. 2018;14(8):1435-1455. doi: 10.1080/15548627.2018.1474314.

Meskauskas A, Dinman JD. Ribosomal protein L3: gatekeeper to the A site. Mol Cell. 2007 Mar 23;25(6):877-88. doi: 10.1016/j.molcel.2007.02.015.

Molavi G, Samadi N, Hosseingholi EZ. The roles of moonlight ribosomal proteins in the development of human cancers. J Cell Physiol. 2019 Jun;234(6):8327-8341. doi: 10.1002/jcp.27722.

Mosca L, Pagano M, Pecoraro A, Borzacchiello L, Mele L, Cacciapuoti G, Porcelli M, Russo G, Russo A. S-Adenosyl-l-Methionine Overcomes uL3-Mediated Drug Resistance in p53 Deleted Colon Cancer Cells. Int J Mol Sci. 2020 Dec 24;22(1):103. doi: 10.3390/ijms22010103. (a)

Mosca L, Vitiello F, Coppola A, Borzacchiello L, Ilisso CP, Pagano M, Caraglia M, Cacciapuoti G, Porcelli M. Therapeutic Potential of the Natural Compound S-Adenosylmethionine as a Chemoprotective Synergistic Agent in Breast, and Head and Neck Cancer Treatment: Current Status of Research. Int J Mol Sci. 2020 Nov 13;21(22):8547. doi: 10.3390/ijms21228547. (b)

O'Donohue MF, Choesmel V, Faubladier M, Fichant G, Gleizes PE. Functional dichotomy of ribosomal proteins during the synthesis of mammalian 40S ribosomal subunits. J Cell Biol. 2010 Sep 6;190(5):853-66. doi: 10.1083/jcb.201005117.

Ofir-Rosenfeld Y, Boggs K, Michael D, Kastan MB, Oren M. Mdm2 regulates p53 mRNA translation through inhibitory interactions with ribosomal protein L26. Mol Cell. 2008 Oct 24;32(2):180-9. doi: 10.1016/j.molcel.2008.08.031.

Ogloblina AM, Khristich AN, Karpechenko NY, Semina SE, Belitsky GA, Dolinnaya NG, Yakubovskaya MG. Multi-targeted effects of G4-aptamers and their antiproliferative activity against cancer cells. Biochimie. 2018 Feb;145:163-173. doi: 10.1016/j.biochi.2017.11.020.

Onofrillo C, Galbiati A, Montanaro L, Derenzini M. The pre-existing population of 5S rRNA effects p53 stabilization during ribosome biogenesis inhibition. Oncotarget. 2017 Jan 17;8(3):4257-4267. doi: 10.18632/oncotarget.13833.

Pagliara V, Saide A, Mitidieri E, d'Emmanuele di Villa Bianca R, Sorrentino R, Russo G, Russo A. 5-FU targets rpL3 to induce mitochondrial apoptosis via cystathionine-β-synthase in colon cancer cells lacking p53. Oncotarget. 2016 Aug 2;7(31):50333-50348. doi: 10.18632/oncotarget.10385.

Paunesku T, Vogt S, Lai B, Maser J, Stojićević N, Thurn KT, Osipo C, Liu H, Legnini D, Wang Z, Lee C, Woloschak GE. Intracellular distribution of TiO2-DNA oligonucleotide nanoconjugates directed to nucleolus and mitochondria indicates sequence specificity. Nano Lett. 2007 Mar;7(3):596-601. doi: 10.1021/nl0624723.

Pecoraro A, Carotenuto P, Franco B, De Cegli R, Russo G, Russo A. Role of uL3 in the Crosstalk between Nucleolar Stress and Autophagy in Colon Cancer Cells. Int J Mol Sci. 2020 Mar 20;21(6):2143. doi: 10.3390/ijms21062143. (a)

Pecoraro A, Carotenuto P, Russo G, Russo A. Ribosomal protein uL3 targets E2F1 and Cyclin D1 in cancer cell response to nucleolar stress. Sci Rep. 2019 Oct 28;9(1):15431. doi: 10.1038/s41598-019-51723-7.

Pecoraro A, Pagano M, Russo G, Russo A. Role of Autophagy in Cancer Cell Response to Nucleolar and Endoplasmic Reticulum Stress. Int J Mol Sci. 2020 Oct 4;21(19):7334. doi: 10.3390/ijms21197334. (b)

Pecoraro A, Virgilio A, Esposito V, Galeone A, Russo G, Russo A. uL3 Mediated Nucleolar Stress Pathway as a New Mechanism of Action of Antiproliferative G-quadruplex TBA Derivatives in Colon Cancer Cells. Biomolecules. 2020 Apr 10;10(4):583. doi: 10.3390/biom10040583. (c)

Pederson T. The nucleolus. Cold Spring Harb Perspect Biol. 2011 Mar 1;3(3):a000638. doi: 10.1101/cshperspect.a000638.

Pinelli M, Carissimo A, Cutillo L, Lai CH, Mutarelli M, Moretti MN, Singh MV, Karali M, Carrella D, Pizzo M, Russo F, Ferrari S, Ponzin D, Angelini C, Banfi S, di Bernardo D. An atlas of gene expression and gene co-regulation in the human retina. Nucleic Acids Res. 2016 Jul 8;44(12):5773-84. doi: 10.1093/nar/gkw486.

Pirota V, Nadai M, Doria F, Richter SN. Naphthalene Diimides as Multimodal G-Quadruplex-Selective Ligands. Molecules. 2019 Jan 24;24(3):426. doi: 10.3390/molecules24030426.

Poppy Roworth A, Ghari F, La Thangue NB. To live or let die - complexity within the E2F1 pathway. Mol Cell Oncol. 2015 Jan 30;2(1):e970480. doi: 10.4161/23723548.2014.970480.

Ristau J, van Hoef V, Peuget S, Zhu J, Guan BJ, Liang S, Hatzoglou M, Topisirovic I, Selivanova G, Larsson O. RITA requires eIF2α-dependent modulation of mRNA translation for its anti-cancer activity. Cell Death Dis. 2019 Nov 7;10(11):845. doi: 10.1038/s41419-019-2074-3.

Rosado IV, Kressler D, de la Cruz J. Functional analysis of Saccharomyces cerevisiae ribosomal protein Rpl3p in ribosome synthesis. Nucleic Acids Res. 2007;35(12):4203-13. doi: 10.1093/nar/gkm388.

Roué G, Pichereau V, Lincet H, Colomer D, Sola B. Cyclin D1 mediates resistance to apoptosis through upregulation of molecular chaperones and consequent redistribution of cell death regulators. Oncogene. 2008 Aug 21;27(36):4909-20. doi: 10.1038/onc.2008.126.

Roxo C, Kotkowiak W, Pasternak A. G-Quadruplex-Forming Aptamers-Characteristics, Applications, and Perspectives. Molecules. 2019 Oct 21;24(20):3781. doi: 10.3390/molecules24203781.

Ruggero D. Revisiting the nucleolus: from marker to dynamic integrator of cancer signaling. Sci Signal. 2012 Sep 11;5(241):pe38. doi: 10.1126/scisignal.2003477.

Russo A, Catillo M, Esposito D, Briata P, Pietropaolo C, Russo G. Autoregulatory circuit of human rpL3 expression requires hnRNP H1, NPM and KHSRP. Nucleic Acids Res. 2011 Sep 1;39(17):7576-85. doi: 10.1093/nar/gkr461.

Russo A, Esposito D, Catillo M, Pietropaolo C, Crescenzi E, Russo G. Human rpL3 induces G_1/S arrest or apoptosis by modulating p21 (waf1/cip1) levels in a p53-independent manner. Cell Cycle. 2013 Jan 1;12(1):76-87. doi: 10.4161/cc.22963.

Russo A, Maiolino S, Pagliara V, Ungaro F, Tatangelo F, Leone A, Scalia G, Budillon A, Quaglia F, Russo G. Enhancement of 5-FU sensitivity by the proapoptotic rpL3 gene in p53 null colon cancer cells through combined polymer nanoparticles. Oncotarget. 2016 Nov 29;7(48):79670-79687. doi: 10.18632/oncotarget.13216. (a)

Russo A, Pagliara V, Albano F, Esposito D, Sagar V, Loreni F, Irace C, Santamaria R, Russo G. Regulatory role of rpL3 in cell response to nucleolar stress induced by Act D in tumor cells lacking functional p53. Cell Cycle. 2016;15(1):41-51. doi: 10.1080/15384101.2015.1120926. (b)

Russo A, Pellosi DS, Pagliara V, Milone MR, Pucci B, Caetano W, Hioka N, Budillon A, Ungaro F, Russo G, Quaglia F. Biotin-targeted Pluronic(®) P123/F127 mixed micelles delivering niclosamide: A repositioning strategy to treat drug-resistant lung cancer cells. Int J Pharm. 2016 Sep 10;511(1):127-139. doi: 10.1016/j.ijpharm.2016.06.118. (c)

Russo A, Russo G. Ribosomal Proteins Control or Bypass p53 during Nucleolar Stress. Int J Mol Sci. 2017 Jan 12;18(1):140. doi: 10.3390/ijms18010140. (a)

Russo A, Saide A, Cagliani R, Cantile M, Botti G, Russo G. rpL3 promotes the apoptosis of p53 mutated lung cancer cells by down-regulating CBS and NFκB upon 5-FU treatment. Sci Rep. 2016 Dec 7;6:38369. doi: 10.1038/srep38369. (d)

Russo A, Saide A, Smaldone S, Faraonio R, Russo G. Role of uL3 in Multidrug Resistance in p53-Mutated Lung Cancer Cells. Int J Mol Sci. 2017 Mar 3;18(3):547. doi: 10.3390/ijms18030547. (b)

Russo A, Siciliano G, Catillo M, Giangrande C, Amoresano A, Pucci P, Pietropaolo C, Russo G. hnRNP H1 and intronic G runs in the splicing control of the human rpL3 gene. Biochim Biophys Acta. 2010 May-Jun;1799(5-6):419-28. doi: 10.1016/j.bbagrm.2010.01.008.

Schmittgen TD, Livak KJ. Analyzing real-time PCR data by the comparative C(T) method. Nat Protoc. 2008;3(6):1101-8. doi: 10.1038/nprot.2008.73.

Shamloo B, Usluer S. p21 in Cancer Research. Cancers (Basel). 2019 Aug 14;11(8):1178. doi: 10.3390/cancers11081178.

Simbulan-Rosenthal CM, Rosenthal DS, Luo R, Samara R, Espinoza LA, Hassa PO, Hottiger MO, Smulson ME. PARP-1 binds E2F-1 independently of its DNA binding and catalytic domains, and acts as a novel coactivator of E2F-1-mediated transcription during re-entry of quiescent cells into S phase. Oncogene. 2003 Nov 20;22(52):8460-71. doi: 10.1038/sj.onc.1206897.

Skalniak L, Kocik J, Polak J, Skalniak A, Rak M, Wolnicka-Glubisz A, Holak TA. Prolonged Idasanutlin (RG7388) Treatment Leads to the Generation of p53-Mutated Cells. Cancers (Basel). 2018 Oct 24;10(11):396. doi: 10.3390/cancers10110396.

Stępiński D. The nucleolus, an ally, and an enemy of cancer cells. Histochem Cell Biol. 2018 Dec;150(6):607-629. doi: 10.1007/s00418-018-1706-5.

Sullivan KD, Galbraith MD, Andrysik Z, Espinosa JM. Mechanisms of transcriptional regulation by p53. Cell Death Differ. 2018 Jan;25(1):133-143. doi: 10.1038/cdd.2017.174.

Sun XX, Dai MS, Lu H. 5-fluorouracil activation of p53 involves an MDM2-ribosomal protein interaction. J Biol Chem. 2007 Mar 16;282(11):8052-9. doi: 10.1074/jbc.M610621200.

Szabo C. H2S and cancer: Give credit where credit is due. Urol Oncol. 2016 Jul;34(7):334. doi: 10.1016/j.urolonc.2016.04.007.

Thomson E, Ferreira-Cerca S, Hurt E. Eukaryotic ribosome biogenesis at a glance. J Cell Sci. 2013 Nov 1;126(Pt 21):4815-21. doi: 10.1242/jcs.111948.

Tsai RY, Pederson T. Connecting the nucleolus to the cell cycle and human disease. FASEB J. 2014 Aug;28(8):3290-6. doi: 10.1096/fj.14-254680.

Virgilio A, Esposito V, Pecoraro A, Russo A, Vellecco V, Pepe A, Bucci M, Russo G, Galeone A. Structural properties and anticoagulant/cytotoxic activities of heterochiral enantiomeric thrombin binding aptamer (TBA) derivatives. Nucleic Acids Res. 2020 Dec 16;48(22):12556-12565. doi: 10.1093/nar/gkaa1109.

Wang CH, Wang LK, Wu CC, Chen ML, Lee MC, Lin YY, Tsai FM. The Ribosomal Protein RPLP0 Mediates PLAAT4-induced Cell Cycle Arrest and Cell Apoptosis. Cell Biochem Biophys. 2019 Sep;77(3):253-260. doi: 10.1007/s12013-019-00876-3.

Wiegering A, Matthes N, Mühling B, Koospal M, Quenzer A, Peter S, Germer CT, Linnebacher M, Otto C. Reactivating p53 and Inducing Tumor Apoptosis (RITA) Enhances the Response of RITA-Sensitive Colorectal Cancer Cells to Chemotherapeutic Agents 5-Fluorouracil and Oxaliplatin. Neoplasia. 2017 Apr;19(4):301-309. doi: 10.1016/j.neo.2017.01.007.

Willis S, Day CL, Hinds MG, Huang DC. The Bcl-2-regulated apoptotic pathway. J Cell Sci. 2003 Oct 15;116(Pt 20):4053-6. doi: 10.1242/jcs.00754.

Wu YX, Kwon YJ. Aptamers: The "evolution" of SELEX. Methods. 2016 Aug 15;106:21-8. doi: 10.1016/j.ymeth.2016.04.020.

Xu H, Di Antonio M, McKinney S, Mathew V, Ho B, O'Neil NJ, Santos ND, Silvester J, Wei V, Garcia J et al. CX-5461 is a DNA G-quadruplex stabilizer with selective lethality in BRCA1/2 deficient tumours. Nat Commun. 2017 Feb 17;8:14432. doi: 10.1038/ncomms14432.

Zhai W, Comai L. Repression of RNA polymerase I transcription by the tumor suppressor p53. Mol Cell Biol. 2000 Aug;20(16):5930-8. doi: 10.1128/mcb.20.16.5930-5938.2000.

Zhang Z, Rigas B. NF-kappaB, inflammation and pancreatic carcinogenesis: NF-kappaB as a chemoprevention target (review). Int J Oncol. 2006 Jul;29(1):185-92.

Zhang Z, Wang H, Li M, Rayburn ER, Agrawal S, Zhang R. Stabilization of E2F1 protein by MDM2 through the E2F1 ubiquitination pathway. Oncogene. 2005 Nov 3;24(48):7238-47. doi: 10.1038/sj.onc.1208814.

Zhou J, Rossi J. Aptamers as targeted therapeutics: current potential and challenges. Nat Rev Drug Discov. 2017 Mar;16(3):181-202. doi: 10.1038/nrd.2016.199.

Zhou X, Hao Q, Liao JM, Liao P, Lu H. Ribosomal protein S14 negatively regulates c-Myc activity. J Biol Chem. 2013 Jul 26;288(30):21793-801. doi: 10.1074/jbc.M112.445122.